Studies of $He+HeH^+$ and $H_2+OH(CN)$ reactive scattering systems using multiconfiguration time-dependent Hartree approach

A thesis submitted by

Sayak Bhattacharya

to

Indian Institute of Technology Guwahati

for the award of the degree of

Doctor of Philosophy





Department of Chemistry
INDIAN INSTITUTE OF TECHNOLOGY GUWAHATI
Guwahati-781039
India

November, 2011

TH-1851_Sayak

Statement

The work contained in this thesis titled '**Studies of He + HeH^+ and H_2 + OH(CN) reactive scattering systems using Multiconfiguration time-dependent Hartree approach**' has been carried out by me under the supervision of Dr. Aditya N. Panda, Assistant Professor, Department of Chemistry, Indian Institute of Technology Guwahati. This work has not been submitted elsewhere for the award of any degree.

Sayak Bhattacharya

Sayak Bhattacharya
IIT Guwahati
November, 2011

TH-1851_Sayak

Certificate I

Certified that the work contained in this thesis titled '**Studies of He + HeH^+ and H_2 + OH(CN) reactive scattering systems using Multiconfiguration time-dependent Hartree approach**' has been carried out by Sayak Bhattacharya, a student of Department of Chemistry, Indian Institute of Technology Guwahati under my supervision. This work has not been submitted elsewhere for the award of any degree.

Aditya Narayan Panda

Aditya N. Panda
Thesis Supervisor
Assistant Professor
Department of Chemistry
IIT Guwahati

TH-1851_Sayak

To

My Parents...

...who taught me the fun of knowledge.

TH-1851_Sayak

Imagination is more important than knowledge.....

- Albert Einstein

TH-1851_Sayak

Acknowledgements

As I conclude my thesis work, its time to acknowledge the immeasurable contributions which have made this work a reality. I would like to express a few words of appreciation and gratitude to the people who have made my journey so far, an unforgettable experience.

To begin with I would like to thank my supervisor Dr. Aditya N. Panda, not only for being so supportive, but also for providing me with the opportunity to travel and interact with people who inspired me to work even harder and pursue science more vigorously. Without him, and his ability to raise my spirits whenever I was the most discouraged, I could have never have made it this far. Always allowing me to pursue my research the way I desired, he gave me the opportunity to learn from my mistakes - being always there by me in all my troubles.

A special word of gratitude goes to the members of my Doctoral committee, Dr. G. Krishnamoorthy(Chairman), Dr. Ashish K. Gupta and Dr. Tarak N. Dey.

I sincerely thank Prof. Arun Chattopadhyay, HoD, Dept. of Chemistry, and Prof. A. T. Khan for guiding me through various stages during my stay at IIT Guwahati. I would also like to thank all faculty and staff at IITG for making my stay here a great learning experience.

I would like to acknowledge Prof. Hans-Dieter Meyer for his invaluable suggestions during my research work and the positive and encouraging feedbacks, which he never forgot to add at the end of his suggestions.

I would like to thank Department of Science and Technology, Govt. of India for funding our high performance cluster.

I would cherish my time spent at IITG due to my friends who made even the depressing

TH-1851_Sayak

of days seem exciting. I have shared my happiest moments at IITG with my batchmates Vijendra, Atul, Devender, Somashekhar, Francis, Sadhu, Mohan Lal, Faizi, Razzaq and Partho.

A special word of appreciation and gratitude goes for my labmates and juniors, Satya, Amey, Koushik, Debasish. I would like to specially mention Debasish for the immense help he has rendered in the final days of my thesis writing.

I am thankful to Mrs. Morris, Mrs. Anjali Roy, Mrs. Angana Chowdhury, Mr. Uday Bhanu Roy, Mr. Sukumar Mukherjee, Dr. Sanjeeb Ganguly, Prof. Rita Kakkar, Prof. S. K. Dogra for having moulded me as a student in different steps of my career.

Words are not sufficient to express my gratitude towards my grandparents, Late Sri Karunamoy Chakrabarty and Late Smt. Kalyani Chakrabarty who helped me grow up, encouraging me to aim higher at every step of life. I would like to express my gratitude to my parents and my sister who have given it their all to make my dreams come true. They have been the strength behind this accomplishment throughout, for which, I believe mere expression of gratitude doesn't suffice. I would also like to mention Shreeja who came as a bundle of joy to our family and cheered me up in my last days of my PhD.

Finally, I would like to thank Dr. Anindita Sengupta, simply for being with me and making me believe that nothing is impossible. Had it not been for her immense support and continuous encouragement, I would have had opted for some other career option, when the going was really tough in my initial days. A famous quote reads - success is how you bounce back when you reach bottom - its only because of her and my family that I have been able to rise up after every failure and aspire for the zenith.

Sayak

TH-1851_Sayak

SYNOPSIS

Studies of quantum reactive scattering systems using the time-dependent wave packet approach provides an opportunity to understand the underlying picture of the reaction dynamics. The objective of this work is to carry out a molecular level analysis of the reaction dynamics of three different systems: one tri-atomic ion-molecule system, the He + H^+He and two different tetra-atomic systems, the H_2 + OH and H_2 + CN. The quantum dynamics has been studied by propagating wave packets using the MCTDH algorithm. The importance of inclusion of Coriolis coupling on the reaction attributes for both the tri-atomic ion-molecule and the tetra-atomic reaction systems is investigated. This being the first quantum dynamical study for the reaction probabilities and cross sections on the He + H^+He system, standard wave packet propagation studies using the split operator methodology have also been performed for the same to estimate the accuracy of the MCTDH approach. The H_2 + OH system has been studied on three different potential energy surfaces with this being the first quantum dynamical study on the WSLFH surface. The aim of this comprehensive study is to determine the dependence of the reaction dynamics of the system on the surface characteristics and topology. The H_2 + CN system has been studied with the aim of determining the accuracy of the TSH3 potential energy surface and the exact nature of the C-N bond, which has an ambiguous spectator bond nature, unlike the O-H bond in the H_2 + OH reaction system.

Chapter 1 provides an introduction to the field of quantum reactive scattering.

Chapter 2 presents the MCTDH methodology and the derivation of the working equations. Various features of the MCTDH algorithm like mode combination and

TH-1851_Sayak

the product representation of the Hamiltonian, which improve the performance of this method, have been discussed.

Chapter 3 discusses the Hamiltonian operator for the tri- and tetra-atomic molecules in the appropriate coordinate system. This is followed by a discussion on the preparation of initial wave packets for both tri- and tetra-atomic reaction systems and the formulation of the reaction cross sections and rate constants for the reaction systems.

Chapter 4 consists of the results derived from the study of the He + H^+He system. Both centrifugal sudden and coupled channel studies have been performed using the MCTDH methodology, while the studies performed using the split operator method have been carried out under centrifugal sudden approximation. The centrifugal sudden results obtained from both the MCTDH and the split-operator methodologies have been compared to establish the accuracy of the calculations. The coupled channel results show a distinct difference from the centrifugal sudden results. The observed differences for this system have been analyzed and explained in this study. The importance of inclusion of Coriolis coupling for the reaction in its ro-vibrational excited states have been determined. The importance of the initial orientation of the reagents and the presence of preferred pathways of approach in the reaction dynamics of this system has been discussed.

Chapter 5 presents the dynamics of the H_2 + OH reaction on three different potential energy surfaces. The MCTDH reaction probabilities and cross sections on the WDSE and YZCL2 surfaces are compared with the literature results to determine the accuracy of the MCTDH algorithm in studying the tetra-atomic reactive systems. The quantum dynamical reaction probabilities and cross sections

TH-1851_Sayak

on the WSLFH surface are reported for the first time. The significant differences observed in the cross sections on the different surfaces have been analyzed on the basis of differences in the surface characteristics and the transition state structure on the three surfaces. Vibrationally excited cross sections on the YZCL2 surface are reported for the first time, while previous studies on the WSLFH surface have involved quasi-classical trajectory studies. The study of the reaction cross sections and rate constants for the ro-vibrational excited states of the diatoms reveals a significant dependence of the reaction attributes on the properties of the surfaces considered, along with the pathways of approach and the initial orientation of the reactants.

Chapter 6 reports the results of the application of the MCTDH algorithm to study the H_2 + CN reaction. Reaction probabilities and cross sections are obtained for the ground and vibrational excited states of H_2 and CN. The effect of using an exact form of the Hamiltonian on the reaction dynamics has been analyzed. The exact nature of the CN bond in the reactive system has been ambiguous till date. This study aims to determine the validity of labelling the CN bond as a spectator bond. The accuracy of the TSH3 potential energy surface, on which the reaction dynamics is studied, has also been investigated.

Chapter 7 presents a summary of the work done along with the conclusions derived from our studies on the different systems.

TH-1851_Sayak

List of Abbreviations

TISE	- Time-independent Schrödinger equation
TDSE	- Time-dependent Schrödinger equation
PES	- Potential energy surface
TDWP	- Time-dependent wave packet
DVR	- Discrete variable representation
TDH	- Time-dependent Hartree
SO	- Split operator
DOF	- Degrees of freedom
1D	- One-dimensional
SPF	- Single particle functions
CS	- Centrifugal sudden
CC	- Coupled channel
QCT	- Quasi-classical trajectory
QM	- Quantum mechanical
CAP	- Complex absorbing potential

TH-1851_Sayak

Contents

1 Introduction 1

2 Theory of the MCTDH Method 9

2.1 Standard propagation method and MCTDH 9

2.2 MCTDH equations of motion 11

2.3 The constant mean-field integrator 14

2.4 Mode combination and numerical scaling 15

2.5 Product representation of the Hamiltonian 16

2.5.1 Product representation of potential energy surface 17

2.6 Flux analysis 21

3 Atom-Diatom and Diatom-Diatom Scatterring Systems 25

3.1 Hamiltonian 26

3.2 Initial wave packet 33

3.3 Cross sections 35

3.4 Rate constants 35

4 He + H^+He → HeH^+ + He : A Comparative Study of MCTDH And Split-operator Methodology Wave Packet Propagation 37

4.1 Introduction 37

TH-1851_Sayak

4.1.1 Computational studies 39
4.2 Results and discussion 43
4.2.1 Numerical details 43
4.2.2 Reaction probabilities 44
4.2.3 Integral cross sections 52
4.3 Summary and Conclusions 59

5 $H_2 + OH \rightarrow H_2O + H$: Effect of Surface Topology on Reaction Dynamics 61

5.1 Introduction 61
5.1.1 Experimental results 63
5.1.2 Potential energy surface 67
5.1.3 Theoretical results 72
5.2 Results and discussions 81
5.2.1 Numerical details 81
5.2.2 Reagents in ro-vibrational ground states 87
5.2.3 Reagents in ro-vibrational excited states 99
5.3 Summary and conclusions 115

6 $H_2 + CN \rightarrow HCN + H$: Effect of Inclusion of Coriolis Coupling on Reaction Dynamics 119

6.1 Introduction 119
6.1.1 Experimental results 121
6.1.2 Potential energy surface 123
6.1.3 Theoretical results 125
6.2 Results and discussion 129
6.2.1 Numerical details 129

TH-1851_Sayak

6.2.2 Reaction probabilities 134
6.2.3 Integral cross sections 135
6.2.4 Rate constants 141
6.3 Summary and conclusions 146

7 Summary and Conclusions **149**

TH-1851_Sayak

List of Figures

3.1 *Reactant jacobi coordinates for He + HeH^+ reaction.* 26

3.2 *Jacobi coordinates for tetra-atomic reactive scattering system* 28

3.3 *Definitions of the body-fixed frame and the E_2 frames. α, β and γ are the three Euler angles. SF denotes the space-fixed frame. Starting from the SF frame, rotation through α results in the E_1 frame. A second rotation through β results in the E_2 frame. The third rotation through γ results in the body-fixed frame.* 29

3.4 *Coordinates for the tetra-atomic reactive scattering system described in E_2 coordinates.* 31

4.1 *Reaction probabilities obtained by MCTDH(CC), MCTDH(CS) and CS results obtained by split-operator(SO) method[144] for the He + H^+He ($v = 0, j = 0$) $\rightarrow$ HeH^+ + He reaction. The results are plotted for four different J values.* 45

4.2 *Total reaction probabilities obtained by split-operator method for v = 0, 1 and 2 using CS approximation. The probabilities are plotted for four different J values as indicated in the figure.* 47

4.3 *Total reaction probabilities obtained by MCTDH(CC) calculations for v = 0, and 1. The probabilities are plotted for four different J values as indicated in the figure.* 48

4.4 *Total reaction probabilities obtained by a split-operator method for j = 0, 1, 2 and 3 using the CS approximation. The probabilities are plotted for four different J values as indicated in the figure.* 49

TH-1851_Sayak

4.5 *Total reaction probabilities obtained by MCTDH(CC) calculations for j = 0, 1, and 2. The probabilities are plotted for four different J values as indicated in the figure.* 50

4.6 *Comparison of total reaction probabilities between different values of m for two different initial rotational states, at J = 5 and 50. The results have been obtained by MCTDH(CC) calculations.* 51

4.7 *Comparison of integral cross sections obtained by MCTDH(CC), and the CS results obtained by split-operator(SO) method for v = 0, j = 0.* 52

4.8 *Integral reaction cross sections plotted as a function of collision energy for v = 0 and 1 states of HeH^+. The diatom is in its ground rotational state. The MCTDH results have been compared with the CS results obtained by a split-operator method.* 54

4.9 *Integral reaction cross sections plotted as a function of collision energy for j = 0, 1, 2 and 3 of HeH^+ while the diatom is in its ground vibrational state. These CS results are obtained by a wave packet propagation using a split-operator method.* 56

4.10 *Integral reaction cross sections plotted as a function of collision energy for j = 0, 1, and 2. The diatom is in its ground vibrational state. The results are from MCTDH(CC) calculations.* 57

4.11 *Comparison of reaction cross section for different values of m, for rotational states j = 1 and 2. The diatom is in its ground vibrational state. The results are from MCTDH(CC) calculations.* 58

5.1 *Energy distribution of the initial wave packet on the WDSE, WSLFH and YZCL2 surfaces for ground ro-vibrational states of the reactants.* 84

5.2 *Reaction probabilities for J = 0, 3, 5, 7, 10, 13, 17, 20, 24, 30, 36, 40 as a function of collision energy on the WDSE surface are shown in (a) for $H_2(v_1 = 0, j_1 = 0) + OH(v_2 = 0, j_2 = 0)$. Interpolated reaction probabilities upto J= 42 are shown in (b).* 87

5.3 *Reaction probabilities for J = 0, 3, 6, 8, 10, 13, 17, 20, 23, 27, 30, 35 and 42 as a function of collision energy on the YZCL2 surface are shown in (a) for $H_2(v_1 = 0, j_1 = 0) + OH(v_2 = 0, j_2 = 0)$. Interpolated reaction probabilities upto J= 42 are shown in (b).* . . . 88

TH-1851_Sayak

5.4 *Reaction probabilities for J = 0, 5, 10, 17, 20, 24, 30, 36, 40 as a function of collision energy on the WSLFH surface are shown in (a)for $H_2(v_1 = 0, j_1 = 0) + OH(v_2 = 0, j_2 = 0)$. Interpolated reaction probabilities upto J= 40 are shown in (b).* 89

5.5 *Comparison of the reaction probabilities obtained using MCTDH with the results of Goldfield and Gray[203] for J = 0 on the WDSE surface. Results from the Ref. [203] are reproduced with permission.* 89

5.6 *Comparison of reaction probabilities on the WDSE, WSLFH and YZCL2 surfaces for J = 0,10 and 20. The reactants H_2 and OH are in their ground ro-vibrational states.* 90

5.7 *Integral reaction cross sections as a function of collision energy on the WDSE surface (a) and on the YZCL2 surface (b) for $H_2(v_1 = 0, j_1 = 0) + OH(v_2 = 0, j_2 = 0)$. The present MCTDH results[248] are compared with the results of Zhang et al.[202] and Yang et al.[160] Reference results are reproduced with permission.* 92

5.8 *Comparison of integral cross sections on the WDSE, YZCL2 and WSLFH surfaces with the reagents in their ground ro-vibrational states.* 93

5.9 *Comparison of transition state structures of H_2OH on the WDSE, WSLFH and YZCL2 surfaces.* 94

5.10 *Rate constants for the* $H_2(v_1 = 0,j_1 = 0) + OH(v_2 = 0,j_2 = 0)$*reaction. The present MCTDH results are compared with the theoretical results from the following references: Manthe et al.[249], Truhlar et al.[250], Goldfield et al.[203], Troya et al.[205]. Experimental results of Baulch et al.[187], Orkin et al.[185], Tully et al.[175] and Talukdar et al.[183] are also shown.* 95

5.11 *Effect of initial vibrational excitations of the reagents on the integral reaction cross sections. Shown are the cross sections for the reactions $H_2(v_1 = 0,j_1 = 0) + OH(v_2 = 0,j_2 = 0) \rightarrow H_2O+H$, denoted as 00, and $H_2(v_1 = 1,j_1 = 0) + OH(v_2 = 0,j_2 = 0) \rightarrow H_2O+H$, denoted as 10, and $H_2(v_1 = 0,j_1 = 0) + OH(v_2 = 1,j_2 = 0) \rightarrow H_2O+H$, denoted as 01, on (a) WDSE, (b) WSLFH and (c) YZCL2 surfaces. The 6D-CS results of Zhang et al.[231] are also shown for comparison.* 100

TH-1851_Sayak

5.12 *Effect of the reagent vibrational excitations on the rate constants for $H_2(v_1 = 1,j_1 = 0) + OH(v_2 = 0,j_2 = 0) \rightarrow H_2O + H$, denoted as 10, and $H_2(v_1 = 0,j_1 = 0) + OH(v_2 = 1,j_2 = 0) \rightarrow H_2O+H$, denoted as 01, processes on WDSE, WSLFH and YZCL2 surfaces. The results for $H_2(v_1 = 0,j_1 = 0) + OH(v_2 = 0,j_2 = 0) \rightarrow H_2O + H$, denoted as 00[248], are also shown with the experimental results of Zellner et al.[96],Glass et al.[97],Hanf et al.[95]. The 6D-CS results of Zhang et al.[231] are also shown for comparison.* 101

5.13 *Effect of reagent rotations on the integral cross sections for the $H_2(v_1 = 0,j_1 = 2) + OH(v_2 = 0,j_2 = 0) \rightarrow H_2O + H$, denoted as 20, and $H_2(v_1 = 0,j_1 = 0) + OH(v_2 = 0,j_2 = 2) \rightarrow H_2O + H$, denoted as 02, reactions on (a) WDSE, (b) WSLFH and (c) YZCL2 surfaces. The results for $H_2(v_1 = 0,j_1 = 0) + OH(v_2 = 0,j_2 = 0) \rightarrow H_2O + H$, denoted as 00, are also shown.* 106

5.14 *K-dependent cross sections for $H_2(j_1 = 2) + OH(j_2 = 0)$ on (a) WDSE, (b) WSLFH and (c) YZCL2 surfaces. The reagents are in their vibrational ground states.* 108

5.15 *K-dependent cross sections for $H_2(j_1 = 0) + OH(j_2 = 2)$ on (a) WDSE, (b) WSLFH and (c) YZCL2 surfaces. The reagents are in their vibrational ground states.* 108

5.16 *Dependence of the rate constants on initial rotational states of the reagents. Results for $H_2(v_1 = 0,j_1 = 2) + OH(v_2 = 0,j_2 = 0) \rightarrow H_2O+H$, denoted as 20, and $H_2(v_1 = 0,j_1 = 0) + OH(v_2 = 0,j_2 = 2) \rightarrow H_2O+H$, denoted as 02, on (a) WDSE, (b) WSLFH and (c) YZCL2 surfaces are shown. The MCTDH results for ground ro-vibrational states (denoted as 00) are also shown. The mentioned reference is Zhang et al.[202](5D-CC).* 111

5.17 *Integral cross sections for (a)$H_2(v_1 = 1,j_1 = 2) + OH(v_2 = 0,j_2 = 0)$ (denoted as 1200) and (b) $H_2(v_1 = 0,j_1 = 0) + OH(v_2 = 1,j_2 = 2)$ (denoted as 0012) on the WSLFH surface. The cross sections for other ro-vibrational state combinations such as 0000, 0200 and 0002 are shown for comparison.* 113

5.18 *Integral cross sections for (a)$H_2(v_1 = 1,j_1 = 2) + OH(v_2 = 0,j_2 = 0)$ (denoted as 1200) and (b) $H_2(v_1 = 0,j_1 = 0) + OH(v_2 = 1,j_2 = 2)$ (denoted as 0012) on the YZCL2 surface. The cross sections for other ro-vibrational state combinations such as 0000, 0200 and 0002 are shown for comparison.* 113

TH-1851_Sayak

5.19 *Effect of simultaneous ro-vibrational excitation on the rate constants for $H_2(v_1,j_1)$ + $OH(v_2,j_2)$ on the (a)WSLFH and (b)YZCL2 surfaces.* 114

6.1 *Energy distribution of the initial wave packet on the TSH3 surface with a momentum of 6.0 a_0 and width of 0.22 a_0.* 131

6.2 *Reaction probabilities for $H_2(v_1 = 0,j_1 = 0)$ + $CN(v_2 = 0,j_2 = 0)$ for selected J's as a function of translational energy.* 134

6.3 *Interpolated reaction probabilities for $H_2(v_1 = 0,j_1 = 0)$ + $CN(v_2 = 0,j_2 = 0)$ for J = 0-50.* 135

6.4 *Comparison of MCTDH integral cross sections for the $H_2(v_1 = 0)$ + $CN(v_2 = 0)$ reaction as a function of translational energy with results of Zhang et al.[286].* 136

6.5 *Comparison of the CC and CSA integral cross sections with the J-shifting results from Zhu et al.[285] for the $H_2(v_1 = 0,j_1 = 0)$ + $CN(v_2 = 1,j_2 = 0)$ reaction as a function of translational energy with both the diatoms at their respective rotational ground states. The mixed quantum-classical results of Coletti et al.[287] and the present CC cross sections for $H_2(v_1 = 0,j_1 = 0)$ + $CN(v_2 = 0,j_2 = 0)$ are also plotted for reference. The reactants are in their respective rotational ground states.* 137

6.6 *Comparison of CC integral cross sections with the approximate cross sections of Zhu et al.[285] for the $H_2(v_1 = 1,j_1 = 0)$ + $CN(v_2 = 0,j_2 = 0)$ reaction. The mixed quantum-classical results of Coletti et al.[287] and the CC cross sections for $H_2(v_1 = 0,j_1 = 0)$ + $CN(v_2 = 0,j_2 = 0)$ are also shown for reference.* 138

6.7 *Comparison of the present initial state selected rate constants for $H_2(v_1 = 0,j_1 = 0)$ + $CN(v_2 = 0,j_2 = 0)$ with CS results of Zhang et al.[286] and experimental results of Smith et al.[262] and Sun et al.[264].* 142

6.8 *Comparison of the present initial state selected rate constants for the reaction $H_2(v_1, j_1 = 0)$ + $CN(v_2, j_2 = 0)$ with the theoretical results of Zhang et al.[286], Zhu et al.[285] and experimental results of Sims et al.[262] and Li et al.[258].* 143

TH-1851_Sayak

List of Tables

4.1 *Numerical parameters of the MCTDH calculations for the He + HeH^+ system(in atomic units if not otherwise stated).* 43

4.2 *Parameters for the primitive basis sets employed for each degree of freedom. KLeg is a two-dimensional extended Legendre DVR [150].* . . 44

5.1 *Numerical parameters of the MCTDH calculations for the $H_2(v_1 = 0,j_1 = 0) + OH(v_2 = 0,j_2 = 0)$ system(in atomic units if not otherwise stated) The parameters for calculations involving vibrationally excited reagents($v_{1(2)}$=1) are given in brackets if those differ from the earlier parameters.* 81

5.2 *Parameters for the primitive basis sets employed for each degree of freedom. The brackets indicate the mode combinations. HO is a harmonic oscillator DVR; KLeg is a two-dimensional extended Legendre DVR [150].* 85

5.3 *Numerical parameters for the potential fit for the H_3O system on the WDSE, WSLFH and YZCL2 PESs.* 86

5.4 *Comparison of MCTDH initial state selected rate constants on the WDSE, WSLFH and YZCL2 surfaces for $H_2(v_1 = 0,j_1 = 0) + OH(v_2 = 0,j_2 = 0) \rightarrow H_2O+H$ with theoretical results of [a] Manthe et al.[249], [b] Zhang et al.[231], [c] Zhang et.al.[202] [d] Truhlar et al.[250], [e] Goldfield et al.[203], [f] Troya et al.[205] and experimental results of [g] Talukdar et al.[183], [h] Tully et al.[175] and [i] Baulch et.al.[187], and [j] Orkin et al.[185].* 98

5.5 *Comparison of MCTDH initial state selected rate constants on the WDSE, WSLFH and YZCL2 surfaces for $H_2(v_1 = 1,j_1 = 0) + OH(v_2 = 0,j_2 = 0) \rightarrow H_2O + H$ with the theoretical results of [a] Zhang et al.[231](6D-CS) and the experimental results of [b] Hanf et al.[95].* 102

TH-1851_Sayak

5.6 *Comparison of MCTDH initial state selected rate constants on the WDSE, WSLFH and YZCL2 surfaces for* $H_2(v_1 = 0,j_1 = 0) + OH(v_2 = 1,j_2 = 0) \rightarrow H_2O + H$ *with results of* [a] *Zhang et al.[231](6D-CS).* 103

5.7 *Comparison of MCTDH rate constants on the WDSE and WSLFH surfaces for* $H_2(v_1 = 0,j_1 = 2) + OH(v_2 = 0,j_2 = 0) \rightarrow H_2O+H$ *with results of* [a] *Zhang et al.[202](5D-CC).* 109

5.8 *Rate constants for* $H_2(v_1 = 0,j_1 = 0) + OH(v_2 = 0,j_2 = 2) \rightarrow H_2O+H$ *on the WDSE and WSLFH surfaces. The MCTDH results are shown in comparison to the 5D-CC results of* [a] *Zhang et al.[202].* 109

6.1 *Numerical parameters of the MCTDH calculations for the* $H_2(v_1 = 0,j_1 = 0) + OH(v_2 = 0,j_2 = 0)$ *system(in atomic units if not otherwise stated). The parameters for calculations involving vibrationally excited reagents* $H_2(v_1 = 1)$ *and* $CN(v_2 = 1)$ *are given in brackets if those differ from ground state parameters.* 129

6.2 *Parameters for the primitive basis sets employed for each degree of freedom. The brackets indicate the mode combinations, and the last column gives the number of single-particle functions used for the modes. HO is a harmonic oscillator DVR; KLeg is a two-dimensional extended Legendre DVR [150].* 132

6.3 *Numerical parameters for the potential fit for the TSH3 PES.* 132

6.4 *Comparison of the present initial state selected rate constants for* $H_2(v_1 = 0,j_1 = 0) + CN(v_2 = 0,j_2 = 0)$ *with theoretical results of* [a] *Zhang et al.[286]. Experimental results of* [b] *Sims et al.[262] and* [c] *Sun et al.[264] are also shown for comparison.* 141

6.5 Comparison of initial state selected rate constants for the reaction $H_2(v_1, j_1 = 0) + CN(v_2, j_2 = 0)$ obtained using MC TDH with the theoretical results of [a]Zhu et al.[285] and experimental results of [b]Sims et al. [262] and [c]Copeland et al.[274]. 145

TH-1851_Sayak

Chapter 1

Introduction

Accurate prediction of the outcome of a chemical reaction has been the ultimate goal of theoretical chemists since the inception of quantum mechanics in 1920s. Experimental studies using high precision instruments can provide accurate information for various reaction attributes in the measurable range. The focus of theoretical studies is to predict and explain the experimental results along with providing answers to how and why a chemical reaction occurs at a molecular level. A chemical reaction generally results from collisions between molecules, also referred to as scattering. The process in which collision results in breaking of bonds and formation of new molecules is known as a reactive scattering process. A rigorous description of reactions is possible through accurate quantum scattering calculations. In this thesis, the reaction dynamics of a tri- and two tetra-atomic reactive scattering systems in ro-vibrational ground and excited states have been duly investigated.

For accurate studies of a quantum dynamical system, the primary step is to de-

TH-1851_Sayak

termine a potential energy surface(PES) for the reaction system. This is usually achieved by applying the Born-Oppenheimer[1, 2] approximation which allows the separation of nuclear and electronic motions. A potential energy surface is first computed through solving the time-independent Schrödinger equation(TISE) for the electrons, with the atoms held in fixed positions. But it is impossible to obtain an exact solution of the Schrödinger equation for systems with more than one electron. In view of this, the field of electronic structure theory has progressed with the objective of development of various numerical and approximate methodologies to solve the TISE[3]. Once a potential energy surface is obtained, the dynamical studies are performed by solving either the TISE or the time-dependent Schrödinger equation(TDSE).

Initial theoretical investigations of reactive scattering systems started with the simplest atom-diatom system possible, i.e. the H + H_2 system on which the first classical trajectory studies were reported by Hirschfelder et al.[4] in the late 1930s. The earliest study to include quantum effects was by Hulburt and Hirschfelder in the early 1940s[5] to compute the transmission coefficients on a number of empirical potential energy surfaces. Even with the advent of computers in the 1960s, the computation of accurate potential energy surfaces and reaction dynamics simulations remained a cumbersome task. The path-breaking molecular beam studies performed by Lee et al.[6] on the F + D_2 system provided a boost to the theoretical studies of atom-diatom systems. An outline of the quantum mechanical reactive scattering theory for planar atom+diatom systems was presented by Kuppermann et al.[7–9] in the early 1970s, while a review by Connors[10] gives an extensive overview of the initial advancements in the field of reactive scattering. Studies of higher dimensional systems was initiated in the 1980s and the early

TH-1851_Sayak

1990s, when various reduced dimensionality methodologies were developed to successfully tackle bigger systems at affordable computational costs. The evolution of the time-dependent methodologies over the years and its applications to various systems have been reviewed in various studies.[11–18]

Quantum dynamical studies of a reactive scattering system can be carried out by solving either the time-independent(TI) or time-dependent (TD) Schrödinger equation. A time-dependent Hamiltonian merits the use of the time-dependent version of the Schrödinger equation. For time-independent Hamiltonians, however, time-dependent and time-independent approaches are equivalent, but their effectiveness depends on the system under study. Both the methodologies have their inherent advantages and disadvantages. The TI methods require diagonalization of large matrices to solve the eigenvalue value problem and the computation has to be repeated over different energies. This makes it a computationally expensive methodology for large systems. In contrast, the TD wave packet propagation yields a single column of the S-matrix over a continuous range of energies. In the TD methods, an initial wave packet can be prepared, evolved in time and the quantities of interest extracted after the propagation is complete. In addition, the entire reaction dynamics can be pictorially observed and analyzed at various stages of propagation of the wave packet. This presents an excellent opportunity to unravel the complicated dynamics involved in the scattering process. The effectiveness of the TD approach is however limited in reaction systems which feature long-lived resonances. The propagation of the wave packets have to be carried out for long times to enable decay of the resonance states to the products. An exhaustive review by Hu and Schatz[16] covers the development of both TI and TD methodologies, along with their application to atom-diatom, ion-molecule and

TH-1851_Sayak

diatom-diatom systems.

The first time-dependent wave packet treatment (TDWP) of reactive scattering was reported by Mazur and Rubin in 1959[19], while it was McCullough and Wyatt who reported the first full quantum dynamics simulation in 1969[20, 21]. In the mid 1980s there were two important developments in the field of reactive scattering. The introduction of grid-based Fourier transform method by Feit et al.[22, 23], Kosloff and Kosloff[24] and the discrete variable representation (DVR) by Light and co-workers [25, 26] enabled the rapid computation of the action of the Hamiltonian operator on the wave packet. The time-evolution of the wave packet became highly efficient with the introduction of the split-operator methods[22, 23] and the Chebyshev expansion[27–29]. A common drawback of the TDWP calculations is the artificial reflection of wave packets from the numerical grid end. The reflected wave packets interact with the wave packets still under propagation, and distort those leading to erroneous results. Using a large enough grid minimizes the reflection but subsequently makes the computation numerically expensive. This problem is overcome by employing an absorbing potential to absorb the wave functions as they reach the grid end[30–35]. The evolution of the TDWP methodology, different modifications and its applications have been the focal point of various reviews in the last two decades[36–42].

One of the major aims of developing new methodologies in the TI and TD domains was to improve the numerical scaling factor. This would help in extending the quantum reactive scattering studies to systems with more than three atoms. The standard TI methods scale as N^3[37] with N being the number of basis functions. This results in prohibitively high computational costs for systems with more than 3 degrees of freedom as the number of basis sets required grows geometrically

TH-1851_Sayak

with the spatial dimensionality of the system. The introduction of finite difference scheme[20, 21] reduced the scaling to N^2 which was improved to N with the introduction of the second order differencing scheme[43]. With the advent of Fourier method[22, 23] the scaling was further improved to $N\log N$. In spite of the marked improvements in the scaling factors, rigorous dynamical treatment for systems with four or more atoms using the TDWP methodology still remained a cumbersome affair. This made it essential to search for approximate methods to obtain results with acceptable accuracy with minimized usage of resources.

The time-dependent Hartree (TDH) approach[27, 44–46], is one such approximate method. A multidimensional time-dependent wave function is approximated by a product of one-dimensional functions. This reduces the f-dimensional Schrödinger equation to f variationally optimized, coupled one-dimensional differential equations. Each time-dependent wave function is time evolved under the influence of a mean-field potential determined by the instantaneous dynamics of other modes. This method results in significant savings in computational efforts thus making quantum mechanical treatment of larger systems feasible. However the main drawback of this method is the ignorance of spatial correlations between different degrees of freedom, which is essential for any dynamical calculation. The TDH method was subsequently improved upon by the introduction of the time-dependent rotated Hartree[47] method and the multiconfigurational self consistent field method(MC-TDSCF)[27, 48–50]. A more efficient formalism, the multiconfiguration time-dependent Hartree method (MCTDH), applicable for both an arbitrary number of configurations and degrees of freedom, was proposed by Meyer and co-workers[51–56]. The wave packet is expressed in terms of products of configuration coefficients and one-dimensional (1D) wave functions

TH-1851_Sayak

which are optimized using the Dirac-Frenkel variational method leading to a set of coupled 1D TDSEs. A minimal number of optimal configurations which result automatically from the equations of motions is used to describe the total state. In the MCTDH algorithm, both the expansion coefficients and the basis functions, called single-particle functions (SPFs), are time dependent. This enables the use of an optimal number of basis functions to describe the wave function, resulting in an improvement in scaling factors. Inclusion of the maximum number of SPFs leads to a numerically exact calculation while use of a single SPF results in the time-dependent Hartree method. The memory requirements of an MCTDH application can be further reduced by utilizing the idea of mode combination where more than one degrees of freedom can be combined to represent a single mode. The multi-dimensional SPFs thus describe a set of degrees of freedom rather than just one, leading to a significant reduction in the size of the coefficient vector. Over the last two decades, the efficiency and accuracy of the MCTDH methodology in studying wave packet propagation studies have been established in various fields. The MCTDH method has been successfully applied to a wide range of problems including scattering[57–65], photo-dissociation[52, 66–68], proton transfer reactions[69–71], infrared spectroscopy[72, 73], vibronically coupled systems[74–76] and intra-molecular vibrational energy redistribution[77–79]. While the MCTDH algorithm has been used to study systems with upto 80 degrees of freedom, various new forms of the algorithm like the S-MCTDH[80] and the multi-layer MCTDH (ML-MCTDH)[81–83] have been developed to treat even larger systems. The MCTDHB[84] and MCTDHF[85] codes have been developed to enable studying bosonic and fermionic systems.

In this thesis, the MCTDH algorithm has been employed to study the reaction

TH-1851_Sayak

dynamics of a tri-atomic and two tetra-atomic systems. While there have been different studies on the protonated Xe_2H^+ (X = rare gas) clusters[86–90], not much has been reported on the reaction dynamics of the He + $H^+He \rightarrow HeH^+$ + He system. Given the importance of Helium in atmospheric chemistry and the absence of any experimental data on this ion-molecule combination, accurate theoretical predictions of the reaction dynamics and the reactivity of the rare gas atoms is of high practical interest. The system has been studied by both standard methodology using the split-operator method and the MCTDH algorithm. While the standard methodology has been applied under the centrifugal sudden (CS) approximation, an accurate Hamiltonian has been used for the MCTDH studies. This would test the accuracy of the MCTDH algorithm to study an ion-molecule reactive scattering system along with determining the importance of inclusion of Coriolis coupling in calculations for this system.

The study has been subsequently extended to the H_2 + OH and the H_2 + CN systems. The study on the H_2 + OH system has been performed over three different potential energy surfaces, i.e. WDSE[91, 92], WSLFH[93] and YZCL2[94], to understand the significance of the topology of the surfaces on the reaction dynamics. In the absence of any quantum dynamical studies on the WSLFH surface, the accuracy of the surface has not been properly determined till date. Recently reported experimental data using latest methodologies[95] on vibrational excitation of H_2 show a big variance with erstwhile experimental results[96, 97], which served as a standard for previous theoretical investigations. This motivates accurate theoretical studies on all three surfaces, for ro-vibrational excitation of the reagents. Comparison with experimental results will determine the accuracy of the surface in question. Since the only reported theoretical results on vibrational

TH-1851_Sayak

excitation of reagents are on the WDSE surface using the CS approximation, the present studies would show the accuracy of the later surfaces and also underline the importance of the inclusion of the Coriolis coupling in the calculations for all the surfaces. For the H_2 + CN system, the exact role played by the CN bond in the reaction dynamics has been debated over the last two decades. An accurate quantum dynamical study of the effect of vibrational excitation of the reagents and subsequent comparison with experimental values, would strongly establish the exact nature of the bond. Similar to the H_2 + OH system, finding out the extent to which the inclusion of Coriolis coupling affects the reaction dynamics is again of primary importance in this study. Moreover, the accuracy of the TSH3 potential energy surface[98], including the barrier height would be rigorously tested in the study of vibrationally excited states.

TH-1851_Sayak

Chapter 2

Theory of the MCTDH Method

2.1 Standard propagation method and MCTDH

Quantum dynamical studies are performed in the time-dependent frame by solving the time-dependent Schrödinger equation(TDSE),

$$i\hbar\frac{\partial\Psi(x.t)}{\partial t} = \hat{H}\Psi(x,t). \tag{2.1}$$

The TDSE is generally solved by expanding the system wave function in a time-independent product basis set as

$$\Psi(q_1,...,q_f,t) = \sum_{j_1=1}^{N_1}....\sum_{j_f=1}^{N_f} C_{j_1...j_f}(t)\prod_{\kappa=1}^{f}\chi_{j_\kappa}^{(\kappa)}(q_\kappa). \tag{2.2}$$

Here $\chi_{j_\kappa}^{(\kappa)}$ represents the one-dimensional time-independent basis set for each degree of freedom κ. Usually, the basis functions are represented in a discrete variable

TH-1851_Sayak

representation(DVR)[25, 26]. f specifies the number of degrees of freedom. q_1 , . . . , q_f are nuclear coordinates, $C_{j_1 \ldots j_f}$ denote the time-dependent expansion coefficients, and N_κ is the number of basis functions used. A set of coupled linear first-order differential equations results by using Dirac-Frenkel variational principle[99, 100], $\langle \delta\Psi | H - i\frac{\delta}{\delta t} | \Psi \rangle = 0$. The principal drawback of this exact time-dependent methodology is the strong exponential scaling where the computational time increases as fN^{f+1} and the memory requirements as N^f. This limits the method to smaller systems.

In the MCTDH scheme[51–56], the scaling factor is improved by the introduction of a smaller but time-dependent basis of so-called single-particle functions(SPFs). The MCTDH wave function is written as

$$\begin{aligned} \Psi(q_1, ..., q_f, t) &= \sum_{j_1=1}^{n_1} .... \sum_{j_f=1}^{n_f} A_{j_1 \ldots j_f}(t) \prod_{\kappa=1}^{f} \varphi_{j_\kappa}^{(\kappa)}(q_\kappa, t) \\ &= \sum_{J} A_J \Phi_J, \end{aligned} \tag{2.3}$$

where n_κ is considerably smaller than N_κ. The Hartree product Φ_J is an f-dimensional product of SPFs. $J = (j_1 \ldots j_f)$ is a composite index while the A-vector represented by $A_J \equiv A_{j_1 \ldots j_f}$ denote the MCTDH expansion coefficients. The SPFs, $\varphi_{j_\kappa}^{(\kappa)}$, are represented as a linear combinations of the primitive basis

$$\varphi_{j_\kappa}^{(\kappa)}(q_\kappa, t) = \sum_{i_\kappa=1}^{N_\kappa} c_{i_\kappa j_\kappa}^{(\kappa)}(t) \chi_{i_\kappa}^{(\kappa)}(q_\kappa). \tag{2.4}$$

The MCTDH methodology contains the time-dependent Hartree(TDH)[27, 44–46] and the exact methods as limiting cases. In the TDH approach, a multidimensional time-dependent wave function is written as a product of one-dimensional functions

TH-1851_Sayak

and this is achieved by having n_κ=1 in Equation 2.3. Increase in n_κ leads to more correlation and by having n_κ=N_κ, the MCTDH wave function converges to the exact one.

2.2 MCTDH equations of motion

As both the coefficients and the SPFs in Equation 2.3 are time-dependent, the wave function representation is not unique. Imposition of additional constraints on the SPFs[52–56] are required to obtain uniquely defined equations of motion. The constraints are

$$\langle \varphi_j^{(\kappa)}(0) | \varphi_l^{(\kappa)}(0) \rangle = \delta_{jl}, \tag{2.5}$$

and

$$\langle \varphi_j^{(\kappa)}(t) | \dot{\varphi}_l^{(\kappa)}(t) \rangle = -i \langle \varphi_j^{(\kappa)}(t) | g^\kappa | \varphi_l^{(\kappa)}(t) \rangle. \tag{2.6}$$

where g^κ denotes a hermitian operator acting on κ-th DOF. The choice of constraints ensures the orthonormality of the SPFs at all times. The choice of the constraint operator g^κ determines the equations of motion, as will be discussed below.

To write down the equation of motion for the SPFs and the coefficients, the *single-hole functions* Ψ_l^κ are introduced

$$\Psi_l^\kappa = \langle \varphi_l^\kappa | \Psi \rangle = \sum_J^\kappa A_{J_l^\kappa} \prod_{v \neq \kappa} \varphi_{j_v}^{(v)}, \tag{2.7}$$

TH-1851_Sayak

where J_l^κ denotes a composite index J with the κth entry set at l, and $\sum_J^\kappa$ denotes the sum over the indices for all degrees of freedom excluding the κth. Next, the *mean field* is defined as

$$\langle H \rangle_{jl}^{\kappa} = \langle \Psi_j^{(\kappa)} | H | \Psi_l^{(\kappa)} \rangle, \tag{2.8}$$

and *density matrices* as

$$\rho_{jl}^{(\kappa)} = \langle \Psi_j^{(\kappa)} | \Psi_l^{(\kappa)} \rangle = \sum_{J^\kappa} A_{J_j^\kappa}^* A_{J_l^\kappa}. \tag{2.9}$$

The mean-field matrix elements in Equation 2.8 are obtained by applying the operators on the κth DOF. Finally, the MCTDH *projector* is defined as

$$P^\kappa = \sum_{j=1}^{n_\kappa} |\varphi_j^{(\kappa)}\rangle\langle\varphi_j^{(\kappa)}|. \tag{2.10}$$

The Hamiltonian can be split into separable and correlated terms

$$H = \sum_{\kappa=1}^{f} h^{(\kappa)} + H_R, \tag{2.11}$$

where $h^{(\kappa)}$ acts only on the κth DOF and residual part, H_R, includes all the correlations between the DOFs.

The MCTDH equations of motion are derived by applying the Dirac-Frenkel variational principle[99, 100] to the ansatz in Equation 2.3. The resultant equa-

TH-1851_Sayak

tions are[54]

$$i\dot{A}_J = \sum_L \langle \Phi_J | H_R | \Phi_L \rangle A_L + \sum_{\kappa=1}^{f} \sum_{l=1}^{n_\kappa} (h^{(\kappa)}_{j_\kappa l} - g^{(\kappa)}_{j_\kappa l}) A_{J^\kappa_l} \tag{2.12}$$

and

$$\begin{aligned} i\dot{\boldsymbol{\varphi}}^{(\kappa)} &= g^{(\kappa)} \mathbf{1}_{n_\kappa} \boldsymbol{\varphi}^{(\kappa)} + (1 - P^{(\kappa)}) \\ &\times [(\boldsymbol{\rho}^{(\kappa)})^{(-1)} \langle \boldsymbol{H_R}^{(\kappa)} \rangle + (h^{(\kappa)} - g^{(\kappa)}) \mathbf{1}_{n_\kappa}] \boldsymbol{\varphi}^{(\kappa)}. \end{aligned} \tag{2.13}$$

Here a vector notation is used for the SPFs with

$$\boldsymbol{\varphi}^{(\kappa)} = (\varphi^{(\kappa)}_1, ... \varphi^{(\kappa)}_{n_\kappa})^T. \tag{2.14}$$

$\boldsymbol{\rho}^{(\kappa)}$ represents the density matrix while $\langle \mathbf{H}^{(\kappa)} \rangle$ represents the matrix of mean field operators, $\mathbf{1}_{n_\kappa}$ denotes the $n^{(\kappa)} \times n^{(\kappa)}$ unit matrix. $h^{(\kappa)}_{jl}$ and $g^{(\kappa)}_{jl}$ are the matrix elements of $h^{(\kappa)}$ and $g^{(\kappa)}$ with respect to the SPFs.

The simplest choice for the constraint operator is to set $g^{(\kappa)}$=0 which yields

$$i\dot{A}_J = \sum_L \langle \Phi_J | H_R | \Phi_L \rangle A_L + \sum_{\kappa=1}^{f} \sum_{l=1}^{n_\kappa} h^{(\kappa)}_{j_\kappa l} A_{J^\kappa_l} \tag{2.15}$$

and

$$i\dot{\boldsymbol{\varphi}}^{(\kappa)} = (1 - P^{(\kappa)})[h^{(\kappa)} \mathbf{1}_{n_\kappa} + (\boldsymbol{\rho}^{(\kappa)})^{(-1)} \langle \boldsymbol{H_R}^{(\kappa)} \rangle] \boldsymbol{\varphi}^{(\kappa)}. \tag{2.16}$$

Setting $H_R = H$ (neglecting the partitioning of the Hamiltonian). the equations of motion are written as

$$i\dot{A}_J = \sum_L \langle \Phi_J | H | \Phi_L \rangle A_L, \tag{2.17}$$

$$i\dot{\boldsymbol{\varphi}}^{(\kappa)} = (1 - P^{(\kappa)})(\boldsymbol{\rho}^{(\kappa)})^{(-1)} \langle \mathbf{H}^{(\kappa)} \rangle \boldsymbol{\varphi}^{(\kappa)}. \tag{2.18}$$

TH-1851_Sayak

Choosing $g^{(\kappa)}=h^{(\kappa)}$, it yields a different set of equations of motion

$$i\dot{A}_J = \sum_L \langle\Phi_J|H_R|\Phi_L\rangle A_L, \tag{2.19}$$

$$i\dot{\boldsymbol{\varphi}}^{(\kappa)} = [h^{(\kappa)}\mathbf{1}_{n_\kappa} + (1-P^{(\kappa)})(\boldsymbol{\rho}^{(\kappa)})^{(-1)}\langle\mathbf{H}^{(\kappa)}\rangle](\boldsymbol{\varphi}^{(\kappa)}). \tag{2.20}$$

Although the choice of constraints will affect the propagation of the two parts of the equation of motion, the propagation of the total wave packet is however not affected. This is because the different sets of SPFs arising out of the different choice of constraints are connected by unitary transformations. Thus the accuracy of the overall calculation is independent of the choice of constraints.

The MCTDH equations conserve the norm and, for time-independent Hamiltonians, the total energy. This follows directly from the variational principle[53]. The equations of motions are a set of non-linear coupled differential equations. While A depends on φ through the matrix elements of $\hat{H}$ and $\dot{\varphi}$ depends on A through the mean fields.

2.3 The constant mean-field integrator

For a fast and efficient application of the MCTDH algorithm a special dedicated integration scheme, the constant mean field (CMF) integration scheme[53, 55, 101] is applied to solve the equations. The matrix elements $\langle\Phi_J|\hat{H}|\Phi_L\rangle$ and the product of the inverse density with the mean field matrices, $(\boldsymbol{\rho}^{(\kappa)})^{-1}\hat{\boldsymbol{H}}_r^{(\kappa)}$ generally change much slower in time than the MCTDH coefficients and the SPFs. This enables holding the Hamiltonian matrix elements, the density matrices and the mean-

TH-1851_Sayak

field matrices constant for some time τ during the integration of the equations of motion, hence the name CMF integrator. The details about the CMF scheme can be found elsewhere[53, 55].

2.4 Mode combination and numerical scaling

In spite of a drastic improvement in the scaling factor the method remains cumbersome for dealing with systems having higher degrees of freedom. MCTDH allows for a further reduction in the scaling by introducing an algorithm called *mode combination*[53, 55, 56]. By combining d degrees of freedom to form a set of $p = f/d$ particles the wave function can now be written in terms of multi-dimensional SPFs as

$$\begin{aligned} \Psi(q_1, ..., q_f, t) &\equiv \Psi(Q_1, ..., Q_p, t) \\ &= \sum_{j_1=1}^{n_1} .... \sum_{j_p=1}^{n_p} A_{j_1 ... j_p}(t) \prod_{\kappa=1}^{p} \varphi_{j_\kappa}^{(\kappa)}(Q_\kappa, t). \end{aligned} \tag{2.21}$$

where Q_κ are the combined coordinates defined as $Q_\kappa = (q_{1,\kappa}, ...q_{d_\kappa,\kappa})$.

The equations of motion remain unchanged except for replacing the number of DOF, f , with the number of particles, p. The operators h^κ now operate on the particles (combined modes) rather than on DOF.

Assuming that all DOF have same grid length N and numbers of SPFs n, a wave function in the standard method format takes N^f data points, and an MCTDH wave function takes fnN (for the SPFs) + n^f (for the A-vectors) data points. With mode combination the later equation turns into $p\tilde{n}N^d + \tilde{n}^p$, where $\tilde{n}$ represents

TH-1851_Sayak

the number of multi-mode functions needed to represent the particles.

It is clear that the degrees of freedom with a strong coupling between them should be combined to produce a particle. In this way, the correlation is treated on the SPF level and does not appear in the configuration interaction part leading to fewer SPFs and hence to a shorter A-vector.

2.5 Product representation of the Hamiltonian

To solve the differential equations, multidimensional integrals, $\langle\Phi_J|\hat{H}|\Phi_L\rangle$ and $\langle H\rangle^{\kappa}_{jl} = \langle\Psi^{(\kappa)}_j|\hat{H}|\Psi^{(\kappa)}_l\rangle$, have to be evaluated at each step. Evaluation of these multidimensional integrals can be avoided if the residual Hamiltonian $\hat{H}_R$ is written as a linear combination of products of single particle operators

$$\hat{H}_R = \sum_{r=1}^{s} c_r \prod_{\kappa=1}^{p} \hat{h}^{(\kappa)}_r. \tag{2.22}$$

Here $h^{(\kappa)}_r$ operates only on the κth degree of freedom and the expansion coefficients are written as c_r and s denotes the number of expansion terms. Using this equation the matrix elements can be written[53, 55, 56] as

$$\langle\Phi_J|\hat{H}|\Phi_L\rangle = \sum_{\kappa=1}^{f}\langle\varphi^{(\kappa)}_{j\kappa}|\hat{h}^{(\kappa)}|\varphi^{(\kappa)}_{l\kappa}\rangle + \sum_{r=1}^{s} c_r \prod_{\kappa=1}^{p}\langle\varphi^{(\kappa)}_{j\kappa}|\hat{h}^{(\kappa)}_r|\varphi^{(\kappa)}_{l\kappa}\rangle. \tag{2.23}$$

where $\hat{h}^{(\kappa)}$ and $\hat{h}^{(\kappa)}_r$ represent the single particle operators which make up the separable and the residual part of the Hamiltonian, respectively. The mean-field

TH-1851_Sayak

operator can now be written as

$$\langle \hat{H}_R \rangle^{\kappa}_{jl} = \sum_{r=1}^{s} \boldsymbol{H}^{(\kappa)}_{rjl} h^{(\kappa)}_{r}. \tag{2.24}$$

where the elements of the mean-field matrix are written as

$$\boldsymbol{H}^{(\kappa)}_{rjl} = c_r \sum_{J}^{(\kappa)} A^{*}_{J^{\kappa}_{j}} \sum_{l_1} \langle \varphi^{(1)}_{j_1} | \hat{h}^{(1)}_{r} | \varphi^{(1)}_{l_1} \rangle \ldots \sum_{l_p} \langle \varphi^{(p)}_{j_p} | \hat{h}^{(p)}_{r} | \varphi^{(p)}_{l_p} \rangle A_{L^{(\kappa)}_{l}}. \tag{2.25}$$

The kinetic energy operators are normally in the desired product form. The potential energy operator, however, is often not of product form. In the following section a method called POTFIT[53, 102, 103] is described which allows to transform a general PES to a product form.

2.5.1 Product representation of potential energy surface

The available potential surfaces on which the wave packet propagation studies are to be carried out may be present in the form of a grid of *ab initio* points or an analytical fit of the *ab initio* points. By representing the multidimensional surfaces as a linear combination of products of one dimensional functions, the computational effort required for the evaluation of complex integrals can be substantially reduced as discussed in the previous section. The POTFIT scheme[53, 55, 56, 102, 103] has been incorporated in the MCTDH algorithm for an efficient transformation of a multidimensional surface to a linear product form.

The potential energy surface can be transformed to the product form by ex-

TH-1851_Sayak

panding it in a product basis. The given potential is approximated as

$$V^{app}(q_1,...,q_p) = \sum_{j_1=1}^{m_1} ... \sum_{j_p=1}^{m_p} C_{j_1...j_p} v_{j_1}^{(1)}(q_1)...v_{j_p}^{(p)}(q_p), \quad (2.26)$$

where p denotes the number of particles(combined modes) and q_κ denotes the coordinate of the κth degree of freedom. The basis functions $v_{j_\kappa}^{(\kappa)}$ are called single-particle potentials (SPP). An optimization of both the expansion coefficients and the expansion orders ensures an efficient and accurate expansion of the PES.

The full potential is written as

$$V_{i_1....i_p} = V(q_{i_1}^{(1)},...,q_{i_p}^{(p)}), \quad (2.27)$$

where $q_i^{(\kappa)}$ denotes the coordinate for the ith grid point of the κth grid. The approximate potential is written as

$$V_{i_1....i_p}^{app} = \sum_{j_1=1}^{m_1} ... \sum_{j_p=p}^{m_p} C_{j_1...j_f} v_{i_1 j_1}^{(1)} ... v_{i_p j_p}^{(p)}, \quad (2.28)$$

with $v_{ij}^\kappa = v_j^\kappa(q_i^\kappa)$. The SPPs are assumed to be orthonormal on the grid, $\sum_i v_{ij}^\kappa v_{il}^\kappa = \delta_{jl}$. The indices i and k are used to label grid points while j and l are used to label the SPPs.

The optimal coefficients and the SPPs are determined by calculating Δ^2 as

$$\begin{aligned} \Delta^2 &= \sum_{i_1=1}^{N_1} ... \sum_{i_p=1}^{N_p} (V_{i_1..i_p} - V_{i_1..i_p}^{app})^2 \\ &= \sum_I (V_I - V_I^{app})^2 \end{aligned} \quad (2.29)$$

TH-1851_Sayak

and then minimizing it. Here I denotes a composite index which runs over all grid points. Minimizing Δ^2 by varying only the coefficients yields

$$C_{j_1 \ldots j_p} = \sum_{i_1=1}^{N_1} \cdots \sum_{i_p=1}^{N_p} V_{i_1 \ldots i_p} v^{(1)}_{i_1 j_1} \ldots v^{(p)}_{i_p j_p}, \tag{2.30}$$

i.e. the coefficients are given by overlap of the SPPs with the potential. Within POTFIT, the SPPs are defined as eigenvector-vectors of the potential density matrices

$$\begin{aligned} \varrho^{\kappa}_{kk'} &= \sum_{I^\kappa} V_{i_1 \ldots i_{\kappa-1} k i_{\kappa+1} \ldots i_p} V_{i_1 \ldots i_{\kappa-1} k' i_{\kappa+1} \ldots i_p} \\ &= \sum_{I^\kappa} V_{I^\kappa_k} V_{I^\kappa_{k'}}, \end{aligned} \tag{2.31}$$

where similar to above I^κ denotes a composite index which contains all grid indices except the κth one, and in I^κ_k the κth entry is replaced by k. The eigenvectors are ordered according to their eigenvalues with the largest eigenvalue coming first. For the two dimensional cases, this approach is known to provide an optimal approximation. For the general f-dimensional case ($f > 2$), POTFIT is not optimal but provides SPPs which are close enough to optimal ones to be useful.

A. Contraction over one degree of freedom

The numerical effort required to evaluate the product form of the potential, as given in Equation 2.28, depends upon the number of expansion terms, $s = \Pi_{\kappa=1}^{f} m_\kappa$ present in the equation. The number of expansion terms can be reduced by one expansion order m_ν , where ν denotes the DOF over which a contraction

TH-1851_Sayak

is performed. The *contracted expansion coefficients* are defined as

$$D^{\nu}_{j_1 \ldots j_{\nu-1} i_\nu j_{\nu+1} \ldots j_p} = \sum_{j_\nu=1}^{m_\nu} C_{j_1 \ldots j_p} v^{\nu}_{i_\nu j_\nu}. \tag{2.32}$$

Since the expansion order m_ν will not be considered for the evaluation of V^{app} , the upper summation limit m_ν can be set equal to N_ν which will allow the full set of SPPs for this particular DOF. The accuracy of the potential approximation can thus be increased without an increase in the number of expansion coefficients. The approximate potential is now defined as

$$\begin{aligned} V^{app}_{i_1 \ldots i_p} = & \sum_{j_1=1}^{m_1} \cdots \sum_{j_{\nu-1}=1}^{m_{\nu-1}} \sum_{j_{\nu+1}=1}^{m_{\nu+1}} \cdots \sum_{j_f=1}^{m_p} D^{\nu}_{j_1 \ldots j_{\nu-1} i_\nu j_{\nu+1} \ldots j_p} \\ & \times v^{(1)}_{i_1 j_1} \ldots v^{(\nu-1)}_{i_{\nu-1} j_{\nu-1}} v^{(\nu+1)}_{i_{\nu+1} j_{\nu+1}} v^{(p)}_{i_p j_p}. \end{aligned} \tag{2.33}$$

A substantial reduction in the numerical effort for fitting the potential is achieved by contraction over the νth DOF without affecting the accuracy of the evaluation. To maximize the gain, the contraction should be carried for that DOF which requires the largest expansion order.

B. Including weight functions

For a wave packet propagation study on a potential energy surface, not all regions of the surface are equally relevant for the study. The potential energy surface is thus modified by inclusion of non-separable weights. An f-dimensional function ω is incorporated in the potential assigning the weight 1 to the physically relevant regions and a weight of 0 to irrelevant points. The relevant region is usually defined by an energy criterion as the region where the potential is lower

TH-1851_Sayak

than some suitably chosen energy threshold. Restrictions on coordinates can also be set to define a relevant region.

The exact potential V is expanded in the product basis of natural potentials to generate V^{app} given as in Equation 2.26. Then a modified reference potential V^{ref}, which is a linear combination of the exact potential V and the potential fit V^{app} is introduced

$$V_I^{ref} = w_I V_I + (1 - w_I) V_I^{app}. \tag{2.34}$$

At points where $\omega = 1$, the modified reference potential V^{ref} equals the exact potential, while it matches the fitted potential V^{app} for $\omega = 0$. The definition of the reference potential depends on V^{app} which in turn depends on the reference potential. First V is potfitted to generate the reference potential. The reference potential is subsequently potfitted with a new V^{app} to generate a new reference potential. The iteration is continued until some break-off criterion is reached.

2.6 Flux analysis

A complete solution of a quantum-mechanical molecular dynamics problem results from a proper analysis of the inherent information in the S-matrix, obtained after a successful propagation of the initial wave packet. Of the various methods available for determining the reaction attributes from the S-matrix elements. the utilization of the flux operator to determine the reaction probabilities has become a standard procedure in the field of time-dependent reactive scattering. In the MCTDH methodology. reaction probabilities are calculated by using the flux operator in

TH-1851_Sayak

combination with complex absorbing potentials(CAPs). This approach requires only solving Fourier integrals over matrix elements in comparison to the $(E-t)$-Fourier transform of the wave packet at every grid point on the dividing surface in case of standard methods.

CAPs are usually used to absorb the wave function reflected from the end of a finite grid[29, 35, 104]. This enables the use of shorter grids, where the relevant part of the wave function is not affected by the reflected part and the accuracy in results is maintained. In the field of scattering, Neuhauser et al.[32, 105] showed the importance of CAPs by enabling the use of the reactant coordinate set throughout the calculation. The utilization of CAPs in determining the reaction probabilities for an MCTDH wave packet propagation underlines its immense significance. The derivation of an effective approach of applying the CAP to obtain reaction probabilities is given below.

In the MCTDH calculations, monomial CAPs[53] of the form

$$-iW(q) = -i\eta(q-q_c)^b\theta(q-q_c), \tag{2.35}$$

have been employed, where W(q) represent real, non-negative potential operators which are non-zero only in the asymptotic region. For efficient performance, the CAPs have to be sufficiently weak and long[53, 106–109]. The order of the CAP is usually set as $b = 3$. The symbol $\theta(x)$ denotes Heaviside's step function and q_c is the point where the CAP is switched on, i.e. q_c and the end of the grid determine the length of the CAP. The CAP strength η and the CAP length are chosen according to the requirement of the system under study.

Initial state selected reaction probabilities are determined by analyzing the re-

TH-1851_Sayak

active flux into the product arrangement channel γ[61] as

$$P_\nu(E) = \sum_{\nu'} |S_{\gamma\nu',\alpha\nu}|^2 = 2\pi\langle\Psi^+_{E\alpha\nu}|F_\gamma|\Psi^+_{E\alpha\nu}\rangle(\gamma \neq \alpha). \tag{2.36}$$

Here S denotes the S-matrix, the index ν collectively accounts for all initial quantum numbers, including the total angular momentum J, α denotes the initial(reactant) arrangement channel, γ represents the product arrangement channel, and $\Psi^+_{E\alpha\nu}$ is the exact time-dependent scattering solution with outgoing bounding conditions. The flux operator is denoted by F_γ.

For the MCTDH method, the most efficient way to calculate the reaction probabilities is to incorporate the CAP in the system Hamiltonian, H. The Hamiltonian H is replaced by the non-Hermitian operator $\tilde{H}$

$$\tilde{H} = H - iW. \tag{2.37}$$

The initial wave packet Ψ^0_ν is propagated by $\tilde{H}$

$$\Psi_\nu(t) = e^{-i\tilde{H}t}\Psi^0_\nu. \tag{2.38}$$

Equation 2.36 may now be written as

$$P_\nu(E) = \frac{1}{2\pi\ |\Delta E|^2}\int_{-\infty}^{\infty} dt \int_{-\infty}^{\infty} dt' \times \langle\psi^0_\nu|e^{i(\tilde{H}^\dagger - E)t}F_\gamma e^{i(\tilde{H}^\dagger - E)t'}|\psi^0_\nu\rangle, \tag{2.39}$$

where $\Delta(E)$ denotes the energy distribution of the initial wave packet[110]. Ψ^0_ν which is located in the reagent arrangement channel α but outside the CAP. As the propagated wave packet can reach the product arrangement channel $\gamma \neq \alpha$

TH-1851_Sayak

only for positive times, the two lower integral limits can be replaced by zero. The flux operator F_γ is written as[53, 111]

$$F_\gamma \equiv i[H, \Theta_\gamma] = i[\tilde{H}, \Theta_\gamma] = 2W_\gamma + i(\tilde{H}^\dagger - E)\Theta_\gamma - i\Theta_\gamma(\tilde{H} - E). \tag{2.40}$$

Thus

$$\begin{aligned} P_\nu &= \frac{1}{2\pi\ |\Delta E|^2} \int_0^\infty dt \int_0^\infty dt' \\ &\times\ [2\langle\psi_\nu^0|e^{i(\tilde{H}^\dagger - E)t} W_\gamma e^{i(\tilde{H}^\dagger - E)t'}|\psi_\nu^0\rangle \\ &+\ \left(\frac{d}{dt} + \frac{d}{dt'}\right)\langle\psi_\nu^0|e^{i(\tilde{H}^\dagger - E)t}\Theta_\gamma e^{i(\tilde{H}^\dagger - E)t'}|\psi_\nu^0\rangle]. \end{aligned} \tag{2.41}$$

Using Equation 2.38, the last term in the above equation is evaluated as,

$$\frac{1}{\pi\ |\Delta E|^2} Re \int_0^T \langle\Psi_\nu(T)|\Theta_\gamma|\Psi_\nu(t)\rangle^{iET} dt. \tag{2.42}$$

Finally, some transformations are performed to obtain suitable working equations as defined below

$$g_\nu^W(\tau) = \int_0^{T-\tau} \langle\psi_\nu(t)|W_\gamma|\psi_\nu(t+\tau)\rangle\ dt \tag{2.43}$$

and

$$g_\nu^\Theta(\tau) = \frac{1}{2}\ \langle\psi_\nu(T-\tau)|\Theta|\psi_\nu(T)\rangle. \tag{2.44}$$

and finally the reaction probabilities are evaluated as

$$P_i^J = \frac{2}{\pi\ |\Delta E|^2}\ Re \int_0^T [g_\nu^W(\tau) + g_\nu^W(\Theta)]\ e^{iE\tau}\ d\tau. \tag{2.45}$$

TH-1851_Sayak

Chapter 3

Atom-Diatom and Diatom-Diatom Scatterring Systems

The MCTDH algorithm has been applied to study the reaction dynamics for ground and ro-vibrational excited states of the He + H^+He, H_2 + OH and H_2 + CN systems on the available potential surfaces for the respective systems. The specific nature of the Hamiltonian considered for the calculations and the preparation of the intitial wave packets for the MCTDH propagations have been discussed in this chapter. The chapter ends with a mention of the formulations for deriving the cross sections from the reaction probabilities and a subsequent derivation of the rate constants.

TH-1851_Sayak

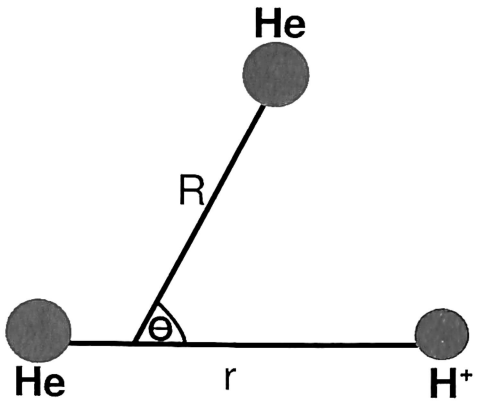


Figure 3.1: *Reactant jacobi coordinates for He + HeH^+ reaction.*

3.1 Hamiltonian

A. Tri-atomic system

The Hamiltonian operator for a triatomic system described in the reactant Jacobi coordinates (R, r and θ) is written as,

$$\hat{\mathbf{H}} = -\frac{1}{2\mu_R}\frac{\partial^2}{\partial R^2} - \frac{1}{2\mu_r}\frac{\partial^2}{\partial r^2} + \frac{(\hat{\mathbf{J}} - \hat{\mathbf{j}})^2}{2\mu_r R^2} + \frac{\hat{\mathbf{j}}^2}{2\mu_r r^2} + V(R, r, \theta). \tag{3.1}$$

Here μ_R is the reduced mass along the R coordinate, the coordinate joining the He atom to the center of mass of HeH^+ diatom, and μ_r is the reduced mass of the diatom. $\mathbf{J}$ and $\mathbf{j}$ are the total angular momentum and rotational angular momentum operators, respectively. The reactant Jacobi coordinates for the tri-atomic He + H^+He are shown in Figure 3.1. To solve the time-dependent Schrödinger equation, the time-dependent wave function is expanded in terms of translational basis for R, the vibrational basis for r, and the body-fixed (BF) total angular basis Y_{lm}[112]. The BF z-axis is chosen to be along R. In terms of the above time-dependent wave function the triatomic Hamiltonian is written as a tridiagonal

TH-1851_Sayak

matrix as[9, 112, 113]

$$\begin{aligned} H &= \Big[-\frac{\hbar^2}{2\mu_R}\frac{\partial^2}{\partial R^2} - \frac{\hbar^2}{2\mu_r}\frac{\partial^2}{\partial r^2} + \frac{j(j+1)}{2\mu_r r^2} + \frac{J(J+1)-K^2}{2\mu_R R^2} \\ &+ V(R,r,\theta)\Big]\delta_{KK'} \\ &- \frac{\hbar^2}{2\mu_R R^2}\lambda^+_{JK}\lambda^+_{jK}\sqrt{1+\delta_{K0}}\delta_{K+1,K'} \\ &- \frac{\hbar^2}{2\mu_R R^2}\lambda^-_{JK}\lambda^-_{jK}\sqrt{1+\delta_{K1}}\delta_{K-1,K'}, \end{aligned} \tag{3.2}$$

where λ is defined as

$$\lambda^{\pm}_{JK} = \sqrt{J(J+1) - K(K\pm 1)}.$$

In Eq. 3.2, K denotes the projection of **J** onto **R**. The last two off-diagonal terms in the above equation couple different K states and their neglection gives rise to the CS approximation. Hence K is a conserved quantity under the CS approximation. It is worth noting here that in the BF-frame, initial K is the initial magnetic rotational quantum number of the diatom.

As has been mentioned in the previous chapter, the system Hamiltonian must be written in a product form for efficient implementation of the MCTDH algorithm. The kinetic energy operrator is in the required product form. The Panda-Satyamurthy potential energy surface[114] used for the calculations on the He_2H^+ system is not in the desired product form. An accurate fit to the potential V was thus generated using the POTFIT algorithm. The potential then assumes the form (see Chapter 2)

$$V(R,r,\theta) = \sum_{i=1}^{m_r}\sum_{j=1}^{m_\theta} D_{ij}(R)v_i^{(2)}(r)v_j^{(3)}(\theta). \tag{3.3}$$

TH-1851_Sayak

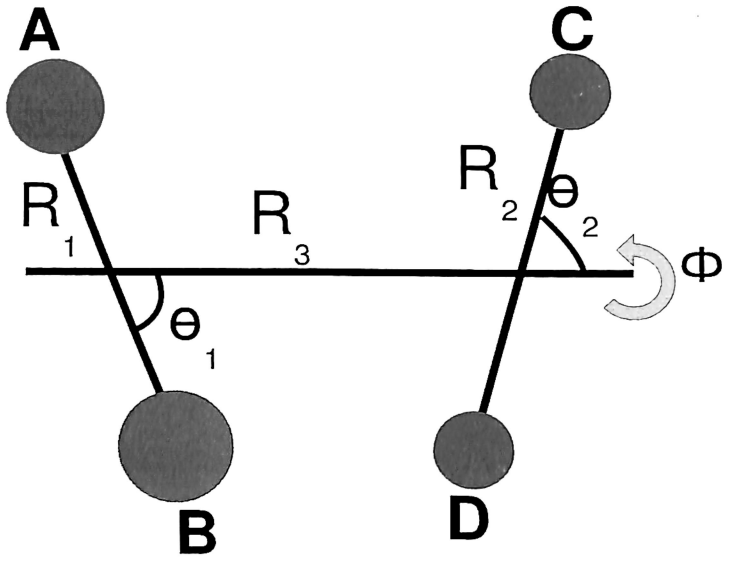


Figure 3.2: *Jacobi coordinates for tetra-atomic reactive scattering system*

B. Tetra-atomic system

For a diatom+diatom system, the Hamiltonian in reactant Jacobi coordinates is written as

$$\begin{aligned}\hat{\mathbf{H}} &= \sum_{i=1}^{3}(-\frac{1}{2\mu_i}\frac{\partial^2}{\partial R_i^2}) + \frac{\hat{\mathbf{j}}_1^2}{2\mu_1 R_1^2} + \frac{\hat{\mathbf{j}}_2^2}{2\mu_2 R_2^2} + \frac{(\hat{\mathbf{J}} - \hat{\mathbf{j}}_1 - \hat{\mathbf{j}}_2)^2}{2\mu_3 R_3^2} \\ &+ V(R_1, R_2, R_3, \theta_1, \theta_2, \varphi).\end{aligned} \tag{3.4}$$

Here R_1 and R_2 are the two diatomic bond distances and R_3 is the distance between the centers of mass of the diatoms. μ_1, μ_2 and μ_3 are the reduced masses along R_1, R_2 and R_3 respectively. $\hat{\mathbf{J}}$ is the total angular momentum operator. $\hat{\mathbf{j}}_1$ and $\hat{\mathbf{j}}_2$ are the rotational angular momentum operators along R_1 and R_2 respectively. θ_1, θ_2 are the polar angles, while φ is the out-of-plane torsional angle. The coordinates are depicted in Figure 3.2

To express the kinetic energy operator in a form suitable for MCTDH calcula-

TH-1851_Sayak

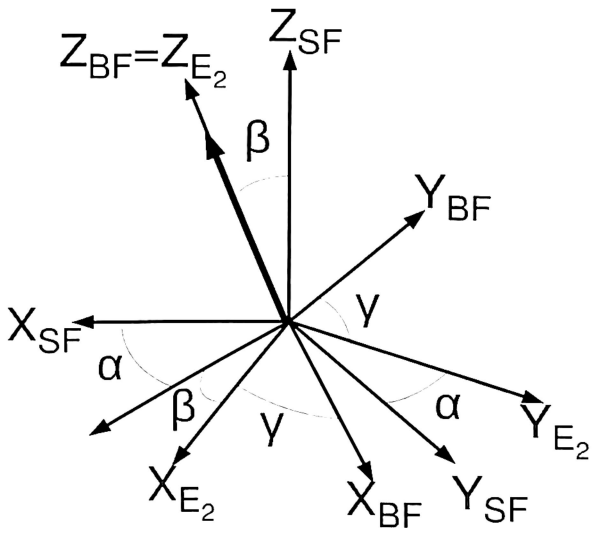


Figure 3.3: *Definitions of the body-fixed frame and the E_2 frames. α, β and γ are the three Euler angles. SF denotes the space-fixed frame. Starting from the SF frame, rotation through α results in the E_1 frame. A second rotation through β results in the E_2 frame. The third rotation through γ results in the body-fixed frame.*

tions, it is convenient to express the body-fixed coordinates in the E_2 frame[115–120]. The E_2 frame, as shown in Figure 3.3, is a coordinate system in which only the first two Euler rotations, through the angles α and β, are considered. The body-fixed frame results from the third rotation over the angle γ. Representation of the tetra-atomic system in the E_2 frame results in a set of seven Jacobi coordinates $(R_1, R_2, R_3, \theta_1, \theta_2, \varphi_1, \varphi_2)$, where θ_1, θ_2 and φ_1, φ_2 denote the polar and azimuthal angles which orient the vectors $\mathbf{R}_1$ and $\mathbf{R}_2$ with respect to the E_2 frame. The dihedral angle $\varphi = \varphi_1$-φ_2 denotes the angle between the planes $(\mathbf{R}_3,\mathbf{R}_1)$ and $(\mathbf{R}_3,\mathbf{R}_2)$. The coordinates are shown in Figure 3.4. The angular basis set for the system in the E_2 coordinate is given as[118, 119]

$$Y_J^K(\beta,0)(-1)^K Y_{j_2}^{k_2}(\theta_2^{BF},\varphi_2^{E_2}) Y_{j_1}^{k_1}(\theta_1^{BF},\varphi_1^{E_2}). \tag{3.5}$$

TH-1851_Sayak

where k_1 and k_2 are the quantum numbers associated with the BF projection of the partial angular momenta j_1 and j_2. K is the BF projection of the total angular momentum J and is defined as $K = k_1 + k_2$, β is the second Euler angle. Using this basis set, the kinetic operator after integration over β, becomes[118]

$$
\begin{aligned}
2\hat{T} &= \sum_{i=1}^{3}\left(-\frac{1}{\mu_i}\frac{\partial^2}{\partial R_i^2}\right) - \left(\frac{1}{\mu_1 R_1^2} + \frac{1}{\mu_3 R_3^2}\right) \\
&\times \left[\frac{1}{sin\theta_1^{BF}}\frac{\partial}{\partial\theta_1^{BF}}sin\theta_1^{BF}\frac{\partial}{\partial\theta_1^{BF}} + \frac{1}{sin^2\theta_1^{BF}}\frac{\partial^2}{\partial\varphi_1^{E_2^2}}\right] \\
&- \left(\frac{1}{\mu_2 R_2^2} + \frac{1}{\mu_3 R_3^2}\right)\left[\frac{1}{sin\theta_2^{BF}}\frac{\partial}{\partial\theta_2^{BF}}sin\theta_2^{BF}\frac{\partial}{\partial\theta_2^{BF}} + \frac{1}{sin^2\theta_2^{BF}}\frac{\partial^2}{\partial\varphi_2^{E_2^2}}\right] \\
&+ \frac{1}{\mu_3 R_3^2}\left(2\frac{\partial^2}{\partial\varphi_1^{E_2^2}}\right) \\
&+ \frac{1}{\mu_3 R_3^2}\left[e^{i\varphi_1^{E_2}}\left(\frac{\partial}{\partial\theta_1^{BF}} + icot\theta_1^{BF}\frac{\partial}{\partial\varphi_1^{E_2}}\right) \times e^{-i\varphi_2^{E_2}}\left(-\frac{\partial}{\partial\theta_2^{BF}} + icot\theta_2^{BF}\frac{\partial}{\partial\varphi_2^{E_2}}\right)\right] \\
&+ \frac{1}{\mu_3 R_3^2}\left[e^{-i\varphi_1^{E_2}}\left(-\frac{\partial}{\partial\theta_1^{BF}} + icot\theta_1^{BF}\frac{\partial}{\partial\varphi_1^{E_2}}\right) \times e^{i\varphi_2^{E_2}}\left(\frac{\partial}{\partial\theta_2^{BF}} + icot\theta_2^{BF}\frac{\partial}{\partial\varphi_2^{E_2}}\right)\right] \\
&+ \frac{1}{\mu_3 R_3^2}\left[J(J+1) + 2\frac{\partial}{\partial\varphi_2^{E_2}}\left(\frac{\partial}{\partial\varphi_2^{E_2}} + \frac{\partial}{\partial\varphi_1^{E_2}}\right)\right] \\
&- \frac{C_+(J,K)}{\mu_3 R_3^2}\left[e^{i\varphi_1^{E_2}}\left(\frac{\partial}{\partial\theta_1^{BF}} + icot\theta_1^{BF}\frac{\partial}{\partial\varphi_1^{E_2}}\right) + e^{i\varphi_2^{E_2}}\left(\frac{\partial}{\partial\theta_2^{BF}} + icot\theta_2^{BF}\frac{\partial}{\partial\varphi_2^{E_2}}\right)\right] \\
&- \frac{C_-(J,K)}{\mu_3 R_3^2}\left[e^{-i\varphi_1^{E_2}}\left(-\frac{\partial}{\partial\theta_1^{BF}} + icot\theta_1^{BF}\frac{\partial}{\partial\varphi_1^{E_2}}\right)\right] \\
&- \frac{C_-(J,K)}{\mu_3 R_3^2}\left[e^{-i\varphi_2^{E_2}}\left(-\frac{\partial}{\partial\theta_2^{BF}} + icot\theta_2^{BF}\frac{\partial}{\partial\varphi_2^{E_2}}\right)\right],
\end{aligned}
\tag{3.6}
$$

where $C_\pm(J,K) = \sqrt{J(J+1) - K(K\pm 1)}$.

Since k_1 and k_2 are actually the conjugate momenta to $\varphi_1^{E_2}$ and $\varphi_2^{E_2}$ and as

TH-1851_Sayak

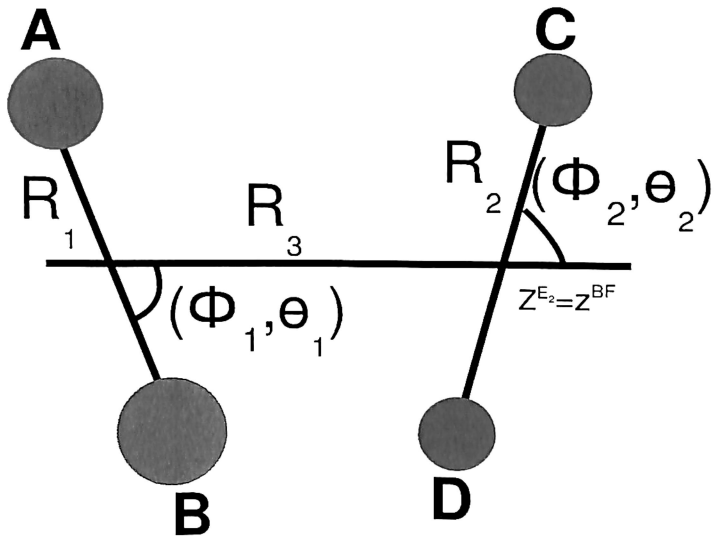


Figure 3.4: *Coordinates for the tetra-atomic reactive scattering system described in E_2 coordinates.*

$K = k_1 + k_2$. the above equation can be rewritten to the following form:

$$\begin{aligned} 2\hat{T} &= \sum_{i=1}^{3}\left(-\frac{1}{\mu_i}\frac{\partial}{\partial R_i^2}\right) + \left(\frac{1}{\mu_1 R_1^2}+\frac{1}{\mu_3 R_3^2}\right)\hat{j}_1^{\,2} + \left(\frac{1}{\mu_2 R_2^2}+\frac{1}{\mu_3 R_3^2}\right)\hat{j}_2^{\,2} + \frac{1}{\mu_3 R_3^2} \\ &\times \left[-2k_1^2 + \hat{j}_{1,+}\hat{j}_{2,-} + \hat{j}_{1,-}\hat{j}_{2,+} + J(J+1) - 2k_2k_1 - 2k_2^2\right] \\ &- \frac{C_+(J,K)}{\mu_3 R_3^2}\left(\hat{j}_{1,+}+\hat{j}_{2,+}\right) - \frac{C_-(J,K)}{\mu_3 R_3^2}\left(\hat{j}_{1,-}+\hat{j}_{2,-}\right), \end{aligned} \tag{3.7}$$

where

$$\hat{j}_i^{\,2} = -\frac{1}{sin\theta_i^{BF}}\frac{\partial}{\partial\theta_i^{BF}}sin\theta_i^{BF}\frac{\partial}{\partial\theta_i^{BF}} + \frac{k_i^2}{sin^2\theta_i^{BF}} \tag{3.8}$$

and

$$\hat{j}_{i,\pm} = \pm\frac{\partial}{\partial\theta_i^{BF}} - k_i cot\theta_i^{BF}.\, k_i \rightarrow k_i \pm 1. \tag{3.9}$$

The expression in Equation 3.7 is in a proper format to be implemented in MCTDH. Dropping the last two terms in Equation 3.7 leads to the CS approxi-

TH-1851_Sayak

mation.

As the potentials used for the H_2 + OH and H_2 + CN calculations don't conform to the the requirements of an efficient MCTDH application, they have to be recast into a sum of products of one-dimensional potentials. The potential energy surface initially expressed in the BF coordinates depends on six internal coordinates given by

$$V = V(R_1, R_2, R_3, \theta_1, \theta_2, \phi^{BF}). \tag{3.10}$$

To express it in E_2 coordinates, a Fourier transformation of the potential is performed as

$$\tilde{V}_\Omega(R_1, R_2, R_3, \theta_1, \theta_2, \Omega) = (2\pi)^{-1} \int_0^{2\pi} e^{-i\Omega\phi^{BF}} V(R_1, R_2, R_3, \theta_1, \theta_2, \phi^{BF})\, d\phi \tag{3.11}$$

Hence,

$$V(R_1, R_2, R_3, \theta_1, \theta_2, \phi^{BF}) = \sum_\Omega \tilde{V}_\Omega(R_1, R_2, R_3, \theta_1, \theta_2)\, e^{i\Omega\phi^{BF}}. \tag{3.12}$$

Since $\varphi^{BF} = \varphi_1^{E_2} - \varphi_2^{E_2}$, the above equation can be written as

$$\sum_\Omega \tilde{V}_\Omega(R_1, R_2, R_3, \theta_1, \theta_2)\, e^{i\Omega\phi} = \sum_\Omega \tilde{V}_\Omega(R_1, R_2, R_3, \theta_1, \theta_2)\, e^{i\Omega\phi_1^{E_2}}\, e^{-i\Omega\phi_2^{E_2}}. \tag{3.13}$$

Hence the action of the potential operator on the wave function is given by

$$\begin{aligned}(\hat{V}\Psi)(R_1, R_2, R_3, \theta_1, k_1, \theta_2, k_2) &= \sum_\Omega \tilde{V}_\Omega(R_1, R_2, R_3, \theta_1, \theta_2) \\ &\times \Psi(R_1, R_2, R_3, \theta_1, k_1 - \Omega, \theta_2, k_2 + \Omega)\end{aligned} \tag{3.14}$$

TH-1851_Sayak

Now $\widetilde{V}_\Omega$ term is refitted by using POTFIT[53, 55, 102, 103] to arrive at a linear combination of products format.

3.2 Initial wave packet

A. Tri-atomic system

The initial wave function is defined as a single Hartree product of a Gaussian wave packet in R, a vibrational eigenfunction function in r, and a rotational eigenfunction function in θ; i.e.

$$A^J_{j_1 j_2 j_3}(t=0) = \delta_{j_1 1}\delta_{j_2 2}\delta_{j_3 3}. \tag{3.15}$$

$$\varphi^{(1)}_1(R, t=0) \equiv \chi_0(R) = (\sqrt{2\pi} d_R)^{-1/2} exp\left[-\left(\frac{R-R_0}{2d_R}\right)\right] e^{-ip_0(R-R_0)}, \tag{3.16}$$

$$\varphi^{(2)}_1(r, t=0) \equiv \varphi_{j_0\nu_0}(r) = vibrational\ eigenfunction. \tag{3.17}$$

$$\varphi^{(3)}_1(\theta, K, t=0) = \sqrt{\frac{2j_0+1}{2}\frac{(j_0-m_0)!}{(j_0+m_0)!}} P^{m_0}_{j_0}(cos\theta)\delta_{K,m_0}, \tag{3.18}$$

where j_0, m_0, ν_0 are the initial ro-vibrational quantum numbers of the free diatom. P^m_j denotes the associated Legendre function, and δ is the Kronecker symbol. The momentum p_0 and width d_r determine the energy distribution ΔE of the initial wave packet.

TH-1851_Sayak

B. Tetra-atomic system

The initial wave packet, Ψ_i^0, is constructed by taking a direct product of an eigenstate ψ_i (with quantum numbers $i = (j_1, m_1, v_1; j_2, m_2, v_2)$) of the internal Hamiltonian and an incoming Gaussian function χ along the collision coordinate:

$$\Psi_i^0(R_1, R_2, R_3, \theta_1, k_1, \theta_2, k_2) = \psi_i(\theta_1, k_1, R_1, \theta_2, k_2, R_2)\ \chi(R_3). \tag{3.19}$$

For the collision coordinate, the Gaussian takes the form

$$\chi(R_3) = \left(\sqrt{2\pi}\, d\right)^{-1/2} \exp\left[-\left(\tfrac{R_3 - R_0}{2d}\right)^2\right] e^{ip_0(R_3 - R_0)}, \tag{3.20}$$

with R_0, p_0 and d denoting its center in coordinate and momentum space and its width, respectively. $\psi_i(\theta_1, k_1, R_1, \theta_2, k_2, R_2)$ is taken as a direct product of two internal functions which define the initial ro-vibrational states of the two diatoms. These are defined as

$$\zeta_{j_i m_i v_i}(\theta_i, k_i, R_i) = \sqrt{\frac{2j_i + 1}{2}\frac{(j_i - m_i)!}{(j_i + m_i)!}} P_{j_i}^{m_i}(\cos\theta)\, \delta_{k_i m_i}\, \xi_{v_i}^{(j_i)}(R_i),\ \ i = 1, 2. \tag{3.21}$$

Here $P_{j_i}^{m_i}(\cos\theta)$ is the associated Legendre Polynomial and $\xi_v^{(j)}$ denotes the v-th vibrational eigenfunction of the diatomic molecule in rotational eigenstate j. Here m_i and m_i' denote the initial and final magnetic quantum numbers, respectively, whereas k_i denotes the corresponding angular momentum variable on which the wave function depends.

TH-1851_Sayak

3.3 Cross sections

The reaction cross sections are calculated from probabilities as

$$\sigma_{v_1 v_2 j_1 j_2}(E) = \frac{1}{(2j_1+1)(2j_2+1)} \sum_{m_1=-j_1}^{j_1} \sum_{m_2=-j_2}^{j_2} \sum_{J=|m_1+m_2|}^{J_{max}} \sigma_{v_1 v_2 j_1 j_2 m_1 m_2 J}(E), \tag{3.22}$$

where

$$\sigma_{v_1 v_2 j_1 j_2 m_1 m_2 J}(E) = \frac{\pi}{k^2}(2J+1)\ P_{v_1 v_2 j_1 j_2 |m_1||m_2| J}(E). \tag{3.23}$$

The momentum k is defined as

$$k = \sqrt{2\mu_R(E - E_{v_1 j_1} - E_{v_2 j_2})}, \tag{3.24}$$

where $E_{v_i j_i}$ is the ro-vibrational energy of the diatom.

3.4 Rate constants

The initial state specific reaction rate constant is given in terms of the total integral cross section

$$k_{v_1 v_2 j_1 j_2}(T) = (\frac{8k_BT}{\pi\mu_R})^{1/2}(k_BT)^{-2} \int_0^\infty dE_t E_t exp(-E_t/k_BT)\sigma_{v_1 v_2 j_1 j_2}(E_t), \tag{3.25}$$

where E_t is the translational energy and k_B is the Boltzmann constant. The rate constant defined in the above equation involves only Boltzmann averaging over translational energy but not rotational energy. The thermal rate constant measured in the experiment involves a Boltzmann averaging over initial ro-vibrational

TH-1851_Sayak

states.

TH-1851_Sayak

Chapter 4

$He + H^+He \rightarrow HeH^+ + He$: A Comparative Study of MCTDH And Split-operator Methodology Wave Packet Propagation

4.1 Introduction

Ion molecule reactions are important processes that occur in many interesting situations such as plasma's, electric discharges, ionosphere and interstellar clouds[121]. Numerous experimental and theoretical works have been carried out in this field over the last few decades. The rare gas dimers are generally known to be weakly bound species[122–125] held together by van der Waals interaction. With a binding energy of only 0.957 meV[123] the helium dimer is known to be the weakest among

TH-1851_Sayak

the rare gas clusters. The subsequent stabilization of X_2H^+(X=rare gas atom), resulting from the insertion of a proton between basically two non-attractive atoms have presented researchers with an intriguing phenomenon over the years.

The initial experimental observation of an X_2H^+(X = He, Ne, Ar) ion was reported nearly three decades ago, in observations by two different groups[126, 127]. This has been followed by various experimental studies for X-H-X(X = Ar, Kr, Xe) and X-H-X′(X≠X′)[86–90] ionic clusters. Earliest theoretical studies on the structure and stability of X_2H^+(X = Ar, Kr, Xe) were performed by Lundell et al. using core potential[128] and DFT approaches[129]. While linear centrosymmetric $[X\text{-}H\text{-}X]^+$ structures, were predicted for Kr and Xe clusters, some ambiguity existed about the bond lengths for the Ar cluster[129, 130]. Subsequent theoretical and experimental studies confirmed the linear centrosymmetric structures for the Ar[89, 131] and Ne[132] cluster. Studies on the X_nH^+ were extended upto n=7[130, 133] for Ar systems, wherein the effect of consecutive addition of Argon atoms on dissociation energy were investigated. Extensive *ab initio* studies were performed by Kim and Lee[132] using second and fourth order Moller-Plesset perturbation theories to determine the potential energy surface for the Ne_2H^+ cluster. A global potential energy surface for Ar_2H^+ developed by Qu et al.[131], employing molecular dynamics simulations paved the way for further studies on the structure and stability of the protonated rare gas clusters[134, 135].

Our interest has been to study the dynamics of such protonated rare gas clusters by quantum mechanical methods. He_2H^+ is the smallest of such clusters and presents an ideal system to study the dynamics at molecular level. The reaction He + H^+He → HeH^+ + He in which a proton is transferred from one heavy atom (helium) to another (helium) presents an interesting scenario on which not

TH-1851_Sayak

much has been reported till date. In the present chapter the proton transfer dynamics of the mentioned process has been studied using the MCTDH algorithm. A literature survey on the theoretical work reported on the system is given in the next section. This is followed by the numerical details of the calculations and a detailed discussion on the results obtained. The chapter ends with a summary of the results obtained and the inferences derived from this study.

4.1.1 Computational studies

Theoretical studies on the He_2H^+ system have mostly involved *ab initio* calculations on the ionic cluster to determine physical parameters of the most stable structure of the ion-molecule cluster resulting from the insertion of a proton in the He_2 molecule. With the development of more accurate methodologies over the years, important parameters like equilibrium bond length (r_e) and dissociation energy(D_e) have been studied exhaustively, to determine the accurate structure of the cluster at its equilibrium state.

The earliest *ab initio* studies on the He_2H^+ system involved valence bond calculations by Poshusta et al.[136] to determine the equilibrium geometries and binding energy of the ion-molecule system. The initial calculations determined a linear symmetric structure for He_2H^+ with H-He bond length of 1.70 a_0 and a dissociation energy of 0.96 eV. Subsequent valence bond configuration interaction calculations by Poshusta and Siems[137] reported a linear symmetrical structure with values of 1.74 a_0 and 0.456 eV, for r_e and D_e. Milleur et al.[138] computed the ground state energies using the linear combination of atomic orbitals-molecular orbital methodology for several geometries for He_2H^+ and reported the most stable

TH-1851_Sayak

geometry corresponding to a linear symmetric configuration with $r_e = 1.75\ a_0$ and a potential well of 0.5757 eV. They also reported a potential energy surface for He_2H^+ for collinear and non-linear configurations. The linear symmetric structure was confirmed by studies performed by Dykstra[139], who obtained $r_e = 1.746\ a_0$ and $D_e = 0.571$ eV with self-consistent electron pair calculations. A value of $r_e = 1.747$ and $D_e = 0.5757$ eV were obtained in the same study for calculations involving substituted coupled cluster methodology. An analytical functional fit to the values computed by Dykstra et al.[139] was subsequently reported by Lee and Secrest[140]. But the potential fit by Lee and Secrest was accurate only near the minimum as the *ab initio* calculations didn't consider a wide range of geometries.

The insertion of a proton into a helium cluster and the subsequent stabilization of the resultant ion-molecule systems resulting from both linear and non-linear approaches of the H^+ ion was studied by Baccarelli et al.[141] employing multireference single and double excitations with configuration interaction calculations. The symmetric insertion of the ionic core at the center of the two helium atoms was found to result in the most stable structure, with $r_e = 1.75\ a_0$ and $D_e = 0.52$ eV. The linear asymmetric arrangement, in which the proton is located outside the dimer, was found to be very weakly bound cluster which can dissociate easily into either He + He + H^+ or HeH^+ + He. A study of the PES over a broad range of nuclear geometries was performed by Baccarelli et al.[141] for collinear $[He\text{-}H\text{-}He]^+$ and $[He\text{-}He\text{-}H]^+$ geometries and for C_{2v} geometries of $[He\text{-}H\text{-}He]^+$. For the equilibrium geometry of He_2H^+ they reported the lowest lying excited state to be about 11.5 eV above the ground state asymptotic fragments and about 19 eV above the Franck Condon region of the symmetric ionic cluster. In a series of subsequent studies, Gianturco et al.[130, 142, 143] investigated the growth of He_nH^+

TH-1851_Sayak

cluster(n = 3-13) around the tri-atomic He_2H^+ ionic core and their structural and dynamical behavior.

An *ab initio* study of the He_2H^+ cluster was performed by Kim and Lee[132], using second and fourth order Moller-Plesset perturbation theories and coupled cluster with single and double excitations approach with various basis sets. which obtained r_e 1.748 a_0 and $D_e = 0.5741$ eV. They reported that due to the presence of charge polarized dipole attraction, electron delocalization was observed resulting in a chemical bond. The studies were also extended to include geometries away from the equilibrium and to higher energy regions on the PES to investigate the existence of the asymmetric species. In a study by Lundell et al.[128] on heavy rare gas dimer-hydrogen atom complexes, it was speculated that there may exist another minimum corresponding to linear X-XH^+(X = Ar, Kr, Xe) geometry on the PES in addition to the global minimum.

There have been few studies on the determination of bound states for the He_2H^+ cluster have been very few in the last three decades. Lee and Secrest[140] studied the rotation-vibration energy levels for total angular momentum $J = 0, 1, 2$ and reported five bound states for the system. The calculations were performed using the variation method on the PES reported by Dykstra[139]. Panda and Satyamurthy[114] performed quantum dynamical calculations on a new PES obtained using coupled cluster single and double excitations with perturbative triple excitations[CCSD(T)] with d-aug-cc-PVTZ basis set and calculated bound states of the He_2H^+ system for total angular momentum $J = 0$. In contrast to the five bound states reported by Lee and Secrest[140]. the study by Panda and Satyamurthy reported seven bound states for the ion-molecule system. An equilibrium bond length of 1.75 a_0 and $D_e = 0.578$ eV was determined in this study.

TH-1851_Sayak

Although ion-molecule clusters involving rare gas atoms have been studied extensively in the last two decades, not much has been reported on the dynamics of the He + H^+He reaction. Also most of the studies on these type of clusters have concentrated on examining the equilibrium structures and on quantifying the number of bound states. In this chapter, a detailed study of the reaction dynamics for both ro-vibrational ground and excited states of the reactant is presented. Owing to the presence of the deep well along the minimum energy path, it is anticipated that the above proton transfer process may be rich in dynamical resonances. Hence, it would be interesting to investigate if the energy dependence of the reaction probability shows signature of reactive resonances and if those resonances survive the l-averaging. Calculations have been performed using the MCTDH algorithm with an exact form of the Hamiltonian on the Panda-Satyamurthy PES[114]. A separate study for the He + H^+He reaction has been performed using the split-operator method under the centrifugal sudden approximation[144]. The accuracy of the CS approximation has been investigated for many ion-molecule reactions[145–149]. Generally, the agreement between the CS and the CC results becomes poorer with increase in J. This can result in large differences in the reaction cross sections, particularly in the high energy region, as has been shown in case of He + H_2^+ [145] and Ne + H_2^+ [146] reactions. The importance of inclusion of Coriolis coupling for the He + H_2^+ reaction system has been analyzed in this chapter.

TH-1851_Sayak

No. of grid points	$N_R/N_r/N_\theta$	80/60/30
Grid points for k_1,k_2	k_{min}/k_{max}	-3/3
Extension of R grid	R_{min}/R_{max}	1.0/12.5
Extension of r grid	$r_{1_{min}}/r_{1_{max}}$	0.5/8.5
CAP order	β_R/β_r	3
CAP strength	η_R/η_r	0.032/0.08
Starting point of CAP	R_c/r_c	8.0/5.50
CAP length	L_R/L_r	4.0/3.0
Center of χ_0	R_0	7.5
Width of χ_0	d_R	0.22
Initial momentum of χ_0	p_0	-6.3
Propagation time	T	1000

Table 4.1: *Numerical parameters of the MCTDH calculations for the He + HeH^+ system(in atomic units if not otherwise stated).*

4.2 Results and discussion

4.2.1 Numerical details

Table 4.1 displays the relevant parameters used in MCTDH calculation for the He + H^+He reaction. The R and r coordinates are represented by sin-DVR grids. The grids for R and r extend from 1 to 12.5 and 0.5 to 8.5 a_0, respectively. A sine DVR of 80 and 60 points is used for R and r respectively. For the angle, a two-dimensional "extended Legendre DVR"[150] has been employed.

The CAP used to absorb the wave packet beyond the analysis point starts at 8.0 a_0 and 5.50 a_0 along R and r respectively. The strengths and orders of the CAPs are (0.032,3) and (0.008,3), along R and r respectively. Calculations have been carried out to obtain reaction attributes upto a translational energy of 0.5 eV. The initial Gaussian is centered at $R = 7.5$ a_0 while the width of the Gaussian wave function is $d_R = 0.22$ a_0. The momentum(p_0) of the initial wave packet is -7.5

TH-1851_Sayak

Mode	Primitive Basis		No. of SPFs
	Type	Size	
R	sin	80	23
(r)	sin	60	17
(θ, k)	KLeg	210	22

Table 4.2: *Parameters for the primitive basis sets employed for each degree of freedom. KLeg is a two-dimensional extended Legendre DVR [150].*

a_0. The number of SPFs used to define the primitive basis sets for the different degrees of freedom are shown in Table 4.2. While a total of 23 SPFs were used to describe the R mode, 17 SPFs were used along r. For the combination of (θ, k), 22 SPFs were used in the calculations. The potential was fitted to the product form required for the MCTDH propagation using the POTFIT algorithm. While applying POTFIT, we have restricted the algorithm to the following space of the surface: $R < 6.54\ a_0$ and $r < 1.98\ a_0$ and $V < 0.5$ eV. The number of natural potentials used along r and θ are 22 and 9 respectively. A total of 10 iterations was used to get an accurate fit.

4.2.2 Reaction probabilities

In Figure 4.1, the MCTDH reaction probabilities obtained using both the centrifugal sudden approximation and coupled channel methodologies are shown for four different J values. The results have been compared with a study performed using the split-operator method under the centrifugal sudden approximation[144].

As can be seen, the probability for lower Js have no threshold for upto $J = 10$. This is an expected behavior of a reaction without any barrier in its reaction path. The main feature of the curves for $J = 10$ is its dense oscillatory structure with

TH-1851_Sayak

a significant number of high intensity peaks in the low energy region. At higher energies, the peaks are of lower intensity. It can also be seen from the figure that the higher values of Js exhibit resonance structures of lesser density. This oscillatory behavior can be related to the potential well of depth 0.578 eV [114]

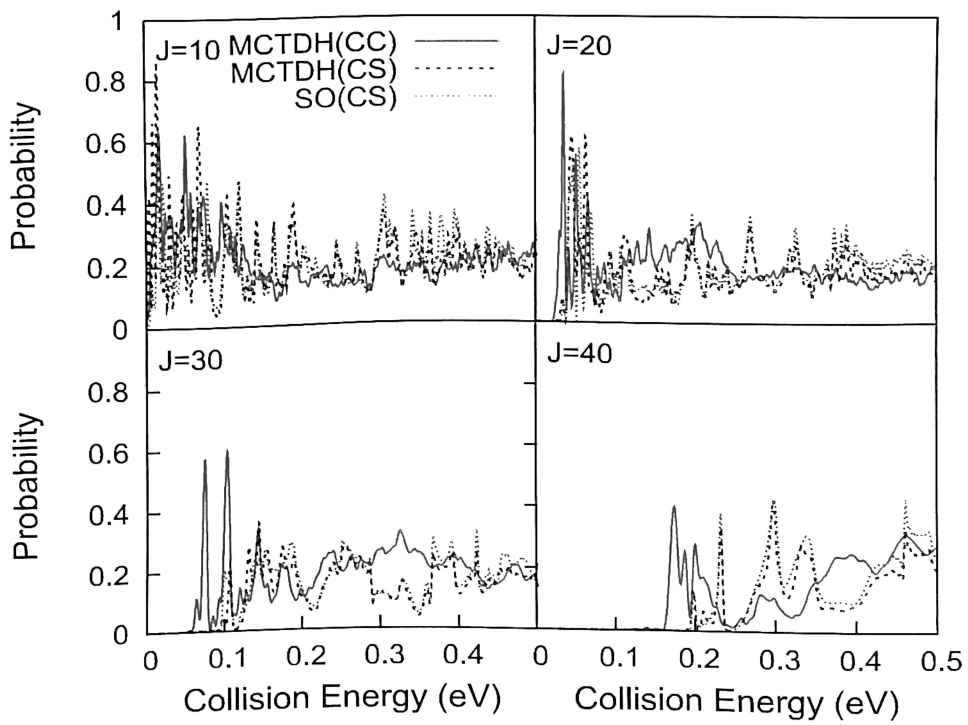


Figure 4.1: *Reaction probabilities obtained by MCTDH(CC), MCTDH(CS) and CS results obtained by split-operator(SO) method[144] for the He + H^+He ($v = 0, j = 0$) $\rightarrow$ HeH^+ + He reaction. The results are plotted for four different J values.*

which is expected to trap wave packets. The properties of resonance states can vary widely from those that are continuum scattering states to those that behave almost like a bound state depending on their relative lifetimes. The eigenvalue spectrum of He_2H^+ for $J = 0$ has been reported to support seven bound states [114]. It is also clear from figure that the threshold energy shifts to higher energy with an increase in J. This is due to the the increase in J dependent centrifugal

TH-1851_Sayak

barrier for the intrinsically barrier-less reaction. The probability peaks for $J = 20$ resemble those of $J = 10$, albeit with a shift in the threshold. For $J = 40$, the number of sharp oscillations is smaller and in fact broad structures can be seen above 0.3 eV.

The CS results obtained from both the MCTDH and the split-operator methodology, show an excellent agreement with each other for all J values considered, over the entire energy range. From here onwards, the CS results would refer to the calculations performed by the split-operator method. The CC calculations show a difference in the structure of peaks compared to the CS results. While sharp resonating structures are observed over the entire energy range for CS calculations, those are not visible for the CC results. This results from the significant influence of Coriolis coupling on resonance intermediates. Coriolis coupling provides an important decay mechanism to the resonance complex[151–153] which results in significantly lower number of oscillations being observed for the CC results. In the CS approximation, K(projection of J and j) remains unchanged during the reaction. Inclusion of Coriolis coupling allows the coupling of K states with K+1 and K-1 states. The significance of K-coupling increases with the value of J, leading to a more pronounced difference between the CS and CC results. For higher Js, the peaks at threshold for the CC results are of significantly higher intensity than those observed for the CS results. Moreover, the threshold for the CC results for higher Js are observed at smaller energies in comparison to the CS results.

The effect of increasing the vibrational energy of the reactant on the reaction probabilities for different J values are shown in Figures 4.2 and 4.3 respectively. While calculations have been carried out till $v = 2$ using the CS approximation, the same has been carried out till $v = 1$ using CC calculations. As observed in

TH-1851_Sayak

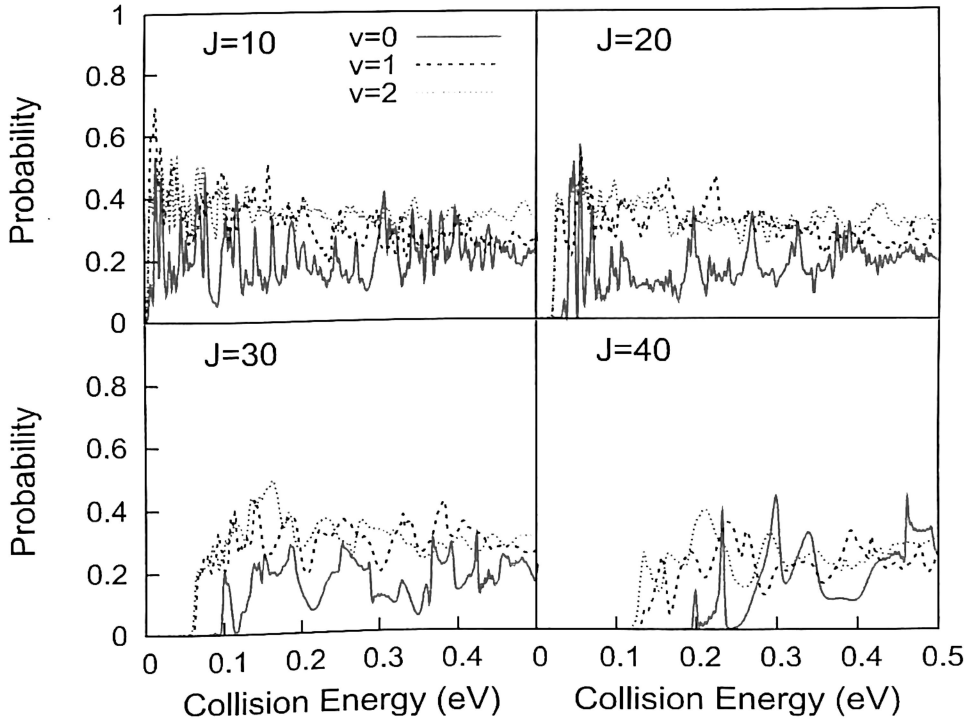


Figure 4.2: *Total reaction probabilities obtained by split-operator method for v = 0, 1 and 2 using CS approximation. The probabilities are plotted for four different J values as indicated in the figure.*

Figure 4.2, the reaction probability values for $J = 0$ are almost unaffected by increase in vibrational energy up to $v = 2$. But the sharp oscillations seen in case of $v = 0$, disappear with increase in v and smaller (and broader) peaks are observed, particularly at higher energies. For $J = 20$ and 30, the probabilities for $v = 1$ and 2 are in the same range. But the values are certainly higher than the ones for $v = 0$. Vibrational excitation does not seem to have much effect on the probability for $J = 40$. Also, a clear decrease in threshold energies for the reaction with increase in vibrational energy is visible for $J = 40$. In case of $J = 20$ and 30, the thresholds for $v = 1$ and 2 are almost the same.

The inclusion of Coriolis coupling in vibrationally excited state calculations dis-

TH-1851_Sayak

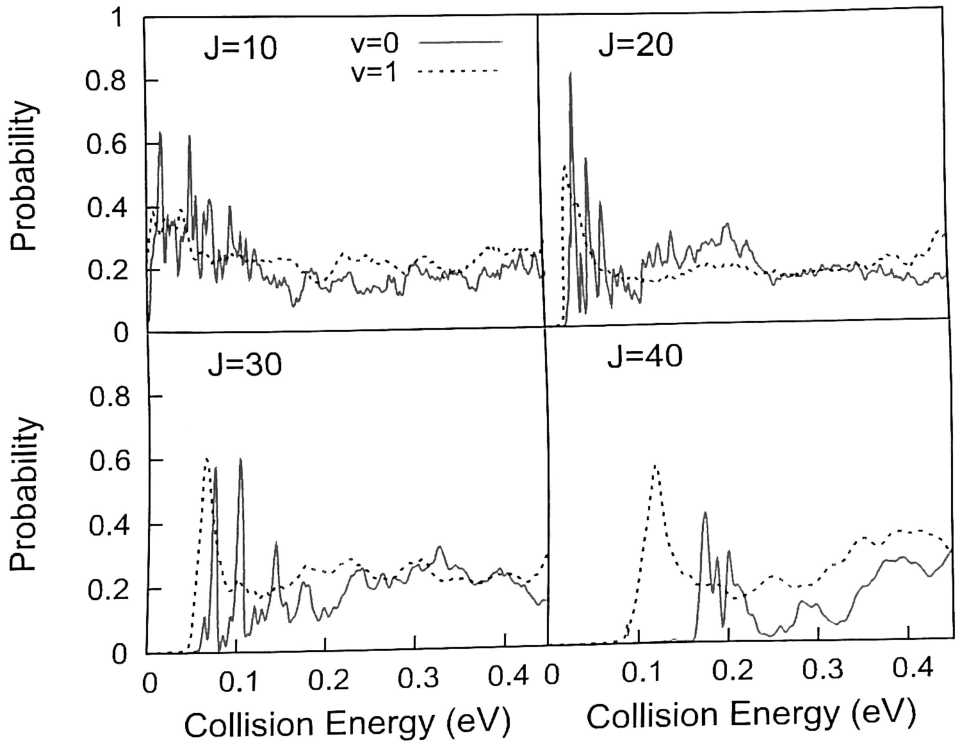


Figure 4.3: *Total reaction probabilities obtained by MCTDH(CC) calculations for $v = 0$, and 1. The probabilities are plotted for four different J values as indicated in the figure.*

plays the same trends as observed for the ground state results as seen in Figure 4.3. The resonance peaks for $v = 1$(CC) are diminished in comparison to $v = 1$(CS) results. The difference in the reaction probabilities between the results for $v = 1$ and $v = 0$ is smaller in case of CC results than the CS results, for $J = 20$ and 30. The shift in the threshold energy, in this case, is similar to that observed in case of the CS results but the probabilities for $J = 30$ and 40 show significantly higher peaks at the threshold. It is also observed that the reaction probabilities for $J = 40$ show an enhancement in reactivity upon vibrational excitation.

Figure 4.4 and 4.5 show the effect of additional reactant rotational energy on the reaction probability for the CS and CC results, respectively. For all the J values

TH-1851_Sayak

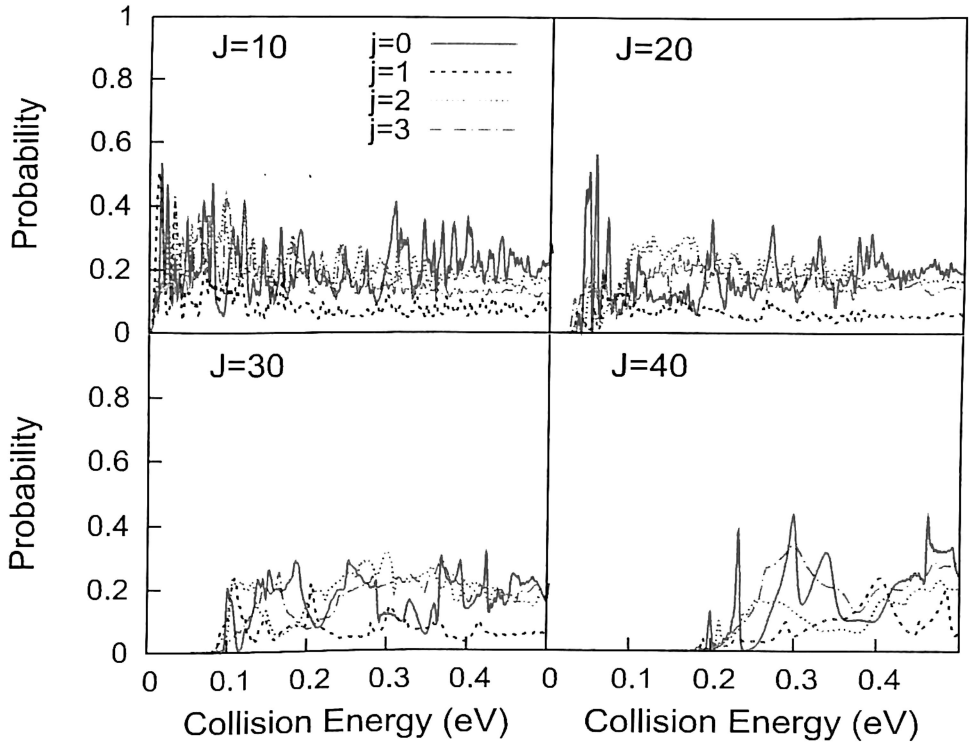


Figure 4.4: *Total reaction probabilities obtained by a split-operator method for j = 0, 1, 2 and 3 using the CS approximation. The probabilities are plotted for four different J values as indicated in the figure.*

in case of CS the reaction probabilities for the rotational excited states show lesser number of high intensity peaks compared to the ground state probabilities, over the entire energy range. Also the peaks become broader with increase in j. The CS and CC results show a significant difference for j =1. While a visible dip in the probability values is observed while going from $j = 0$ to $j = 1$ for all the J values in the CS results, the same is not observed in the case of CC. The reaction probabilities for $j = 1$ in the CC results show almost no significant variance from the $j = 0$ results. A similar effect was also observed for H + D_2 direct reaction[150], where the CC results predicted a slight increase in reactivity on rotational excitation. In contrary, the CS results[154] predicted a decrease

TH-1851_Sayak

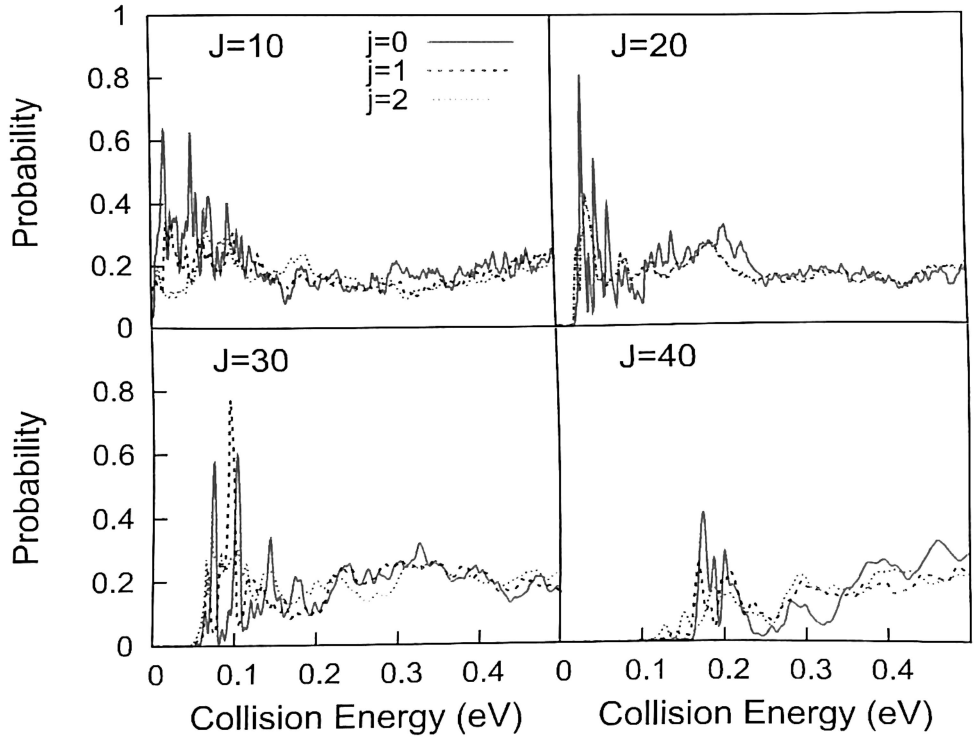


Figure 4.5: *Total reaction probabilities obtained by MCTDH(CC) calculations for j = 0, 1, and 2. The probabilities are plotted for four different J values as indicated in the figure.*

in reactivity. It is clear that the CS approximation is unable to account for the effect of initial rotational excitation of reagents, due to the neglection of the K-coupling[150]. No significant enhancement in reactivity is observed for excitation to higher rotational states. The reaction probabilities for higher Js in the CC calculations show a much smoother structure in comparison to the CS results and a generally good agreement with the peaks observed for $j = 0$.

The variations in reaction probabilities with m(the initial magnetic rotational quantum number of the diatom), for two different rotational levels ($j = 1$ and 2), are shown in Figure 4.6. For a given j. m=0 represents the planar approach of He towards HeH^+ while $m = j$ represents the situation where the orbital motion

TH-1851_Sayak

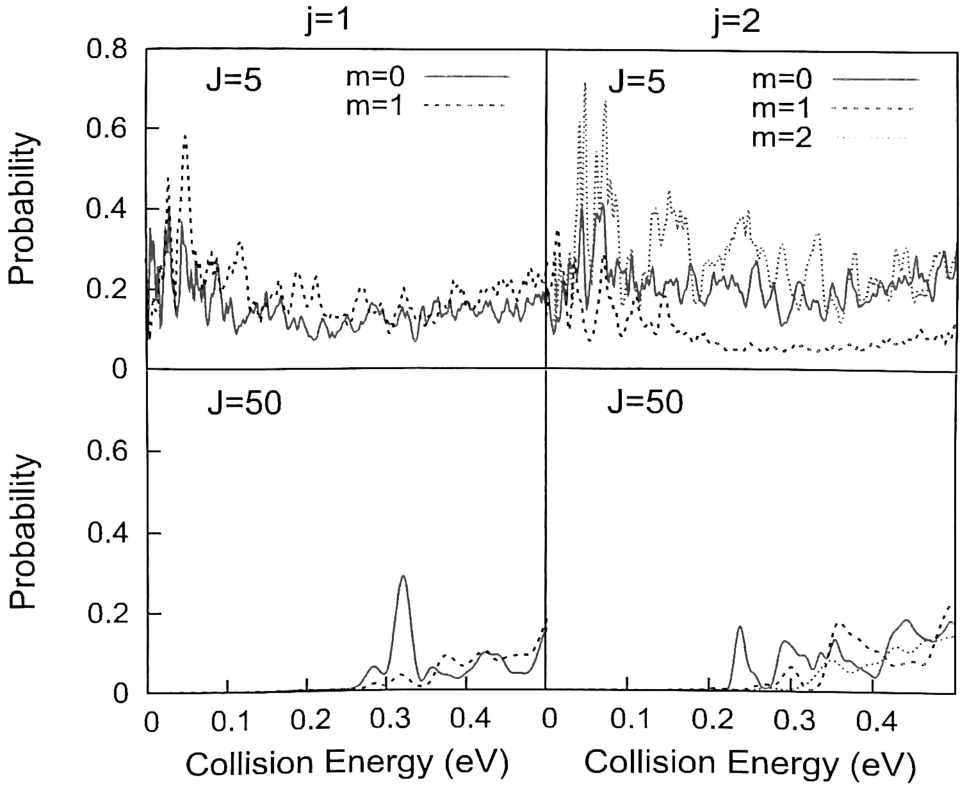


Figure 4.6: *Comparison of total reaction probabilities between different values of m for two different initial rotational states, at $J = 5$ and 50. The results have been obtained by MCTDH(CC) calculations.*

of He with respect to HeH^+ is perpendicular to the plane of rotation of HeH^+. It is clear from the figure that for $J = 5$, $m = 0$ and $m = 1$ have equal contribution to reaction probabilities while for $J = 50$, $m = 0$ has a greater contribution, especially near the threshold. This signifies a preference for a collinear reaction pathway at higher J values, while at lower J's other pathways of approach are equally probable. This is contrary to conclusion on the dynamics of approach of the reactants derived for a similar comparison in the CS results[144]. This is expected in view of the difference in reactivities observed between CS and CC calculations as mentioned earlier. The picture becomes somewhat complicated in case of $j = 2$ for which there are three different values of m. The dominance of m

TH-1851_Sayak

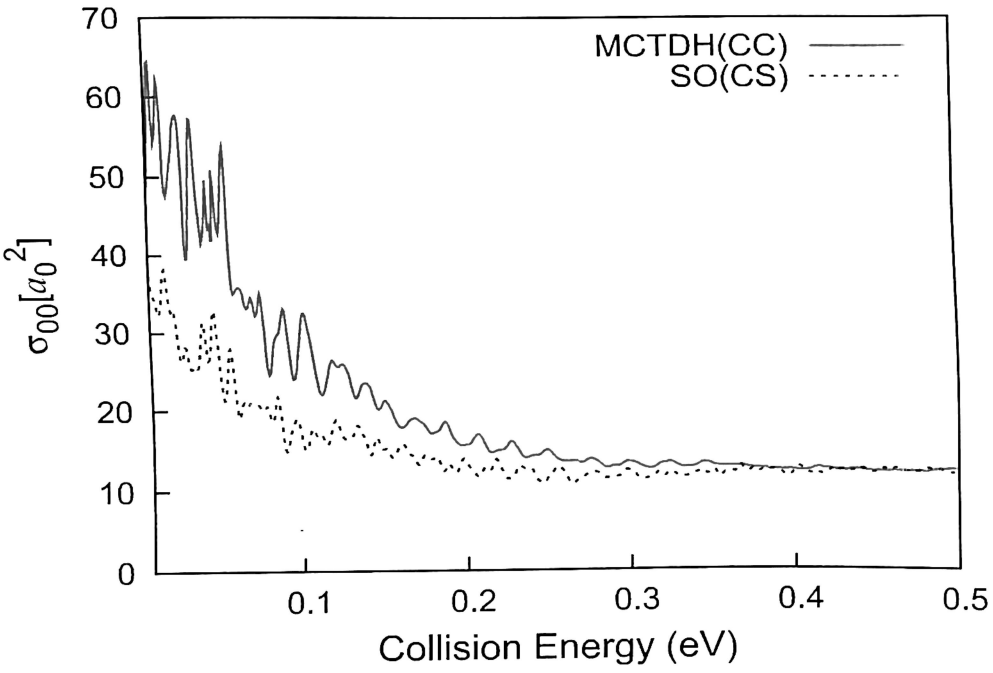


Figure 4.7: *Comparison of integral cross sections obtained by MCTDH(CC), and the CS results obtained by split-operator(SO) method for* $v = 0$, $j = 0$.

$= 2$ over $m = 0$ and 1, in the entire energy range shows a clear preference for a perpendicular approach of reagents at lower Js for the $j = 2$ state of the system. For $J = 50$, variation in m does not have any significant effect on the probability values. It is clear that rotational excitation of the reactant affects the dynamics of this proton transfer process. This is further discussed in the next section where the picture becomes clearer for the integral reaction cross sections.

4.2.3 Integral cross sections

To obtain converged integral reaction cross section, the reaction probabilities were calculated for all the J values in the range $0 \leq J \leq J_{max}$, where J_{max} was between 60-70, depending on the initial vibrational state of the reagent. The integral cross

TH-1851_Sayak

sections obtained from the MCTDH calculations are plotted in Figure 4.7 along with the CS cross sections. The cross sections show no threshold and are very large at low collision energies with conspicuous kink structures in the low energy region. The resonance structures seen in the probability plots are not totally washed out but their number and intensity decrease with increase in energy. In this regard, the dynamics of the present reaction is similar to other reactions with deep well along the reaction path[146, 155, 156].

It is observed that inclusion of Coriolis coupling in the calculations resulted in larger integral cross sections at lower energies with more oscillatory structure. The effect of CS approximation on ion-molecule reactions has been recently reviewed by Chu and Han[145] and E. L. Wu[157] by studying He + H_2^+, D^+ + H_2, D^- + H_2 and the H^- + D_2 systems. For the He + H_2^+ and the D^+ + H_2 systems, the CC cross sections are larger than the CS results at lower energies, while the difference becomes significantly smaller at higher energies. For D^- + H_2, while the CS and CC results show a good agreement at lower energies, the CS approximation clearly overestimates the cross sections at higher energies. The study on H^- + D_2 reaction reveals that the CC results are significantly smaller than the CS cross sections over the entire energy range considered. The effect of inclusion of Coriolis coupling on cross sections for the He + H^+He reaction system is similar to that observed for the He + H_2^+ and the D^+ + H_2 systems[145]. For ion-molecule reactions, the reaction dynamics at low energies is dominated by a complex formation mechanism. The collisions are not sudden in nature and subsequent breakdown of the resonance complexes is favored by the orientational changes of the molecule involved. The CS approximation artificially hinders the collision induced orientational changes in the angular momentum vectors[158] and thus significantly underestimates the

TH-1851_Sayak

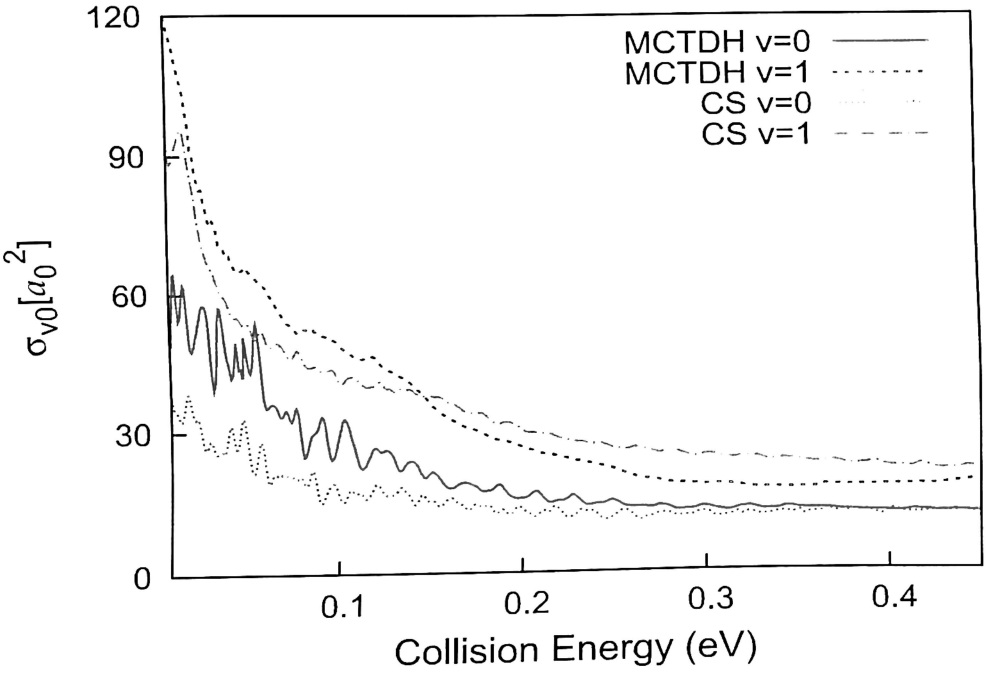


Figure 4.8: *Integral reaction cross sections plotted as a function of collision energy for $v = 0$ and 1 states of HeH^+. The diatom is in its ground rotational state. The MCTDH results have been compared with the CS results obtained by a split-operator method.*

reaction cross sections at low energies. At higher energies, the differences between the CS and CC cross sections decrease and they are almost similar above 0.35 eV. The formation of products at higher energies is facilitated by sudden collisions which results in a significant improvement in the CS results. It is predicted that a short-lived intermediate is formed which breaks down easily at higher energies and this results in improvements in the results from the CS approximation at higher energies. The presence of long-lived complexes would have resulted in larger cross sections from the CC calculations in comparison to the CS results over the entire energy range unlike what is observed for the present reaction system.

The effect of vibrational excitation of the reagent ground state, on integral

TH-1851_Sayak

reaction cross sections is shown in Figure 4.8. The cross sections for $v = 1$ are larger than the ones for $v = 0$ for both CS and CC. Also the oscillatory structures of the $v = 0$ curve are somewhat smeared out in the curve for the excited state plot. The vibrational enhancements in cross sections are almost similar for the CS and CC results in the low energy regime. The observed difference between the ground and excited state cross sections narrows down at higher energies for the CC results. A similar trend is not observed for the CS results, where the $v = 1$ cross sections show a significant enhancement compared to those for $v = 0$ at higher energies. A comparison of the CC and CS results for $v = 1$ show larger cross sections for CC results in lower energies. For energies beyond 0.15 eV, CS approximation results overestimate the exact excited state cross sections. These differences at higher energies for $v = 1$ are in contrast to the $v = 0$ results.

The effect of initial rotational excitation on the integral cross sections is shown in Figure 4.9 and 4.10 for the CS and CC results, respectively. While the CS results reported excited cross sections for $j = 1$, 2 and 3, excited state cross sections using the MCTDH(CC) methodology were calculated for $j = 1$ and 2. It is observed that for both CS and CC calculations, cross sections for $j = 2$ and 3(CS only) at the onset are smaller than those for the rotational ground state. The results for $j = 1$ exhibits values similar to that of $j = 0$. Thereafter, the figure shows a decline in the cross section values for all the rotational states before attaining a constant value. The initial high peaks for $j = 0$, 1, 2 and 3(CS) indicate the existence of a certain orientation of the reagents for which the reagents approaching each other along this path have an enhanced probability to react. The average torque exerted on an initially slowly rotating HeH^+ molecule during the collision time in case the approach of the reagents take place in an unfavored orientation may well

TH-1851_Sayak

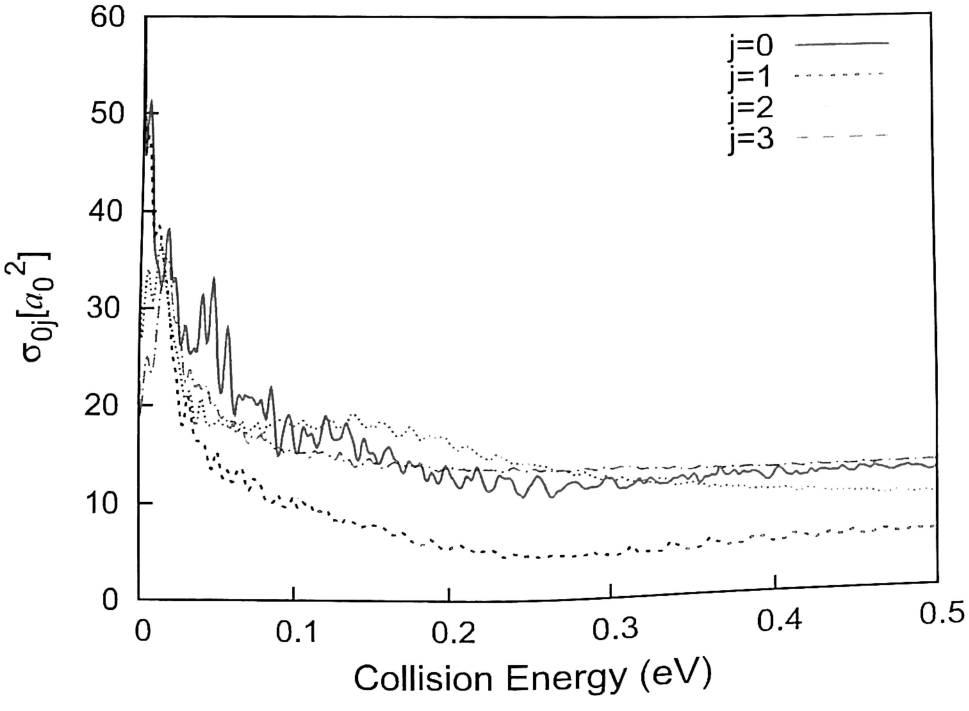


Figure 4.9: *Integral reaction cross sections plotted as a function of collision energy for j = 0, 1, 2 and 3 of HeH^+ while the diatom is in its ground vibrational state. These CS results are obtained by a wave packet propagation using a split-operator method.*

be sufficiently large to force it into the preferred orientation and thus make the reaction possible again. However, with increase in angular momentum the mean restoring action of these torques diminishes and the cross sections decline steeply.

Figure 4.10 shows the effect of inclusion of Coriolis coupling on the reaction cross sections for rotational excitations. It is clear that there is a significant difference in the CC results when compared with the CS results. While the CS results show a significant decrease for j =1 above 0.1 eV in comparison to j = 0, no such decrease is observed in the CC results. This owes its origin to the inadequacy of the CS approach to describe the orientational dynamics. The variation in the

TH-1851_Sayak

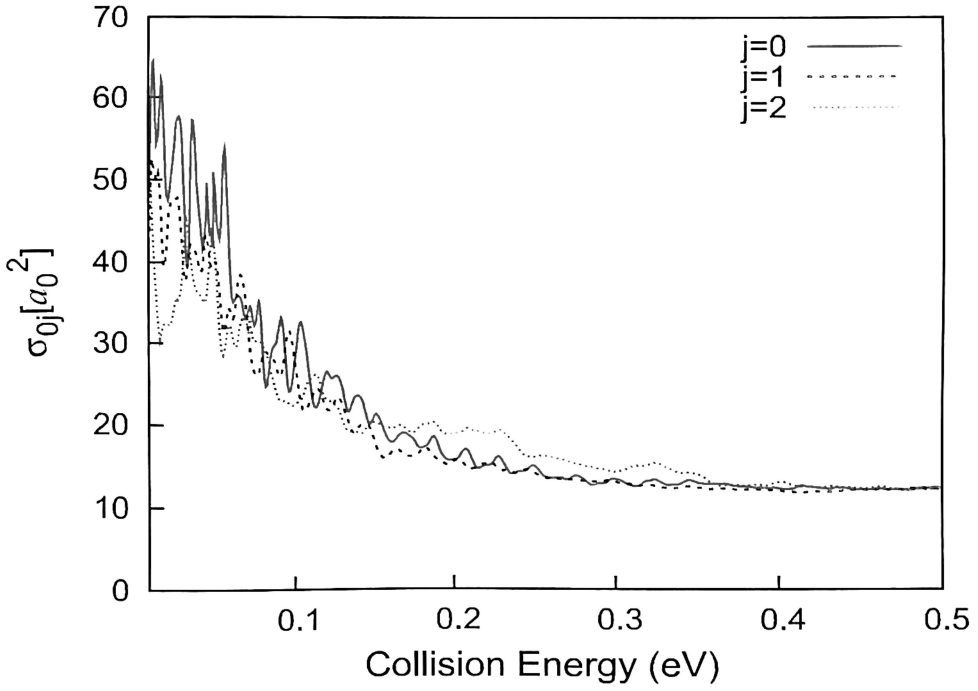


Figure 4.10: *Integral reaction cross sections plotted as a function of collision energy for j = 0, 1, and 2. The diatom is in its ground vibrational state. The results are from MCTDH(CC) calculations.*

cross sections for $j = 2$, in comparison to $j = 0$, are similar for both CS and CC results upto 0.3 eV. At higher energies, the excited state($j = 2$) CC results show an overlap with the ground state cross sections and the CS approximation leads to an underestimation in the cross section values.

The dependence of the CC reaction cross sections on the m-values for $j = 1$ and 2 are shown in Figure 4.11. For $j = 1$, it is observed that the contribution from $m = 0$ is higher than that from $m = 1$ at energies below 0.1 eV. Above 0.3 eV, the trend reverses with $m = 1$ showing higher contributions compared to $m = 0$. This signifies a preference for the planar approach of the reactants at lower energies while a perpendicular approach is preferred at higher energies for the reagents in their initial rotational excited state($j = 1$). For $j = 2$, both the planar(m=0)

TH-1851_Sayak

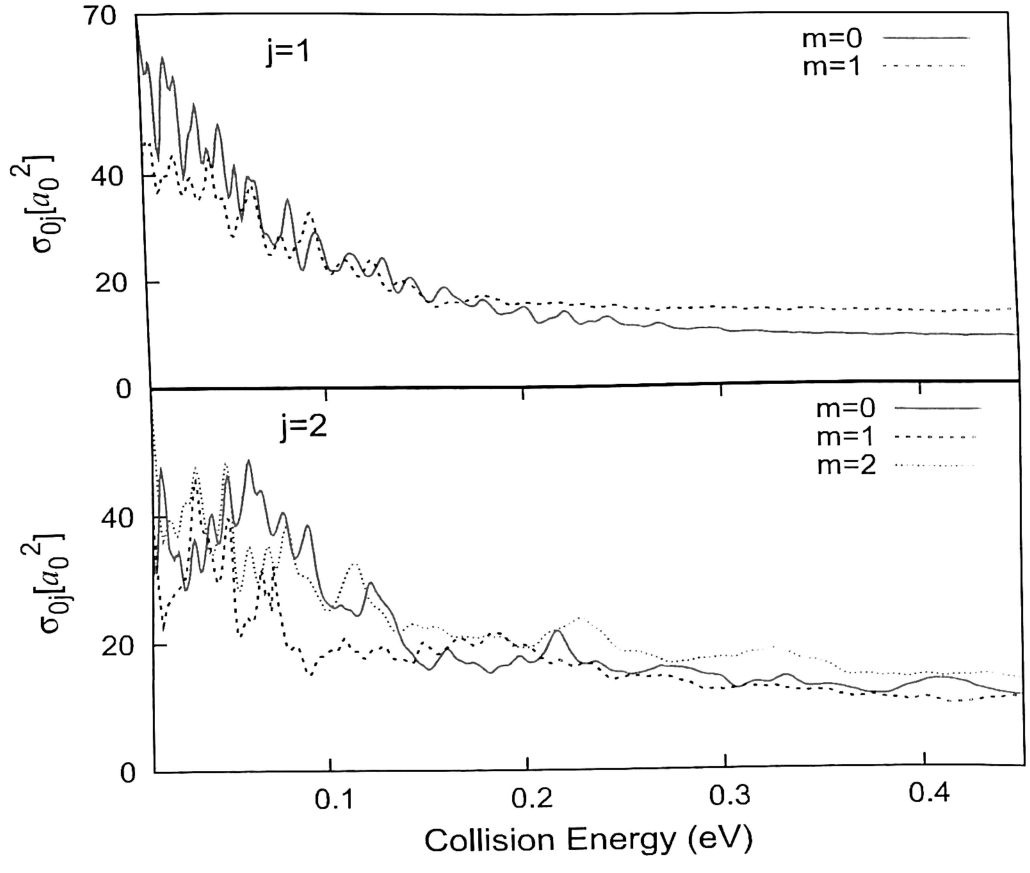


Figure 4.11: *Comparison of reaction cross section for different values of m, for rotational states j = 1 and 2. The diatom is in its ground vibrational state. The results are from MCTDH(CC) calculations.*

and the perpendicular($m = 2$) approach of reagents have similar contribution to the reaction cross section at lower energies. This signifies no preferred pathway of approach in the low energy regime. At energies above 0.2 eV, the $m = 2$ contribution is marginally higher than the contribution from $m = 0$. It can be inferred that for $j = 2$, a perpendicular approach of the reagents is preferred at higher energies which is similar to that observed for $j = 1$.

TH-1851_Sayak

4.3 Summary and Conclusions

Wave packet studies were performed for the ion-molecule He + H^+He system using the MCTDH methodology with an exact form of the Hamiltonian. A comparative study was carried out with the results obtained using an approximate Hamiltonian. The effect of inclusion of Coriolis coupling in ion-molecule reactions varies from system to system and hence it is imperative to carry out exact calculations to arrive at a conclusion. This study throws up various interesting characteristics of this ion-molecule reaction and shows the influence of Coriolis coupling on the reaction dynamics.

The reaction probability curves are characterized by sharp resonance structures, especially at the threshold, while the intensity of the peaks decrease followed by subsequent broadening at higher energies. The CC results show a distinct difference in the structure of peaks and threshold characteristics, in comparison to the CS results. A significantly smaller number of resonance peaks are observed in the CC studies over the entire energy range, compared to the CS results. The importance of inclusion of Coriolis coupling increases with increase in J due to a greater role of K-coupling, which is neglected in the centrifugal sudden approximation. For intermediate and higher Js, the thresholds for the CC reaction probabilities become smaller than the CS results and a sharp increase in intensity is observed at the threshold. The resonance peaks are conspicuously absent in the reaction probabilities for the $v = 1$ state. This is accompanied by a strong threshold shift to lower energies for higher J values. For rotational excitations($j = 1$ and 2), the CC reaction probabilities show no significant changes from the $j = 0$ state. There is a significant underestimation of reaction probabilities for the $j = 1$ state

TH-1851_Sayak

in the CS calculations. The orientational dynamics has been studied for the rotational excited states of the reactants. For $j = 1$, there is a preference for collinear reaction pathways for higher J values. On further rotational excitation($j = 2$), a perpendicular approach is preferred for lower Js, while no particular preferred pathway of approach can be predicted for higher J values.

A comparison of the CC and CS cross sections underlines the significance of inclusion of Coriolis coupling in the dynamics of the present system. The CC cross sections are significantly higher at the threshold and at lower energies, while the difference narrows down at higher energies. The breaking of the collision complex to products is much less favorable within the CS approximation. The presence of a short lived reaction intermediate and the phenomenon of sudden collisions occurring at higher energies, explain the agreement between the CS and CC cross sections in this regime. Comparison of CC and CS cross sections for $v = 1$ shows an interesting feature. While the CC results are larger than the CS results till 0.15 eV, the trend reverses beyond 0.15 eV. Excitation to higher rotational states($j = 1$ and 2) does not affect the CC cross sections in a significant manner. This underlines the inadequacy of the CS methodology in predicting the orientational dynamics for initial rotational excitations. An insight into the preferred pathway of approach for rotationally excited states have been obtained from the study of m-dependent CC cross sections. At the lower energy regime, while a perpendicular approach of reagents is preferred for $j = 1$, all pathways of approach become equally favorable for j =2. For higher energies, a preference for the perpendicular pathway of approach of the reactants is observed. The importance of the initial orientation of the reagents in the reaction dynamics of the He + H^+He system.

TH-1851_Sayak

Chapter 5

$H_2 + OH \rightarrow H_2O + H$: Effect of Surface Topology on Reaction Dynamics

5.1 Introduction

In the field of reaction dynamics, the emphasis on reactions beyond three-atom cases, traditionally represented by A + BC → AB + C has been steadily increasing. *Ab initio* dynamical studies of four-atom reactions of the type AB + CD → ABC + D have evoked considerable interest, specially in the last two decades. Within this class of reactions, for both theoretical and experimental reasons, the process H_2 + OH → H_2O + H has emerged as a prototype for direct four atom reactions that occur without the formation of a collision complex. This reaction is in a number of respects the simplest reaction in which a H-atom is transferred

TH-1851_Sayak

to a molecular free radical. The reaction is exothermic by $\sim$ 0.659 eV[159] and has an energy barrier of 0.234 eV[160] along the reaction path. Apart from the potential importance of this reaction in atmospheric and combustion chemistry, the moderate exoergicity, availability of reasonably good potential energy surfaces [91–94, 161–164], and possibility to compare with experimental results over a wide range of temperatures have made this reaction a natural choice for theoretical investigations. With three of the four atoms in the reaction system being hydrogen, the total number of electrons is relatively small, thus enabling accurate *ab initio* calculations of the potential energy surface. This presents an excellent opportunity for theoretical investigations employing different methodologies, ranging from quasi-classical trajectory methods to reduced and full dimensional quantum scattering calculations.

In the present work, the MCTDH method has been used to perform a detailed and comprehensive study of the H_2 + OH system on three different potential energy surfaces. While MCTDH has been previously applied to study inelastic tetra-atomic systems like H_2 + H_2[118, 119, 165], a successful application for studies on reactive tetra-atomic systems would serve as an effective test for the accuracy and gains envisaged in the algorithm. A successful application is expected to go a long way in studying more complicated systems including those with higher degrees of freedom. The accuracy has been tested on the Walch-Dunning-Schatz-Elgersma (WDSE)[91, 92] and Yang-Zhang-Collins-Lee(YZCL2)[94] surfaces on which exact quantum dynamical results for ro-vibrational ground state calculations serve as an excellent reference. The study has been subsequently extended to the Wu-Schatz-Lendvay-Fang-Harding (WSLFH)[93] surface on which no exact quantum dynamical calculations have been performed till date, for obtaining $J > 0$ reaction

TH-1851_Sayak

probabilities. This chapter begins with a brief look into the available experimental and theoretical results along with a knowledge of the PESs in use, which would help us in formulating the problem and specify our objectives. This is followed by the numerical details of our calculation. The detailed results and discussions for the ro-vibrational ground state and excited state calculations on the WDSE, YZCL2 and WSLFH surfaces are given in the next section. The chapter ends with a summary of all obtained results and the conclusion derived on the importance of surface topology on reaction dynamics.

5.1.1 Experimental results

The H_2 + OH reaction has been subject to various kinetic experiments[95–97, 166–185] performed over a wide range of temperatures (200-3000 K). The experimental activation energy has been measured to be 0.17 eV[161]. Experimental data on the H_2 + OH reaction are mainly related to the measurement of thermal rate constants and studying the influence of initial vibrational excitation, translational excitation and isotopic substitution on the reaction dynamics. The rate constants and their variation with temperature are as well established as for any bimolecular reaction. Experimental work related to the kinetics and the dynamics of the reaction over three decades have been reviewed by Smith et al.[186] and more recently by Baulch et al.[187] Studies of reaction systems like the H_2 + OH which possess a barrier can be broadly based into three different energy regimes: (1) reaction at energies much above the barrier where dynamical effects are dominant (2) reactions at energies comparable to the barrier height where rate coefficients are sensitive to the barrier (3) reactions at very low energies which make passing over the barrier virtually

TH-1851_Sayak

impossible leaving the tunneling phenomenon as the most important pathway. The third scenario is particularly important for the H-atom transfer process, as in the present system and has been duly investigated. While the height and position of the barrier influences the dynamical calculations associated with the first two scenarios, the kinetic parameters at lower energies is expected to show greater dependence on the width and shape of the reaction barrier.

The detailed experimental works have revealed a slight curvature in the Arrhenius plots of ln $k(T)$ *vs.* $1/T$ but various modifications of the Arrhenius expression($k_T = AT^n e^{-E/RT}$) were performed to achieve an accurate fit of the data over the entire range of temperatures considered. The methodologies of experimental studies have greatly evolved over the last few decades. Initial investigations on the $H_2(v_1 = 0, j_1 = 0)$ + $OH(v_2 = 0, j_2 = 0)$ system by Overend et al.[172] involved flash photolysis and they obtained a rate coefficient of 5.79×10^{-15}cm^{3}molecule^{-1}sec^{-1} at 300 K. Pulsed vacuum UV photolysis studies performed by Atkinson et al.[170] over the temperature range 298-425 K yielded a rate coefficient of 6.97 $\pm$0.7 $\times10^{-15}$ cm^3 molecule^{-1} sec^{-1} at room temperature with an Arrhenius expression k_T = 5.79×10^{-12}exp(-2008/T). Tully and Ravishankara[175] performed similar studies over an extended range of temperatures (298-992 K) and reported k_{298} = (6.08 $\pm$0.37) $\times10^{-15}$cm^{3}molecule^{-1}sec^{-1} and k_T = $4.12\times10^{-19}T^{2.44}$exp(-2008/T). Discharge flow studies by Steinert et al.[96] yielded $k_{298} = 6.1\times10^{-15}$cm^{3}molecule^{-1}sec^{-1} in good agreement with previously reported values. At higher temperatures, the reaction is reported to exhibit a non-linear Arrhenius behavior with a pronounced upward curvature[161, 171, 176]. The rate coefficients in the higher temperature range (1700-2500) were measured by Frank and Just[188] using the shock tube methodology with the variation of

TH-1851_Sayak

rate coefficients given by $k_T = 7.9\times10^{-11}$exp(-3067/T). Oldenborg et al.[189] measured k_T over a temperature range of 800-1550 K. They combined their data with those of Ravishankara et al.[176], Tully et al.[175], Sutherland et al.[178], Frank and Just[188] and derived the expression $k_T = 3.56\times10^{-16}T^{1.52}$exp(-1736/T) to cover a broad temperature range of 250-2581 K. This was followed by similar studies by Talukdar et al.[183] using pulsed laser photolysis for investigating rate constants in the low temperature range of 230-420 K. The expression derived by Oldenberg et al.[189] agreed with their results except for temperatures below $\sim$ 250 K where a deviation of $\sim$ 20% was observed. Talukdar et al.[183] presented a modified expression $k_T = 7.2\times10^{-20}T^{2.69}$exp(-1150/T) for a better fit especially in the lower range of temperatures. A very pronounced isotopic effect was observed when the rate constants for HD + OH were measured and compared with those relative to the isotopic variants $H_2/(D_2)$ + OH[183]. A significant decrease of reactivity on going from H to D suggested a strong increase in the importance of tunneling contribution with a decrease in temperature[161, 176, 183].

In addition to the kinetics of the reaction, the reaction dynamics has also been investigated by various groups. The crossed molecular beam experiments by Alagia et al.[161, 190] on D_2 + OH indicate that about two-thirds of the energy released in the exothermic reaction between OH radicals and H_2/D_2 is channeled into the internal motions of the H_2O(HOD) product. Absolute cross sections for the H_2 + OH were measured by Wolfrum et al.[191, 192] using the pump-probe technique. The measured values of the cross section are $\sigma_{H_2+OH} = 0.08\pm0.03$ and 0.60 ± 0.30 Å^2 at the collision energy of 0.17 and 0.22 eV respectively. The transition state region of the title reaction has been investigated by photoelectron spectroscopy of the H_3O^- ion by Neumark, Lineberger and co-workers[182], while Loomis et

TH-1851_Sayak

al.[193] have succeeded in stabilizing the OH and $H_2/(D_2)$ reactants in a weakly bound complex. Although a large number of experimental studies have been performed to give a detailed information for the H_2 + OH reaction in its ro-vibrational ground state, similar studies on the effect of excitation of reagents are very few[95–97, 173]. Experimental information on the reaction dynamics obtained by Light and Matsumoto[173], showed that the reaction rate was appreciably enhanced(by a factor of 150) by excitation of $H_2(v_1 = 0)$ to $H_2(v_1 = 1)$, whereas similar excitation of OH produced at most a 50% increase in reaction rate[97, 174, 177]. Since the reaction considered is a direct reaction, the rate will be enhanced most effectively by excitation of the vibration along the bond that is broken in the reaction(in this case the H-H bond), whereas excitation of any other bond(in this case O-H bond) is much less effective. The flow tube studies by Zellner et al.[96] and Glass et al.[97] reported absolute values of (7.5±3) × 10^{-13} cm^3 $molecule^{-1}s^{-1}$ and (9.9±2.4) × 10^{-13} cm^3 $molecule^{-1}s^{-1}$ respectively for $H_2(v_1 = 1, j_1 = 0)$ + $OH(v_2 = 0, j_2 = 0)$ at room temperatures. This amounted to an enhancement in rate constants by a factor of 120 and 155 respectively at room temperature. The rate constant obtained by recent laser spectroscopic studies performed by Hanf et al.[95] for $H_2(v_1 = 1)$ is (1.2±0.1)10^{-13} cm^3 $molecule^{-1}s^{-1}$ at room temperature indicating significant smaller rate enhancements on excitation of H_2. The differences in the results obtained can be attributed to the inaccuracies accumulated in the older methodologies.

TH-1851_Sayak

5.1.2 Potential energy surface

In order to completely predict the experimental results, it is imperative to carry out both electronic structure calculations to obtain the potential energy surface as well as nuclear dynamics calculations to reliably extract reaction dynamics information. The first *ab initio* calculations for the system were performed by Walch and Dunning[91] who carried out high quality, large-scale polarization configuration interaction calculations on the barrier height and transition state geometry for HHOH. They calculated a barrier height of 0.264 eV which was higher than the experimentally obtained barrier height of 0.17 eV for the reaction system. The saddle point geometry was found to be coplanar and resembling the reactants, as expected from a reaction with high exoergicity. The *ab initio* energy points in the vicinity of the reaction path were evaluated only for planar configuration. The potential energy surface was characterized with an early barrier in the entrance channel followed by a non physical deep well. Schatz and Elgersma[92] obtained an analytic potential energy surface, thereafter called WDSE. based on an approximate fit of the *ab initio* points calculated by Walch and Dunning[91]. The *ab initio* points were fitted to the surface by using a function consisting of two, three and four body terms. In spite of the initial success in studying the reaction dynamics, the WDSE surface has several known defects[194. 195]:(1) some features of the transition state geometry are incorrect, (2) there are spurious wells in the H_2 + OH entrance channel. (3) only one of the H atoms in the water molecule is capable of reacting with the incident H, (4) the H_2O anharmonic force field is inaccurate. Rashed and Brown[196] modified the WDSE surface by adding a cubic spline term to the Morse potential resulting in the removal of the spurious wells observed in the entrance channel of the surface. The character of the poten-

TH-1851_Sayak

tial near the saddle point geometry was retained in the modified surface since the high density of *ab initio* points in the region resulted in a good analytic fit of the original surface. The correction of the spurious minima in the WDSE surface by Rashed and Brown[196] in turn introduced spurious peaks in the potential in the form of a non physical barrier as pointed out in subsequent studies by Harrison and Mayne[197]. In view of this inaccuracy, Clary[159] in a later work sought to remove the non physical features in the WDSE surface by multiplying the four body term in the functional form of the potential by a function which damps out the non physical well and the long range barrier in the H_2 + OH entrance channel. This damping function however left the geometry and energy of the transition state unaffected.

Issacson[198] proposed a new PES for modelling the dynamics of the title reaction. This new potential form not only resulted in better fits of the available data at the saddle point compared to the previous surfaces[92, 196], but also reproduced the new barrier shape computed by Dunning et al.[199] The importance of the assumed functional form of the PES was underlined, as fitting of different functional forms to the same set of data resulted in profoundly different predictions for the rate constant. Two key properties of the PES were pointed out which determined the choice of the functional form. Firstly, the barrier height, which strongly affects the reaction rate by determining the number of collisions that have sufficient energy to react. Secondly, the barrier shape or width, which significantly affects the reaction tunneling along with determining the particular reaction path curvature for a given functional form. In spite of the better fit to the *ab initio* data, the surface had some inherent deficiencies. Firstly, the hydrogen atoms of the H_2 diatom had not been treated equivalently which rendered the surface unsuitable

TH-1851_Sayak

for accurate quantum dynamics calculations. Secondly, spurious local minima and maxima remained, which led to inaccuracies in the results. Truong[200] carried out a direct dynamics study of vibrational state selected reaction rates. This approach calculates a reaction path using accurate *ab initio* theory and a full variational transition state theory plus multidimensional semi-classical tunneling approximations within a statistical diabatic model. Calculated thermal and state selected rates for the $H_2(v_1 = 0,j_1 = 0) + OH(v_2 = 0,j_2 = 0)$, $H_2(v_1 = 1,j_1 = 0) + OH(v_2 = 0,j_2 = 0)$ and $H_2(v_1 = 0,j_1 = 0) + OH(v_2 = 1,j_2 = 0)$ reactions were found to be in excellent agreement with available experimental data. Comparison with reference data on the WDSE surface led to a conclusion that the potential energy function for the WDSE surface is too large which explains the large kinetic isotope effects at lower temperatures on the WDSE surface. This approach, however, does not yield a potential energy surface that can be used in more general dynamics calculations such as quantum scattering and QCT computations.

Although a large number of quantum dynamical studies have been performed on the WDSE PES, different groups have concluded that the rate coefficients obtained on the WDSE surface have been considerably larger than the experimental results, especially at lower temperatures[201–203]. To improve the accuracy of results, Alagia et al.[161] developed a new surface known as Kliesh-Werner-Clary(KWC) surface based on extensive *ab initio* calculations. Among the many anomalies pointed out in the WDSE surface, the incorrect transition state structure affects the reaction dynamics significantly. This was corrected for the first time in the KWC PES with a correct "cis" form of transition state structure. In the longer range region for both reactants and products, damping functions were utilized to damp out both spurious wells and barriers. In spite of the improve-

TH-1851_Sayak

ments on the earlier surfaces, certain inaccuracies remained in the new surface. Firstly, not enough *ab initio* points were calculated for positions far away from the saddle point region to achieve an accurate global fit. As a result, properties like reaction dynamics at high energy, or photo-detachment spectra of H_3O^-, that depend on the geometry well away from the transition state region or the minimum energy path are not expected to be accurate. The *ab initio* energies of Alagia et al.[161] was used by Ochoa de Aspuru and Clary to construct the OC surface[163] on which QCT[204, 205] and full dimensional QM[206] studies were reported. At temperatures below 300 K, the calculated rate constants were seen to be above the experimental values, thus suggesting either the surface allows for too much tunneling due to a narrow minimum energy path or the vibrational adiabatic barrier is too low. Schatz and collaborators produced a new PES, known as WSLFH[93], which is symmetric with respect to the two hydrogen atoms of the water molecule. The WSLFH surface is a functional fit to a more extensive and reasonably accurate *ab initio* data compared to the WDSE surface. QCT studies on both OC and WSLFH surfaces were reported by Troya and co-workers[205]. The OC surface was observed to overestimate the cross sections close to the threshold for the reverse reaction when the water is vibrationally excited while the WSLFH surface showed the trend predicted from *ab initio* calculations[207]. It was also observed that the product state distributions for the reverse reaction were better reproduced by QCT calculations using the WSLFH PES than by the OC PES[208]. The presence of a broad attractive well in the OC surface differentiates it from the WSLFH surface which is well behaved and devoid of any spurious features. Goldfield et al.[203] carried out six-dimensional wave packet propagation on the WSLFH surface and concluded that the WSLFH potential energy surface underestimates the experimental rate constant by a factor of 2-4 over a broad temperature range. In

TH-1851_Sayak

spite of significant improvements in the WSLFH surface compared to the previous PESs, it has some inherent deficiencies. Firstly, the WSLFH surface allows only one H-atom in the H_2 diatom to react[204, 209] and secondly, the influence of the second low lying degenerate electronic state in the H_2 + OH entrance channel was not taken into account in the WSLFH surface.

At the beginning of this decade, Bettens et al.[164] and Zhang et al.[210]reported two new PESs for the H + $H_2O \rightarrow H_2$ + OH reaction with the former surface denoted as BJCZ surface. Both the PES's were constructed using interpolation of high-level *ab intio* data over the full six-dimensional configuration space and including a large range of molecular geometries. The later surface by Zhang et al.[210] was more accurate of the two as in contrast to the former surface[164], no additive or scaling approximation of the gradients had been employed. Both PESs accurately described the entrance channel for the H_2O + H system upto the saddle point extending only a little further into the H_2 + OH channel. The presence of a second low-lying nearly degenerate state in the entrance channel of the H_2 + OH reaction resulted in an impediment to accurate description of the H_2 + OH entrance channel as there is considerable difficulty in application of *ab intio* methods which are based on a single reference determinant. Yang et al.[160] developed a new global PES known as YZCL1 for the H_2 + OH reaction. The near degeneracy of the ground and first excited states was taken into account by employing the CMRCI+Q method in a substantial part of the H_2 + OH entrance channel. For other regions, QCISD(T)/6-311++G(3*df*,2*pd*) level of theory was employed. The resultant ground state PES was thus a hybrid of a number of *ab initio* estimates of the electronic energy. To improve the YZCL1 surface, an additional 1600 energies were calculated using the unrestricted coupled-cluster

TH-1851_Sayak

HI-TECH TEMP

theory (UCCSD(T)/aug-cc-pVQZ) level of theory. The barrier heights for the YZCL1 and YZCL2 surfaces relative to the H_2 + OH equilibrium reactants are 0.248 eV and 0.234 eV, respectively. A significant difference is observed in the reaction dynamics on the two surfaces with the YZCL2 surface giving better and highly accurate results in comparison to the experimental data.

Very recently, a new PES was developed by Xiao et al.[211] and calculations were performed for the HD + OH $\rightarrow$ H_2O + D reaction. This PES was purely based on coupled-cluster with single and double and perturbative triplet excitations[CCSD(T)] *ab initio* calculations. This PES is more accurate than the YZCL2 PES which was built with a mixture of CCSD(T) and MCRI *ab initio* methods.

5.1.3 Theoretical results

A. Ro-vibrational ground states

Early dynamical studies on the H_2 + OH reaction have been dominated by quasi-classical trajectory[196, 197, 212–214], transition state[212, 215–218] and classical path[219, 220] calculations. Initial theoretical studies on the H_2 + OH reaction system were performed by Walch and Dunning[91] who did polarization configuration interaction calculations on the barrier height and the transition state geometries. The O-H distance in the transition state was found to be similar to that of the OH molecule, in accordance with its spectator bond nature, as reported by experimental studies. The H-H bond in the transition state showed a ~14% increase in comparison to that of the H_2 molecule. Transition state theory calculations were also performed over a range of 300-2000 K to determine the rate constants. Schatz and Elgersma[212] carried out quasi-classical trajectory

TH-1851_Sayak

calculations on the WDSE surface to determine product vibrational distributions in the reaction. They concluded that at $E = 0.3$ eV, 56% of the total energy available to the products goes to H_2O vibration, while 9% goes to rotation and 35% goes to translation. Slightly modified versions of the WDSE surface were used in other QCT calculations by Rashed and Brown[196] and by Harrison and Mayne[197]. The main conclusion of all these studies was that the translation energy is the most efficient form of energy for promoting reactivity. The reaction cross section showed a steep increase with increase in translational energy. Quasi-classical trajectory studies have been performed by Clary et al.[221] and compared with quantum dynamical calculations, both exact($J = 0$) and approximate. While there is a very good agreement between QCT and quantum cumulative reaction probabilities, the rate constants differ at low energies. The quantum rate constants are 30-50% above the QCT ones due to the tunneling effects at play.

QCT studies on the OC surface by Progrebnya et al.[206] and Rodríguez et al.[204] have analyzed the effectiveness and inaccuracies in the PES in describing the H_2 + OH reaction. The OC PES overestimates the rate constants at lower temperatures while they underestimate the experimental rate constants at higher temperatures. The calculated cross sections on OC PES are smaller than the measured ones indicating the necessity of modifying the entrance channel in a way that would route the trajectories to the products more efficiently. Quasi-classical studies have been performed on the most recent and accurate YZCL2 surface[222] and the results have been compared with QCT results obtained on the OC[223] and WSLFH[93, 205] surface. The experimental rate constants have been excellently reproduced on the YZCL2 surface. The QCT calculations on the WSLFH surface reproduce the experimental rate constants at lower temperatures

TH-1851_Sayak

but underestimate the rate constants at lower temperatures. To circumvent the problem of tunneling and possible zero point energy leakage in the QCT calculations, variational transition state theory was used to calculate rate constants. The variational transition state theory rate constants show a fairly good agreement with experimental values for highest level of tunneling theory used(μOMT) used while the agreement is good at higher temperatures for all tunneling corrections. Tunneling was shown to account for more than half the reactivity below 400 K.

Since six coordinates are required to describe the system, exact quantum dynamical calculations are difficult to carry out. Quantum mechanical(QM) scattering calculations of rate constants, integral cross sections and differential cross sections were performed for the first time by Clary[159, 195] and by Nyman and Clary[224] on both H_2 + OH and D_2 + OH, on the WDSE surface, using the rotating bond approximation(RBA). In these studies the total number of degrees of freedom were constrained to be three and reaction probability, cross sections and product distributions were calculated. This method involved using hyperspherical coordinates to account for the H_2 vibration and one local OH stretching vibration of H_2O, accounting for both the rotation of OH and the bending mode of H_2O with a spherical harmonic basis set, and applying a version of the bending-corrected rotating line approximation to treat the rotation of H_2 and the vibration of initial OH. Rate constants determined over a temperature range of 250-1050 K were higher than the experimental values by 20%-40% for the whole temperature range. In the 3 dimensional rotating bond approximation, Clary included two rotating coordinates and one bending coordinate explicitly, while Bowman et al.[225] developed an "adiabatic bend approximation" which included three radial coordinates explicitly in their calculation while treating the three angles by

TH-1851_Sayak

the adiabatic approximation. Echave and Clary[226] further extended the RBA model to the planar calculation, in which they included four degrees of freedom in the scattering calculation by constraining the system to a planar configuration. They obtained accurate state-to-state reaction probabilities for the coplanar reaction which were in good agreement with results obtained using RBA approximation. These theoretical works do not treat the reaction in its full dimensionality, but rather use reduced dimensionality scattering calculations or calculations with constrained geometry to reduce the number of degrees of freedom from six to a maximum of three or four.

In the absence of any accurate quantum dynamic calculation that include all the important degrees of freedom, the validity and accuracy of the reduced dimensionality calculations are hard to gauge. It is also difficult to ascertain the accuracy of the PES and determine parameters such as the barrier height. Within a time-dependent treatment Baer and co-workers[227. 228] calculated cross sections for the energy range 0.2-0.7 eV. The obtained results were at variance with the previous cross sections obtained by Clary et al.[159, 195], which were carried out with a frozen OH bond. Balakrishnan and Billing[229, 230] carried out a mixed quantum classical study of H_2 + OH reaction. They developed a semi-classical scheme in which the total number of degrees of freedom was divided into a quantal and a classical part. The vibration as well as translational motion was treated quantally while the rotational motion was treated classically. They computed initial state-selected total reaction probabilities at a number of translational energy values of the reactants. Vibrational excitation of H_2 was found to significantly enhance the reaction probability. It was also found that for ground rotational states of the reactants, one quantum rotational excitation of the reagents had no effect while a

TH-1851_Sayak

similar excitation of H_2 was marked by an increase in reaction probability. They also compared the reaction probabilities from the original WDSE PES and the modified version by Clary[159] and concluded that the unphysical barriers in the original PES resulted in a significant enhancement in reaction probabilities. The computed rate constants were found to be in good agreement with the full dimensional wave packet calculations by Zhang et al[231]. The total cross sections were slightly low near the threshold region but increased much more quickly with collision energy, in comparison to the wave packet calculation results. The computed rate constants were higher than the experimental results by a factor of 3 at 300 K, although the difference narrowed down at higher temperatures. The calculated results, on the other hand, showed a good agreement with 6D results of Manthe et al.[201, 232], thus underlining the accuracy of the theoretical approach. Thompson and Miller[233] developed a reduced dimensionality approach to calculate initial state selected reaction probabilities for H_2 + OH and photo-detachment intensities for HOH_2^- in connection with the experimental work of Neumark[182]. This was followed by a series of five dimensional calculations to compute initial state selected reaction probabilities. Zhang et al.[234, 235] employed a time-dependent wave packet method to compute initial state specific total reaction probabilities for the reaction on the WDSE PES.

All six internal degrees of freedom were treated for the first time in calculations of the cumulative reaction probability and the thermal rate constant by Manthe et al.[201, 232] and later by Zhang et al.[236]. The reaction probabilities for $J = 0$ were subsequently determined by Zhang and co-workers[231, 237, 238] using time-dependent wave packet calculations in six dimensions. This was followed by the calculation of reaction probabilities for the values of $J > 0$ using

TH-1851_Sayak

the centrifugal sudden(CS) approximation[239]. Simultaneous full dimensional quantum mechanical studies were also reported by Neuhauser[240]. Numerically exact calculations, without the CS approximation, were carried out by Zhang and co-workers[202]. They reported fully converged integral reaction cross sections for different ro-vibrational states of the reactant and examined the accuracy of the CS approximation for this reaction. The CS approximation was found to work very well for the ground ro-vibrational and accuracy decreased with increasing reagent rotational excitation. The CS approximation was also found to work better in the higher energy regions compared to the lower energy regions.

While exhaustive quantum dynamical studies on the WDSE have been widely reported, accurate quantum dynamical studies on the WSLFH surface for the H_2 + OH system have been largely restricted to $J = 0$. Goldfield and Gray [203] have used the J-shifting approximation for non zero angular momentum values, while the reactant-product decoupling approach was used by Cvitaš and Althorpe [241, 242] for calculating state-to-state reaction probabilities for total angular momentum $J = 0$ on this surface. Studies on the WSLFH surface for the isotopic D_2 + OH system have involved both quantum dynamical[243] and QCT[205] approaches. A series of fully-dimensional quantum scattering calculations were reported at the beginning of this decade by Zhang et al.[160. 244, 245]. These calculations used the YZCL1 and the YZCL2 PESs to calculate fully converged integral reaction cross-sections for the ground and ro-vibrational states using TDQM method. For temperatures upto 1050 K, excellent agreement between theoretical and experimental rate coefficients was achieved on the more exact YZCL2 PES. Very recently, Xiao et al.[211] calculated differential cross sections for the isotopic HD + OH system on a newly developed potential energy

TH-1851_Sayak

HI-TECH TEMP

surface and achieved an excellent agreement with experimental results.

B. Ro-vibrational excited states

Early classical trajectory studies on the effect of rotational excitation of the reagents on the WDSE surface by Schatz[213] showed a decrease in reactivity with rotational excitation, with a greater decrease observed for H_2 in comparison to that for excitation of OH. Rashed and Brown[196] found a similar decrease in reactivity for both reagents on the Rashed and Brown surface[196]. Later quantum dynamical studies by Zhang and co-workers[246] using CS approximation concurred with earlier results for H_2 rotational excitation showing substantial reduction in cross section. Excitation of OH resulted in a small enhancement of reaction cross section. Fully coupled channel(CC) calculations reported by Zhang et al.[202] on the WDSE surface showed a decrease in accuracy of the approximate results with increasing rotational excitation. The CS approximation was observed to underestimate the enhancement due to OH rotational excitation at low energy while overestimating the decrease due to rotational excitation of H_2. Quasi-classical studies on the effect of rotational excitation of reagents for the WSLFH surface gave a completely contrasting picture[205]. While excitation of H_2 shows an increase in reactivity that of OH shows a decrease in reactivity. No exact quantum dynamical studies are available currently to give a accurate explanation of this contrasting behavior. Studies of rotational effects on the recent and most accurate surface by Yang et al.(YZCL2)[94, 160] gives results differing from the WDSE and WSLFH surfaces. Excitation of H_2 leads to an initial increase of cross sections at lower energies while at higher energies cross sections show a steady decrease. Rotational excitation of OH leads to a steady decrease in cross sections over the entire energy range. The widely varying effects of rotational ex-

TH-1851_Sayak

citation depending on surfaces considered merits an thorough quantum dynamical coupled channel(CC) study on all surfaces to analyze the differences.

Vibration excitation of reagents on the WDSE surface have been studied using QCT[92, 213], mixed quantum classical[229] and also reduced[226] and full dimensional quantum dynamical methodology[231]. Full dimensional quantum dynamical studies performed by Zhang et al.[231] involved the use of CS approximation. Excitation of the reactive H_2 bond produced a strong enhancement in reaction probabilities characterized by sharp resonance peaks at low energies. Similar peaks were also observed in quantum dynamical calculations performed by Goldfield et al.[203] for $J = 0$. The appearance of peaks were discussed in terms of the presence of the wells in the entrance channel. Vibrational excitation of the non-reactive OH bond was reported to show only a marginal enhancement in reaction probabilities, thus emphasizing its spectator bond nature. QCT calculations on the WSLFH surface found the enhancement in cross sections on vibrational excitation of H_2 to be moderate in comparison to that on the WDSE surface. There have been no studies reported on the WSLFH and YZCL2 surfaces for vibrational excitation of reagents till date for the present system.

To summarize the theoretical results, exhaustive theoretical studies have been performed to study the dynamics and the reaction kinetics of the H_2 + OH reaction and its isotopic variants for the last three decades. Several inherent flaws in the WDSE surface stood out during the studies performed by various groups. This led to various modifications of the WDSE surface with the aim of removing the spurious wells in the surface which were giving rise to erroneous features in the reaction attributes. Attempts to correct the other flaws, namely the incorrect transition state conformer, barrier height and asymmetry of the H-atoms of the

TH-1851_Sayak

H_2 diatom led to development of a number of improved PESs over the last two decades. The H_2 + OH system also served as a benchmark for development of various new quantum dynamical methodologies to study reaction dynamics. In spite of improved computational capabilities, exact full dimensional studies of a tetra-atomic system is a cumbersome task till date. We have used the WDSE surface to study the effectiveness of the MCTDH algorithm in reproducing the literature values for the reaction cross sections and rate constants for the reagents in the ground state. In view of the absence of 6D CC studies of reagents in their rotational excited state($j_{1(2)} = 2$), we have also performed studies on rotational excitation. The literature values available on the vibrational excitation of reagents are obtained using CS approximation which has motivated us to perform CC studies to understand the importance of using an exact Hamiltonian in excited state calculations. Theoretical work on the WSLFH surface have been limited to TST and QCT calculations, although it is a much improved surface, in comparison to the WDSE surface, having a a proper symmetry with respect to the two hydrogen atoms of water and devoid of any spurious structures. We have performed studies on the WSLFH surface for the reagents in their ground state and also in their ro-vibrational excited states. The highly accurate surface for the H_2 + OH reaction system was developed at the beginning of this decade and studies were performed for reagents in their ground an rotational excited states. This serves as an excellent reference for the numerical accuracy of the MCTDH algorithm which is being used to study reactive tetra-atomic systems for the first time. We have also performed calculations for reagents in vibrational excited state($v_{1(2)} = 1$) on the YZCL2 surface and compared them with recent experimental studies to ascertain the accuracy of the surface in describing the reaction dynamics of reagents in their excited states. We have also performed a comparative analysis of our results

TH-1851_Sayak

Parameters		Surfaces		
		WDSE	WSLFH	YZCL2
No. of radial grid points	$N_{R_3}/N_{R_1}/N_{R_2}/$	99/8/21	-do-	-do-
No. of angular grid points	$N\theta_1/N\theta_2$	17/10	-do-	-do-
No. of grid points for k_1,k_2	k_{min}/k_{max}	-4/4	-do-	-do-
R_3 grid	$R_{3_{min}}/R_{3_{max}}$	1.5/14.0	-do-	-do-
R_1 grid	$R_{1_{min}}/R_{1_{max}}$	0.8/3.06	0.8/2.90(3.07)	0.8/2.80
R_2 grid	$R_{2_{min}}/R_{2_{max}}$	0.4/6.0	-do-	-do-
CAP order	β_{R_3}/β_{R_2}	3	-do-	-do-
CAP strength	η_{R_3}	0.008(0.006)	0.0006(0.015)	0.008
CAP strength	η_{R_2}	0.005(0.004)	0.0005(0.01)	0.005(0.015)
Starting point of CAP	R_{3_c}/R_{2_c}	11.0/3.0	10.0(11.0)/3.0	11.0/3.0
CAP length	L_{R_3}/L_{R_2}	3.0/3.0	4.0(3.0)/3.0	3.0/3.0
Center of χ_0	R_0	12.0	11.0	12.0
Width of χ_0	d_R	0.18(0.3)	-do-(0.3)	-do-(0.3)
Initial momentum of χ_0	p_0	-8.2(3.0)	-7.8(5.8)	-8.2(4.7)
Propagation time	T	200(fs)(1000)	-do-	-do-(500)

Table 5.1: *Numerical parameters of the MCTDH calculations for the* $H_2(v_1 = 0,j_1 = 0) + OH(v_2 = 0,j_2 = 0)$ *system(in atomic units if not otherwise stated) The parameters for calculations involving vibrationally excited reagents*($v_{1(2)}=1$) *are given in brackets if those differ from the earlier parameters.*

on all the three surfaces to evaluate the dependency of the reaction dynamics on features of the surface topology.

5.2 Results and discussions

5.2.1 Numerical details

Table 5.1 displays the relevant parameters used in MCTDH calculation for the $H_2(v_1 = 0,j_1 = 0) + OH(v_2 = 0,j_2 = 0)$ reaction. As shown in the Chapter 3(See Figure 3.4), a set of seven coordinates was used to parametrize the Hamiltonian. Here R_1 and R_2 denote the H_2 and OH bond distances and R_3 is the distance between the centers of mass of the two diatoms. θ_1, θ_2 are the polar angles. The

TH-1851_Sayak

torsion angle φ is written as φ_1 and φ_2 in the E_2 frame of reference. The parameters used for estimation of reaction attributes for reagents in their rotational excited state($j_{1(2)} = 2$) are the same as the ro-vibrational ground state parameters. The parameters for vibrational excited state ($v_{1(2)} = 1$) calculations have been shown in brackets if those differ from the ground state parameters and are discussed below.

We have carried out extensive test calculations to check the convergence of our results with respect to the number of SPFs considered for each mode and the size of DVR grid for each DOF. Decreasing the number of spfs along the translational coordinate leads to a greater variance with the previous theoretical result at higher energies. It has been observed that decreasing the number of basis functions used for R_3, R_1 and R_2 leads to a substantial decrease in computational time but at the cost of convergence, especially in the low energy regions. Increasing the grid length along the OH coordinate R_1 shows an interesting effect. For longer grids along R_1, the probabilities are consistently larger than the reported result although the threshold remains the same.

The R_3 and R_2 coordinates are represented by sin-DVR grids. The grids for R_3 and R_2 extend from 1.5 to 14 and 0.4 to 6.0 a_0, respectively. A sine DVR of 99 and 25 points is used for R_3 and R_2 respectively on the three surfaces. For R_1, which basically acts as a spectator bond, a harmonic oscillator DVR of 8 points is used to represent the grid points on all the three surfaces considered. The R_1 grid extends from 0.8 to 3.06 a_0 on the WDSE surface, while the corresponding values are 0.8 to 2.90 a_0 and 0.8 to 2.80 a_0 on the WSLFH and YZCL2 surfaces respectively. For $v_{1(2)}$=1 calculations, the R_1 grid was extended to 3.07 a_0 for attaining proper convergence. For the angles, a 2-dimensional "extended Legendre DVR"[150] has been employed.

TH-1851_Sayak

Calculations have been carried out to obtain reaction attributes upto a translational energy range of 0.6 eV. The initial Gaussian is placed at $R_3 = 12.0$ au for the WDSE and YZCL2 surfaces and at 11.0 au for the WSLFH surface. The width of the Gaussian wave function is $d_R = 0.18$ on all the three surfaces. For the $v_{1(2)} = 1$ calculations, the width was increased to $d_R = 0.3$ on all the three surfaces. The momentum(p_0) of the initial wave packet is 8.20 on the WDSE and YZCL2 surfaces and is 7.20 for the WSLFH surface. A smaller value of initial momentum was required for the wave packet for the $v_{1(2)} = 1$ calculations. The initial momentum values were changed to 3.0, 5.8 and 4.7 on the WDSE, WSLFH and YZCL2 surfaces, respectively. The initial position, width and momentum of the wave packet significantly affects the reaction probabilities and the parameters used have been considered so as to cover the entire energy range. The momentum and width of the wave packet determines the energy distribution and detailed calculations have underlined the importance of a perfect energy distributions on the convergence of reaction probabilities. It has been observed that a good energy distribution strongly influences proper convergence especially at lower energies. The energy distributions of the initial wave packet for ground ro-vibrational states of the reagent on the WDSE, WSLFH and YZCL2 surfaces are shown in Figure 5.1 for reference.

The complex absorbing potential starts at $R_3 = 11$ au on the WDSE and YZCL2 surfaces and at $R_3 = 10$ au on the WSLFH surface. The CAP along R_2 starts at $R_2 = 3$ au on the three surfaces. The strengths and the orders of the CAPs are (0.008,3) and (0.005,3) along R_3 and R_2, respectively for both the WDSE and the YZCL2 surfaces. For the WSLFH surface, the corresponding figures are (0.0006,3) and (0.0005,3). The CAP parameters show a significant change for the excited

TH-1851_Sayak

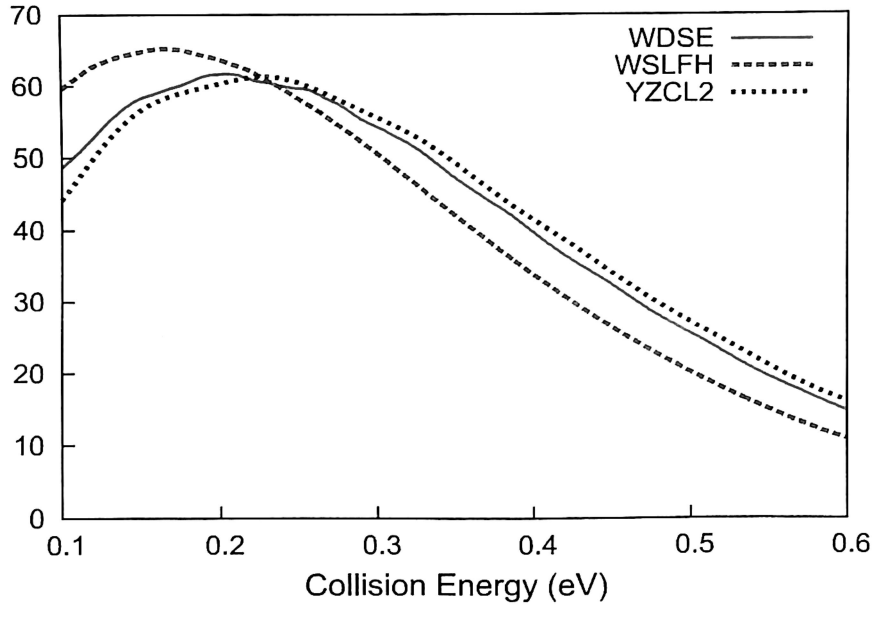


Figure 5.1: *Energy distribution of the initial wave packet on the WDSE, WSLFH and YZCL2 surfaces for ground ro-vibrational states of the reactants.*

state($v_{1(2)}$= 1) calculations. The corresponding numbers for $v_{1(2)}$= 1 on the WDSE surface are (0.006,3) and (0.004,3) along R_3 and R_2, respectively. On WSLFH, the CAP strengths were increased to 0.015 and 0.01 along R_3 and R_2, respectively. On the YZCL2 surface, the strength remains unchanged along R_3 while along R_2 the corresponding parameters are (0.015,3). The surface parameters are chosen so as to minimize the effect of wave packet reflection from the grid ends. Since the initial wave packet in R_3 is already located inside the CAP area, we have used an automatic CAP which is switched on after 40 fs, when the initial wave packet has moved outside the CAP area. Extensive tests on all parameters have been carried out on all parameters have been carried out to attain convergence in results.

For the propagation, we have used a set of three MCTDH particles. The parameters for the primitive basis sets employed for each degree of freedom are shown in Table 5.2. While the R_3 and R_2 are combined to one mode, the spectator bond R_1

TH-1851_Sayak

Mode	Primitive Basis		No. of SPFs		
	Type	Size			
		WDSE/WSLFH/YZCL2	WDSE	WSLFH	YZCL2
(R_3, R_2)	(sin.sin)	(99,21)	40	32	42
$(R_1.\theta_1, k_1)$	(HO,KLeg)	(8,153)	42	42	46
(θ_2, k_2)	KLeg	90	30	32	36

Table 5.2: *Parameters for the primitive basis sets employed for each degree of freedom. The brackets indicate the mode combinations. HO is a harmonic oscillator DVR; KLeg is a two-dimensional extended Legendre DVR [150].*

is combined with a two-dimensional angular grid, θ_1, k_1. Hence, the mode combination looks like $\{(R_3, R_2),(R_1, \theta_1, k_1),(\theta_2, k_2)\}$. We have also carried out tests with the mode combination of the form $\{(R_3),(R_1, \theta_1, k_1),(R_2, \theta_2, k_2)\}$. but the huge increment in computational time required made it improbable to proceed with. The number of single particle functions used for the $\{(R_3, R_2),(R_1, \theta_1, k_1),(\theta_2, k_2)\}$ mode combinations are 40, 42, 30 on the WDSE surface. While the spfs are 42, 46, 36 for the same mode combination on YZCL2, the WSLFH surface required 32, 42 and 32 spfs for the results to converge. The results are converged with respect to the number of spfs. The quality of convergence has been checked by checking the maximum over time of populations of the least occupied natural orbitals which was close to 10^{-5} for all calculations.

The numerical parameters used for the potential fit of the surfaces used. are tabulated in Table 5.3. We used $\Omega = 1$ for the transformation on the WDSE PES and $\Omega = 2$ on the YZCL2 and WSLFH PESs. Then each transformed potential was fitted separately, 300 natural potentials were used for $\Omega = 0$, 1 and 2. While applying POTFIT, we have have restricted the surface to a certain region in space, *eg.* $1.5< R_3 <8.0$, $0.8< R_2 <4.0$, $1.2< R_1 <2.2$ and V<1.0 eV. Total 10 iterations were used to get an accurate fit. The relative error was found to be less than 2

TH-1851_Sayak

Number of natural potentials	l_2/l_3	30/10
Relevant region for R_3 coordinate, au	$R_{3_{min}}/R_{3_{max}}$	1.50/8.00
Relevant region for R_1 coordinate, au	$R_{1_{min}}/R_{1_{max}}$	1.20/2.20
Relevant region for R_2 coordinate, au	$R_{2_{min}}/R_{2_{max}}$	0.8/4.00
Relevant region for θ_1 coordinate,	$\theta_{1_{min}}/\theta_{1_{max}}$	0.00/3.00
Relevant region for θ_2 coordinate,	$\theta_{2_{min}}/\theta_{2_{max}}$	0.00/3.00
Number of iterations	N_{iter}	10
Potential cutoff(V_{min}=0.0 eV)	V_{max}	1.0 eV

Table 5.3: *Numerical parameters for the potential fit for the H_3O system on the WDSE, WSLFH and YZCL2 PESs.*

meV, in the relevant region defined above.

TH-1851_Sayak

5.2.2 Reagents in ro-vibrational ground states

A. Reaction probabilities

Reaction probability values for a few selected values of J on the WDSE surface are shown in Figure 5.2. The reaction probabilities for higher J values exhibit smooth curves without any major structural distortions or oscillatory behavior.

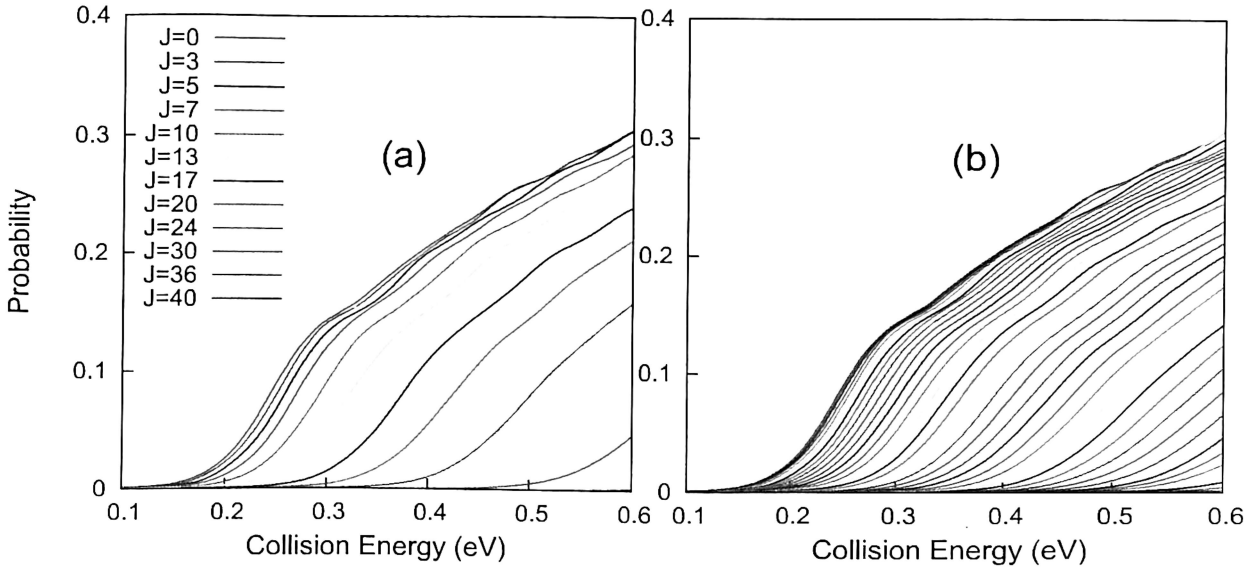


Figure 5.2: *Reaction probabilities for J = 0, 3, 5, 7, 10, 13, 17, 20, 24, 30, 36, 40 as a function of collision energy on the WDSE surface are shown in (a) for $H_2(v_1 = 0, j_1 = 0) + OH(v_2 = 0, j_2 = 0)$. Interpolated reaction probabilities upto J = 42 are shown in (b).*

This has enabled us to use the J-interpolation algorithm[61] which gives us the interpolated probabilities between two accurately calculated probabilities. Every third reaction probability has been accurately calculated and the intermediate reaction probabilities have been obtained using the J interpolation algorithm. The interpolated reaction probabilities for all the J values are shown in Figure 5.2(b). Extensive tests have been carried out to ensure that the interpolated results are not in substantial variance with the exact ones for the same. Exact calculations

TH-1851_Sayak

have been carried out till $J = 42$ to attain convergence.

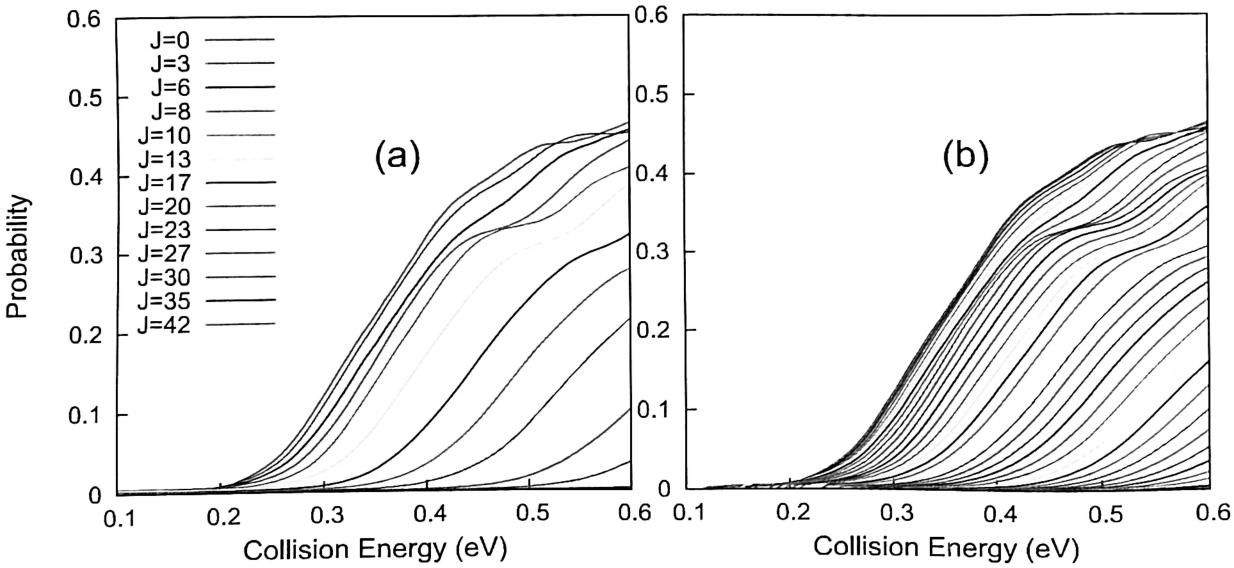


Figure 5.3: *Reaction probabilities for J = 0, 3, 6, 8, 10, 13, 17, 20, 23, 27, 30, 35 and 42 as a function of collision energy on the YZCL2 surface are shown in (a) for $H_2(v_1 = 0, j_1 = 0)$ + $OH(v_2 = 0, j_2 = 0)$. Interpolated reaction probabilities upto J= 42 are shown in (b).*

A few selected reaction probabilities calculated on the YZCL2 surface over the collision energy range of 0.1-0.6 eV are given in Figure 5.3(a) while the interpolated probabilities are shown in Figure 5.3(b). The curves appear smooth over the entire energy range except a few small humps between 0.4 and 0.55 eV energy range which eventually smoothen out for higher J values. Similar features were also observed for the WDSE reaction probabilities near 0.5 eV. Figure 5.4 shows the calculated and the interpolated reaction probabilities for the WSLFH surface.

Figure 5.5 displays the total reaction probability for $J = 0$ obtained by the MCTDH method along with the results of Goldfield et al.[203] on the WDSE surface upto 0.6 eV. The reaction probabilities for $J = 3$, 15, 24 have been separately reported by Zhang et al.[202] Our results show a perfect agreement with the reported results (not compared in the figure) over the entire energy range

TH-1851_Sayak

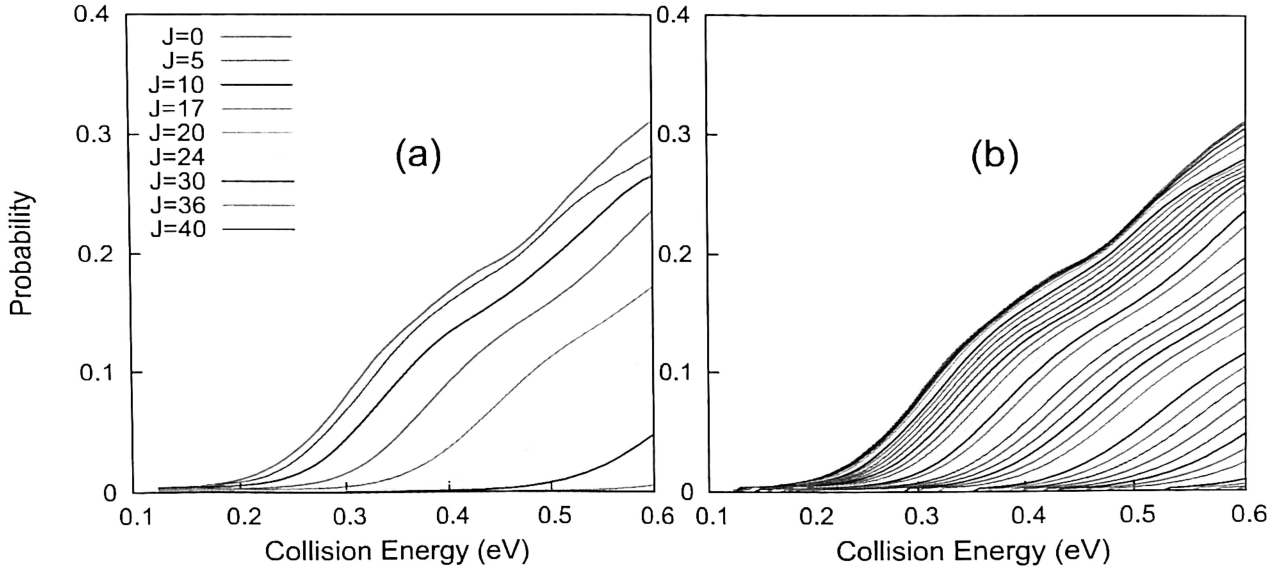


Figure 5.4: *Reaction probabilities for $J = 0, 5, 10, 17, 20, 24, 30, 36, 40$ as a function of collision energy on the WSLFH surface are shown in (a)for $H_2(v_1 = 0, j_1 = 0) + OH(v_2 = 0, j_2 = 0)$. Interpolated reaction probabilities upto $J = 40$ are shown in (b).*

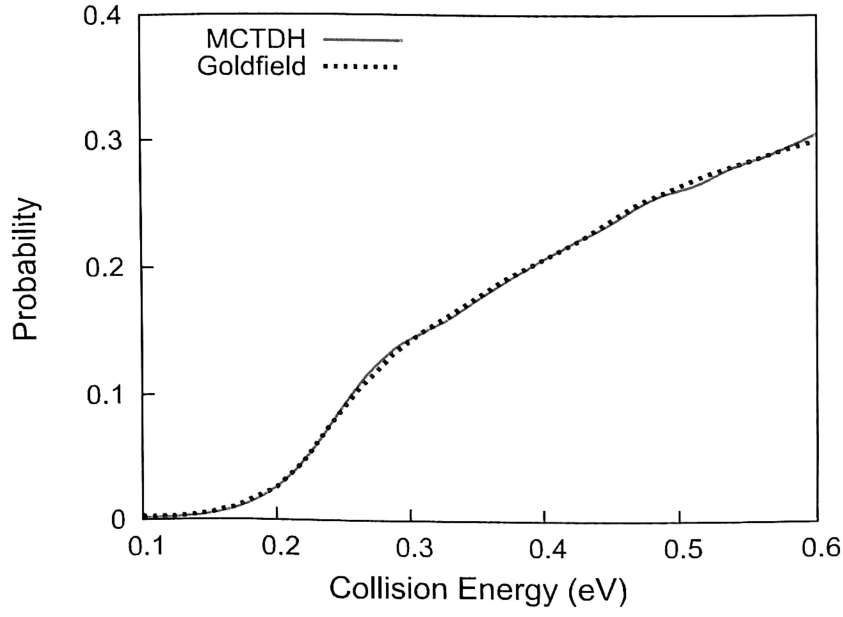


Figure 5.5: *Comparison of the reaction probabilities obtained using MCTDH with the results of Goldfield and Gray[203] for $J = 0$ on the WDSE surface. Results from the Ref. [203] are reproduced with permission.*

TH-1851_Sayak

considered.

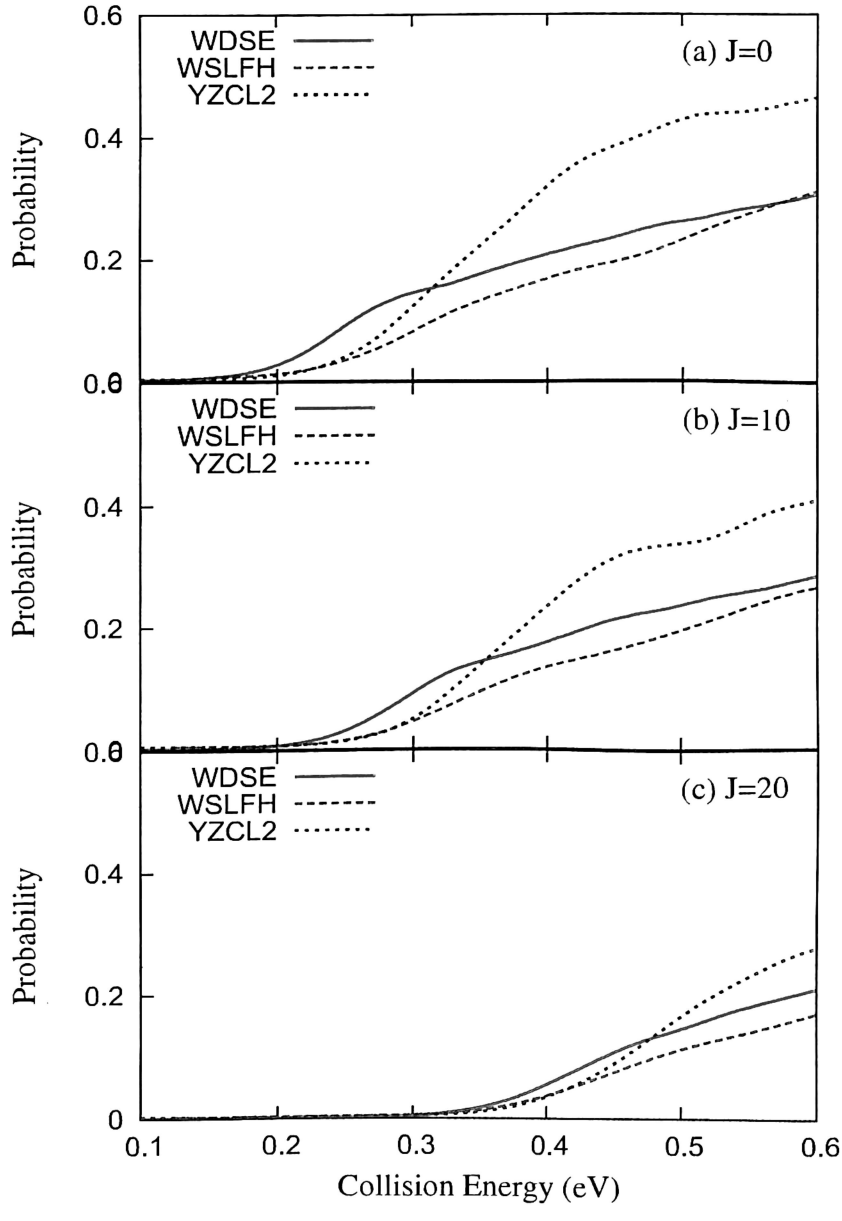


Figure 5.6: *Comparison of reaction probabilities on the WDSE, WSLFH and YZCL2 surfaces for J = 0,10 and 20. The reactants H_2 and OH are in their ground ro-vibrational states.*

Figure 5.6 shows a detailed comparison of the reaction probabilities on the WDSE, WSLFH and YZCL2 surfaces for three different J values. It is clearly evident that at energies near the threshold, reaction probabilities for J= 0 on the

TH-1851_Sayak

WDSE surface are higher in comparison to those on WSLFH and YZCL2 surfaces. The same trend is observed for higher J's too. This is expected, given the incorrect "trans "nature of the transition state structure which accounts for lower steric hindrance and higher reaction probabilities. At higher energies, the YZCL2 reaction probabilities become more dominant for all Js considered. This arises from the differences in barrier height on the WDSE and YZCL2 surfaces, with the lower barrier height accounting for the ease of reaction on the YZCL2 surface. Absence of any van der Waals well in the WSLFH surface, unlike the WDSE and YZCl2 surfaces, results in a decreased focussing effect[247] on the trajectories towards the products. This accounts for the low probabilities on the WSLFH surface for all Js over the entire energy range.

B. Integral cross sections and rate constants

The cross sections show a steep enhancement with increase in translational energy in accordance with the trend observed for exothermic reactions. Fig 5.7 displays the converged integral reaction cross sections, calculated on the WDSE and YZCL2 surfaces and their comparison with the respective reference results. The cross section obtained on the WDSE surface is in excellent agreement with the fully converged numerically exact integral reaction cross section reported by Zhang and co-workers[202] over the entire energy range. The YZCL2 results are given in comparison to that of Yang et al.[160]. The MCTDH results are in good agreement with those of Yang et al. at lower energies. The resonance structures visible in the reaction probabilities for YZCL2 are washed out by the summation over J in the cross section results.

The integral cross sections obtained on the WDSE, YZCL2 and WSLFH surfaces

TH-1851_Sayak

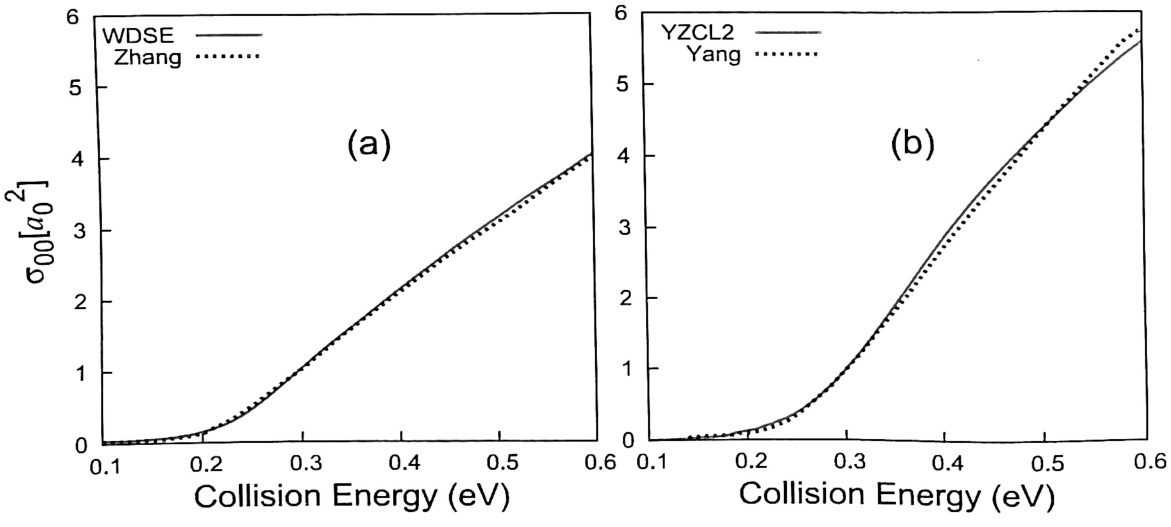


Figure 5.7: *Integral reaction cross sections as a function of collision energy on the WDSE surface (a) and on the YZCL2 surface (b) for* $H_2(v_1 = 0, j_1 = 0)$ + $OH(v_2 = 0, j_2 = 0)$. *The present MCTDH results[248] are compared with the results of Zhang et al.[202] and Yang et al.[160] Reference results are reproduced with permission.*

are compared in Figure 5.8. The reaction threshold has a small positive energy shift for the YZCL2 surface. The WSLFH surface shows significantly lower cross sections over the entire energy range, compared to the WDSE and YZCL2 surfaces. This is expected to result from the difference in the topology of the reagent valleys. The presence of a van der Waals minimum in the entrance channel for both WDSE and YZCL2 surfaces results in increased reactivity by virtue of a focussing effect on the trajectories towards the saddle point region [247]. The absence of any such well in the WSLFH surface contributes to the overall reduced reactivity. The cross sections on the WDSE PES is marginally higher than the cross sections on the YZCL2 surface at lower energies. In the higher energy range, the results on YZCL2 show a significant enhancement over the WDSE cross sections.

There are two competing factors at play which influence the contrasting trends

TH-1851_Sayak

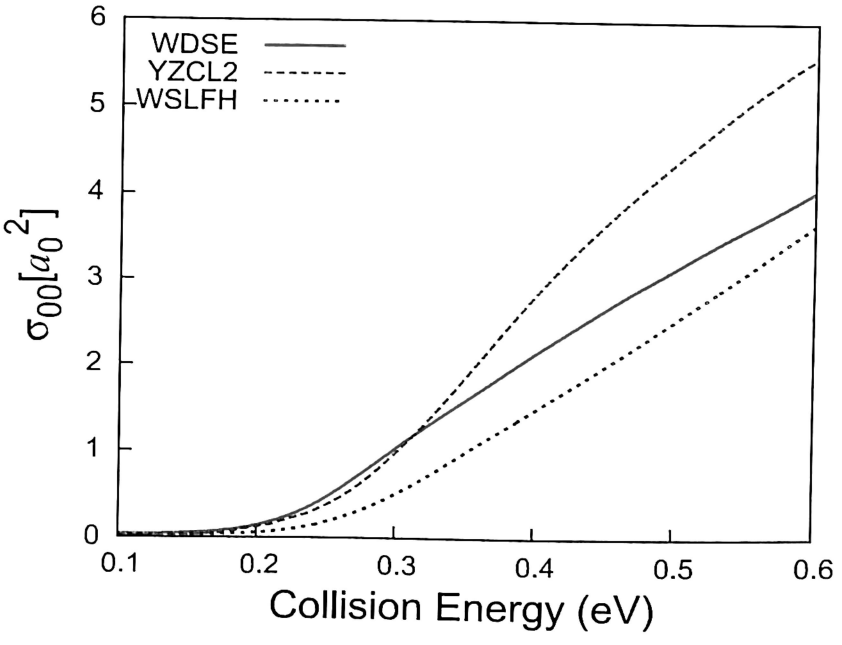


Figure 5.8: *Comparison of integral cross sections on the WDSE, YZCL2 and WSLFH surfaces with the reagents in their ground ro-vibrational states.*

on the three surfaces. At higher energies, the difference in cross sections is due to the difference in barrier heights between the two surfaces. The energy difference between H_2 + OH and the saddle point for the abstraction reaction are 0.264 eV and 0.234 eV on the WDSE and YZCL2 surfaces, respectively. This results in enhanced reaction probability with increase in translational energy. The dependence on the barrier height solely is unable to account for the higher cross sections for the WDSE at lower energies. We have to consider the transition state structures of H-O-H-H on the two PESs as shown in Figure 5.9. The transition state is a *cis* structure on the YZCL2 and WSLFH PESs while it is a *trans* on the WDSE PES, which has been shown to be incorrect by later studies[203]. For the formation of the *cis* structure, the H_2 molecule will have to encounter considerable steric hindrance on its approach to the OH moiety. The WDSE transition state would be attained with comparatively lesser hindrance resulting in favor-

TH-1851_Sayak

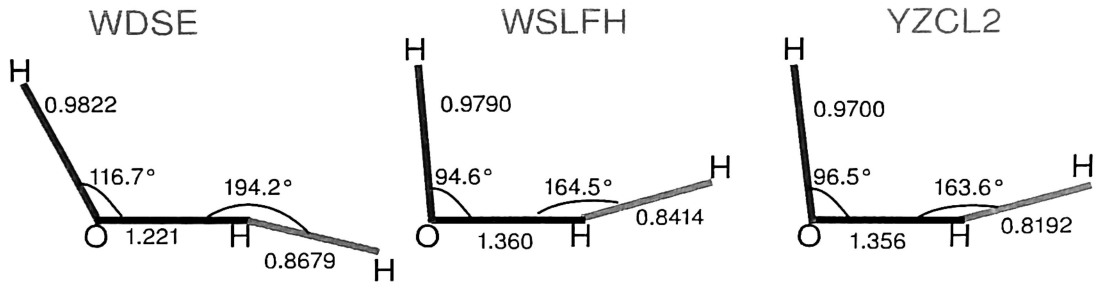


Figure 5.9: *Comparison of transition state structures of H_2OH on the WDSE, WSLFH and YZCL2 surfaces.*

able formation of products at lower energies. At higher translational energies, the reagents have enough energy to overcome the steric hindrance and it is the barrier height which becomes more influential. The reactive H-H bond makes an angle of 163.6° with the non-spectator O-H bond in the transition state on the YZCL2 surface and 194.2° for the WDSE surface. The bond length of the reactive H-H bond in the transition state is 0.8192 Å on the YZCL2 PES and 0.8679 Å on the WDSE surface. This results in greater ease of bond cleavage at lower energies for the WDSE surface leading to formation of H_2O. A similar pattern is observed for the non-spectator O-H bond which is formed simultaneously with the H-H bond cleavage. The O-H bond length being 1.221 Å on the WDSE PES is closer to the product O-H bond length of 0.96 Å than the YZCL2 transition state bond length of 1.356 Å. The bond lengths of the WDSE transition state structure indicate a smoother conversion to the product H_2O molecule at lower translational energies compared to the transition state on the YZCL2 PES.

Figure 5.10 displays the rate constants we obtained for the WDSE, WSLFH and YZCL2 surfaces along with previously published experimental and theoretical results. The rate constants obtained on all the three surfaces are also tabulated in Table 5.4 along with the reference theoretical and experimental re-

TH-1851_Sayak

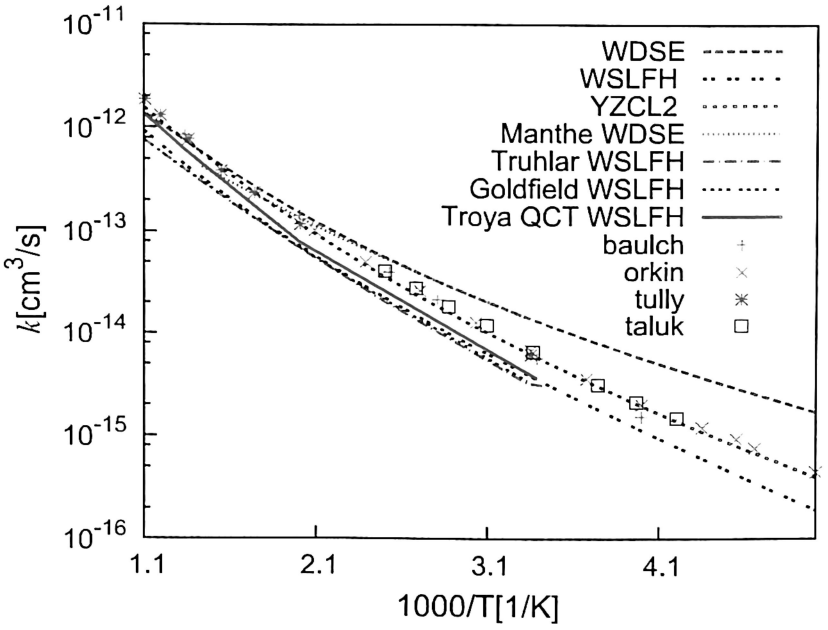


Figure 5.10: *Rate constants for the* $H_2(v_1 = 0, j_1 = 0) + OH(v_2 = 0, j_2 = 0)$ *reaction. The present MCTDH results are compared with the theoretical results from the following references: Manthe et al.[249], Truhlar et al.[250], Goldfield et al.[203], Troya et al.[205]. Experimental results of Baulch et al.[187], Orkin et al.[185], Tully et al.[175] and Talukdar et al.[183] are also shown.*

sults. The WDSE surface results show a good agreement with experimental results[175, 183, 185, 187] above 400 K. But at lower temperatures, the rate constants are clearly overestimated. While the experimental rate at 200 K is 4.30×10^{-16} cm^3 molecule$^{-1}s^{-1}$[185], the calculated rate on the WDSE surface is 1.65×10^{-15} cm^3 molecule$^{-1}s^{-1}$ being higher by a factor of ~ 4. The higher reactivity at lower temperatures owes its origin to the erroneous but favorable "trans" transition state on the WDSE surface. At lower temperatures, initial reactivity remains much higher compared to the other surfaces which have a corrected "cis" structure as discussed in the previous section. This is evident from the rate constants obtained on the WSLFH and YZCL2 surfaces, which are 1.85×10^{-16} cm^3 molecule$^{-1}s^{-1}$ and 3.81×10^{-16} cm^3 molecule$^{-1}s^{-1}$ respectively at 200 K, be-

TH-1851_Sayak

ing lower than the experimental rate constant. The rate constants obtained on the WDSE surface at higher temperatures are comparatively closer to the experimental values. The rate constant of 7.37×10^{-13} cm^3 molecule$^{-1}s^{-1}$, obtained on the WDSE surface agrees well with the experimental value of 8.3×10^{-13} cm^3 molecule$^{-1}s^{-1}$[187] at 750 K.

Rate constants for WSLFH obtained using full dimensional quantum calculations including the Coriolis coupling are being reported for the first time and presents a proper estimate on the accuracy of the potential energy surface. A corrected initial orientation for the transition state structure results in much improved agreement for reactivity at lower temperatures, in comparison to the WDSE surface. In analogy with the variation seen between the J-shifting and exact results on the WDSE surface, Goldfield and Gray[203] had predicted that the exact rate constants on WSLFH surface to be lower than the J-shifting results by a factor of 2 and subsequently by a factor of 4 in comparison with the experimental results. The results we have obtained at low temperatures are an improvement over the J-shifting results and much closer to the experimentally reported rate constants. The calculated rate constant at 330 K is 7.15×10^{-15} cm^3 molecule$^{-1}s^{-1}$ which is less than the experimentally obtained rate constant of 1.26×10^{-14} cm^3 molecule$^{-1}s^{-1}$[185] by a factor of $\sim$ 1.7. At 500 K, the MCTDH rate constant of 7.11×10^{-14} cm^3 molecule$^{-1}s^{-1}$ is closer to the experimental value of 1.4×10^{-13} cm^3 molecule$^{-1}s^{-1}$. In comparison a value of 6.9×10^{-14} cm^3 molecule$^{-1}s^{-1}$ was obtained by Goldfield and Gray[203] and 6.82×10^{-14} cm^3 molecule$^{-1}s^{-1}$ by Truhlar et al.[250] The QCT rate constant obtained by Troya et al.[205] at 500 K is 1.12×10^{-13} cm^3 molecule$^{-1}s^{-1}$ is closer to the experimental result, in comparison to the quantum results. This could be an "accidental" accuracy, since the QCT

TH-1851_Sayak

results would have shown agreement with the quantum results, if they were accurate. The rate constant values on the WSLFH surface show an underestimation in comparison to experimental values, on account of the absence of the van der Waals attractive well in the *ab initio* calculations for the WSLFH surface resulting in decreased reactivity over the entire energy range. The results on the YZCL2 surface, the most exact surface reported till date, show an excellent agreement with the experimental rate constants over the entire range of temperatures considered. The rate constant calculated on the YZCL2 surface at 576 K is 2.35×10^{-14} cm^3 molecule$^{-1}s^{-1}$ with the corresponding experimental value being 2.34×10^{-14} cm^3 molecule$^{-1}s^{-1}$[175]. The variation from the experimental results over the entire range of temperatures is limited to a factor of ~ 1.1.

TH-1851_Sayak

TH-1851_Sayak

$T(K)$	MCTDH			Literature Theory					Experiment
	WDSE	WSLFH	YZCL2	WDSE		WSLFH			
				Manthe[a]	Zhang[b,c]	Tru[d]	GG[e]	Troya[f]	
200	1.65E-15	1.85E-16	3.81E-16						4.30E-16[j]
215	2.51E-15	3.43E-16	6.58E-16						7.40E-16[j]
220	2.85E-15	4.14E-15	7.78E-16						9.10E-16[j]
230	3.64E-15	5.89E-15	1.07E-15						1.185E-15[j]
238	4.37E-15	7.67E-15	1.36E-15						1.46E-15[g]
250	5.66E-15	1.11E-15	1.92E-15						1.98E-15[j]
272	8.70E-15	2.03E-15	3.38E-15						3.55E-15[j]
290	1.20E-14	3.13E-15	5.12E-15			2.98E-15			
295	1.30E-14	3.50E-15	5.71E-15					3.56E-15	5.6E-15[i]
298	1.37E-14	3.74E-15	6.09E-15						6.67E-15[j]
300	1.41E-14	3.91E-15	6.35E-15	1.40E-14	1.55E-14[c]	3.18E-15	3.4E-15		
330	2.24E-14	7.15E-15	1.15E-14						1.266E-14[j]
350	2.96E-14	1.02E-14	1.63E-14	2.95E-14	3.14E-14[c]				
356	3.20E-14	1.13E-14	1.81E-14						2.1E-14[i]
370	3.84E-14	1.41E-14	2.27E-14						2.58E-14[j]
396	5.26E-14	2.08E-14	3.35E-14						3.9E-14[i]
400	5.51E-14	2.20E-14	3.54E-14	5.37E-14	5.88E-14[c]	1.95E-14	2.1E-14		4.03E-14[g]
419	6.81E-14	2.84E-14	4.59E-14						4.954E-14[j]
450	9.39E-14	4.15E-14	6.77E-14	8.81E-14	1.01E-13[c]				
479	1.24E-13	5.73E-14	9.41E-14						1.008E-13[j]
500	1.49E-13	7.11E-14	1.17E-13	1.33E-13	1.63E-13[c]	6.82E-14	6.9E-14	7.73E-14	1.4E-13[i]
550	2.23E-13	1.13E-13	1.89E-13	1.90E-13	2.03E-13[b]				
576	2.70E-13	1.40E-13	2.35E-13						2.34E-13[h]
600	3.18E-13	1.69E-13	2.85E-13	2.58E-13	3.50E-13[c]	1.55E-13	1.6E-13		
648	4.30E-13	2.38E-13	4.04E-13						3.84E-13[h]
650	4.35E-13	2.42E-13	4.10E-13	3.35E-13	4.09E-13[b]				
700	5.74E-13	3.32E-13	5.65E-13	4.22E-13	6.32E-13[c]	3.00E-13	3.1E-13		
750	7.37E-13	4.40E-13	7.52E-13		7.10E-13[b]			6.02E-13	8.3E-13[i]
800	9.21E-13	5.71E-13	9.72E-13		1.01E-12[c]	4.99E-13	5.0E-13		

Table 5.4: *Comparison of MCTDH initial state selected rate constants on the WDSE, WSLFH and YZCL2 surfaces for* $H_2(v_1 = 0, j_1 = 0) + OH(v_2 = 0, j_2 = 0) \rightarrow H_2O + H$ *with theoretical results of* [a] *Manthe et al.[249],* [b] *Zhang et al.[231],* [c] *Zhang et.al.[202]* [d] *Truhlar et al.[250],* [e] *Goldfield et al.[203],* [f] *Troya et al.[205] and experimental results of* [g] *Talukdar et al.[183],* [h] *Tully et al.[175] and* [i] *Baulch et.al.[187], and* [j] *Orkin et al.[185].*

540
BHA/S
P11

THESIS
Lakshminath Bezbaroa Central Library
Indian Institute of Technology Guwahati
ACC. No. TH 1851
Date 28/3/19

5.2.3 Reagents in ro-vibrational excited states

5.2.3.1 Effect of reagent vibration

Figure 5.11 shows the effect of vibrational excitation of the two reagents on reaction cross section for the three surfaces. The $v_{1(2)}$= 1 results on the WDSE and YZCL2 surfaces are compared with the cross sections for the ground ro-vibrational states[248] and the literature values[160, 202]. For the WSLFH surface, we report the exact quantum dynamical results reported for the ground as well as for the excited states. It is worth mentioning here that the vibrationally excited cross sections for the H_2 + OH system on the YZCL2 PES are being reported for the first time while previous calculations on WSLFH by Troya et al.[205] used the QCT methodology for the $H_2(v_1,j_1 = 1)$ + $OH(v_2,j_2 = 2)$ process.

For $H_2(v_1 = 1)$ on the WDSE surface, the present results show sharp peaks in accordance with the previous CS results. But these peaks are absent in the results for WSLFH and YZCL2 surfaces. These peaks for WDSE owe their origin to the presence of unphysical wells in the entrance channel and has been discussed in the literature[231]. The initial high peaks in the probabilities contribute significantly to the large values of cross sections for $H_2(v_1 = 1)$ on the WDSE surface. The cross sections for vibrational excitation of H_2 show a steady and significant increase on both the YZCL2 and WSLFH surfaces in comparison to the respective ground state cross sections. For $OH(v_2 = 1)$, although both the present CC and CS[231] cross sections show an enhancement in comparison to $OH(v_2 = 0)$ on the WDSE surface, there is a difference in the quantum of enhancement observed. At lower energies, the CC cross sections are larger than the CS cross sections while at higher energies the CS calculations overestimate the exact cross sections. On the

TH-1851_Sayak

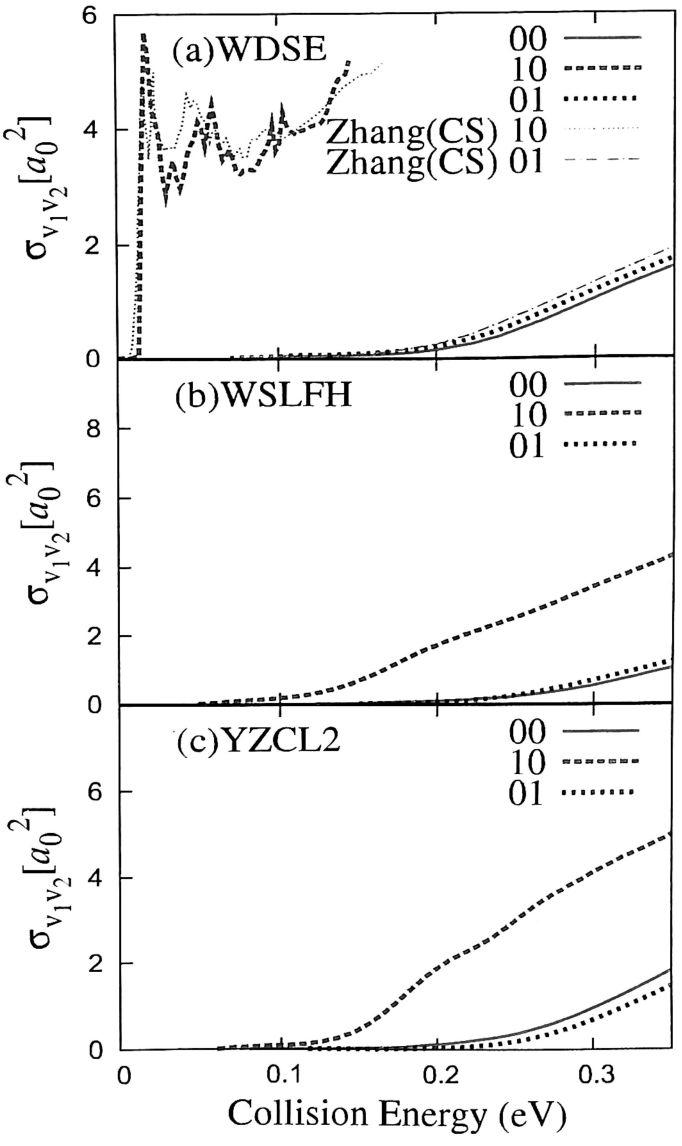


Figure 5.11: *Effect of initial vibrational excitations of the reagents on the integral reaction cross sections. Shown are the cross sections for the reactions* $H_2(v_1 = 0,j_1 = 0) + OH(v_2 = 0,j_2 = 0) \rightarrow H_2O+H$, *denoted as 00, and* $H_2(v_1 = 1,j_1 = 0) + OH(v_2 = 0,j_2 = 0) \rightarrow H_2O+H$, *denoted as 10, and* $H_2(v_1 = 0,j_1 = 0) + OH(v_2 = 1,j_2 = 0) \rightarrow H_2O+H$, *denoted as 01, on (a) WDSE, (b) WSLFH and (c) YZCL2 surfaces. The 6D-CS results of Zhang et al.[231] are also shown for comparison.*

WSLFH surface, the cross sections show a marginal decrease at lower energies and an increase at higher energies while the results show an uniform decrease over the

TH-1851_Sayak

entire range of energies for the YZCL2 surface.

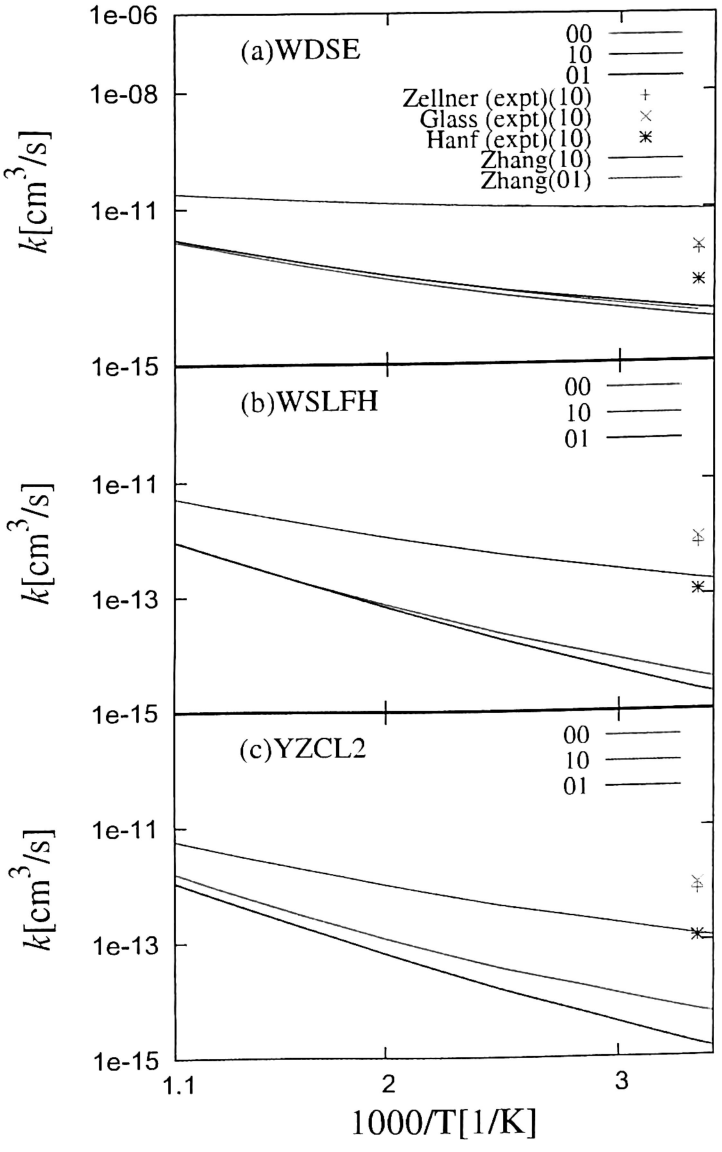


Figure 5.12: *Effect of the reagent vibrational excitations on the rate constants for* $H_2(v_1 = 1,j_1 = 0) + OH(v_2 = 0,j_2 = 0) \rightarrow H_2O + H$, *denoted as 10, and* $H_2(v_1 = 0,j_1 = 0) + OH(v_2 = 1,j_2 = 0) \rightarrow H_2O+H$, *denoted as 01, processes on WDSE, WSLFH and YZCL2 surfaces. The results for* $H_2(v_1 = 0,j_1 = 0) + OH(v_2 = 0,j_2 = 0) \rightarrow H_2O + H$, *denoted as 00[248], are also shown with the experimental results of Zellner et al.[96],Glass et al.[97],Hanf et al.[95]. The 6D-CS results of Zhang et al.[231] are also shown for comparison.*

The enhancement of reactivity is expected to be strongest for excitation along

TH-1851_Sayak

$T(K)$	MCTDH			Literature	
	WDSE	WSLFH	YZCL2	WDSE[a]	Experiment[b]
300	9.00E-12	1.89E-13	1.27E-13	9.02E-12	1.2E-13
400	1.13E-11	5.28E-13	4.32E-13	1.16E-11	
500	1.38E-11	1.08E-12	9.99E-13		
600	1.64E-11	1.85E-12	1.83E-12		
700	1.91E-11	2.80E-12	2.91E-12		
800	2.17E-11	3.89E-12	4.19E-12		

Table 5.5: *Comparison of MCTDH initial state selected rate constants on the WDSE, WSLFH and YZCL2 surfaces for* $H_2(v_1 = 1, j_1 = 0) + OH(v_2 = 0, j_2 = 0) \rightarrow H_2O + H$ *with the theoretical results of* [a] *Zhang et al.[231](6D-CS) and the experimental results of* [b] *Hanf et al.[95].*

the bond which is broken in the reaction. The same trend is visible on all the three surfaces with the enhancement in cross sections for vibrational excitation along the H-H bond being much higher compared to that along the O-H bond[94]. The OH bond remains essentially unchanged during the course of the reaction while the H-H bond length shows a significant enlargement in the transition state geometry and this results in a distinct enhancement in reactivity. The increment in H-H bond length at the transition state is approximately around 14 percent for WDSE and WSLFH surfaces while being around 10 percent for the YZCL2 surface[94]. This is quite a significant value considering the almost unchanged O-H bond length. This confirms the spectator nature of the O-H bond whereas the H-H bond couples strongly with the reaction coordinate motion and its vibrational excitation influences reactivity.

Our computed rate constants for vibrational excitation of the reagents are shown in Figure 5.12 while the data are tabulated in Table 4.5 and Table 4.6. The effect of excitation of H_2 on the rate constants for all the three surfaces considered is shown in Figure 5.12(a) and compared with experimental results. We should keep in

TH-1851_Sayak

$T(K)$	MCTDH			Literature
	WDSE	WSLFH	YZCL2	WDSE[a]
300	2.72E-14	2.19E-15	1.67E-15	1.90E-14
400	7.63E-14	1.71E-14	1.53E-14	7.26E-14
500	1.89E-13	6.50E-14	6.43E-14	1.96E-13
600	3.83E-13	1.67E-13	1.77E-13	4.15E-13
700	6.73E-13	3.36E-13	3.75E-13	7.40E-13
800	1.06E-12	5.79E-13	6.68E-13	1.18E-12

Table 5.6: *Comparison of MCTDH initial state selected rate constants on the WDSE, WSLFH and YZCL2 surfaces for* $H_2(v_1 = 0, j_1 = 0) + OH(v_2 = 1, j_2 = 0) \rightarrow H_2O + H$ *with results of* [a] *Zhang et al.[231](6D-CS).*

mind that our calculated rate constant is for the reaction at the ground rotational state of the reagents while the experimental results involve thermal averaging over the rotational state of the reagents. Vibrational excitation leads to a significant enhancement in rate constants for excitation for H_2 which is the bond which breaks in the course of the reaction. The WDSE results show a good agreement with the previously reported data on this surface calculated with CS approximation[231] although they highly overestimate the experimental results. The initial high peak in the cross sections arising from the inaccuracy in the surface is responsible for the exceptionally high increase of rate constants on the WDSE surface. Early experimental flow tube studies by Zellner et al.[96] and Glass et al.[97] reported absolute values $(7.5\pm3) \times 10^{-13}$ cm^3 molecule$^{-1}s^{-1}$ and $(9.9\pm2.4) \times 10^{-13}$ cm^3 molecule$^{-1}s^{-1}$ respectively for $H_2(v_1{=}1)$ at room temperatures. This amounted to an enhancement in rate constants by a factor of 120 and 155 respectively at room temperature. The rate constant obtained by recent laser spectroscopic studies performed by Hanf et al.[95] for $H_2(v_1{=}1)$ is $(1.2\pm0.1)10^{-13}$ cm^3 molecule$^{-1}s^{-1}$ at room temperature which is much smaller compared to the previous results. Our calculations on the YZCL2 surface, which is the most accurate surface for

TH-1851_Sayak

this reaction system till date, gives a rate constant value of 1.27 $\times$ 10^{-13} cm^3 $molecule^{-1}s^{-1}$ which shows an excellent agreement with the results of Hanf et al.[95]. The rate constants for $H_2(v_1{=}1)$ increase by a factor of 20 on the YZCL2 surface in comparison to the $H_2(v_1{=}0)$ rate constants. The rate constants obtained on the WSLFH surface is 1.89 $\times$ 10^{-13} cm^3 $molecule^{-1}s^{-1}$ which is higher than that obtained on the YZCL2 surface. The difference in the increments of the H-H bond length at the transition states for the YZCL2 and the WSLFH surfaces affects the rate of enhancement on the two surfaces. The YZCL2 rate constants are observed to be smaller than those for WSLFH at lower temperatures while in the higher temperature range the rate constants for the YZCL2 surface are larger.

Figure 5.12(b) shows the rate constants of OH($v_2 = 1$) in comparison to the ground state rate constants. Excitation of the non-reactive OH bond gives a relatively small but non-negligible enhancement over the entire range of temperatures for the WDSE surface in accordance with previously reported results[231]. An enhancement factor of 1.6 is obtained for OH($v_2 = 1$) with respect to OH($v_2 = 0$) in our CC results which is comparable with the factor of 1.7 obtained by Zhang et al. in their CS calculations[231]. An experimental study performed by Glass et al.[177] to obtain rate constant for OH($v_2 = 1$) have reported an upper limit of 1 $\times$ 10^{-14} cm^3 $molecule^{-1}s^{-1}$ at room temperatures. Similar studies performed by flow tube methodology for $H_2(v_1 = 1)$[97] have been shown to highly overestimate the rate constants in comparison to recent laser spectroscopic studies[95] which questions the accuracy of the values obtained for OH($v_2 = 1$). The rate constant on the YZCL2 value at 300 K is 1.7 $\times$ 10^{-15} cm^3 $molecule^{-1}s^{-1}$ while that on the WSLFH surface is 2.2 $\times$ 10^{-15} cm^3 $molecule^{-1}s^{-1}$. For the WSLFH surface the effect of excitation of OH is seen to be negligible over the entire temperature

TH-1851_Sayak

range with $k(v_2 = 1)/k(v_2 = 0)$ being close to 1 over the entire range. For the YZCL2 surface, a steady decrease in rate constants is observed over the entire temperature range considered.

5.2.3.2 Effect of reagent rotation

The effect of rotation of the reagents on the reactivity has been studied over the last two decades[160, 196, 197, 202, 205, 246, 249]. In Figure 5.13, we present the 6D-CC results on all the three surfaces. Previously reported results on WDSE by Zhang et al. were either 6D-CS[246] or 5D-CC[202] calculations. For WSLFH, this is the first set of quantum dynamical calculations for rotational excitations and the results are in sync with the QCT results performed earlier[205]. We also show in the same figure the MCTDH results on YZCL2 and compare against the 6D-CC results available[160]. Below we provide a comprehensive analysis of the present results in comparison with the literature results and the dependence of the results on the surface topology.

For rotational excitation of H_2, the observed decrease in reactivity in comparison to the ground state results are similar to that observed for 6D-CS[246] and 5D-CC[202] results on WDSE. For the WSLFH surface, the cross sections shows an increase with increase in rotation throughout the entire energy range. This is in accordance with the effects of rotational excitation observed in QCT calculations[205]. The YZCL2 surface shows an initial increase in reactivity at lower energies followed by a decrease at higher energies, although to a lesser extent compared to the results on WDSE. The initial transition state conformation is favorable for the WDSE surface[248] and this is evident from higher ground

TH-1851_Sayak

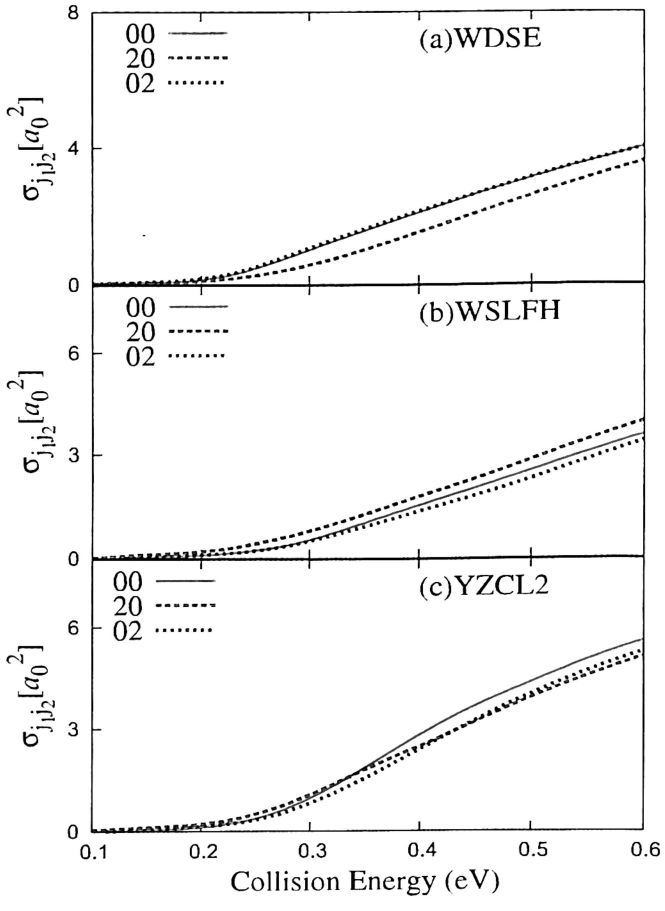


Figure 5.13: *Effect of reagent rotations on the integral cross sections for the* $H_2(v_1 = 0, j_1 = 2) + OH(v_2 = 0, j_2 = 0) \rightarrow H_2O + H$, *denoted as 20, and* $H_2(v_1 = 0, j_1 = 0) + OH(v_2 = 0, j_2 = 2) \rightarrow H_2O + H$, *denoted as 02, reactions on (a) WDSE, (b) WSLFH and (c) YZCL2 surfaces. The results for* $H_2(v_1 = 0, j_1 = 0) + OH(v_2 = 0, j_2 = 0) \rightarrow H_2O + H$, *denoted as 00, are also shown.*

state cross sections for the WDSE surface compared to the YZCL2 surface at lower energies. On rotation, cross sections on the WDSE surface show a faster decrease as the rotating reagents move away from the favored conformation. For the YZCL2 and WSLFH PESs, initial rotation brings the diatoms to a favored conformation leading to an increase in cross sections at lower energies. The orientational effect is expected to become less important with the increase in collision energy due to the relative decrease in interaction time as compared to the rota-

TH-1851_Sayak

tion period of the diatoms. At higher energies, hence, the ratio of time spent in the approach coordinate to the time required for appreciable rotation needs to be taken into account[251]. The presence of spurious wells in the entrance channel for the WDSE PES significantly increases the time spent in approach leading to a larger ratio and this leads to an uniform decrease in reactivity on H_2 rotation compared to the other surfaces. For the YZCL2 surface, the presence of a van der Waals minimum in the approach channel clearly shows a different effect in comparison to the WSLFH surface which is devoid of one[247]. Thus for the YZCL2 surface there are two competing effects at play; the orientation effect and the well influencing the reaction dynamics at lower and higher energies, respectively. For WSLFH, the absence of wells in the surface leads to an increase in cross sections over the entire energy range on account of the lower ratio as mentioned above.

The rotation of the OH diatom results in a decrease in reaction cross sections for the YZCL2 and the WSLFH surfaces while the effect is negligible for WDSE. The results obtained on the YZCL2 surface are slightly smaller than the 6D-CC results[160] for energies greater than 0.5 eV. The cross section on WSLFH and on WDSE are in sync with the QCT studies on WSLFH[205] and approximate[246] and reduced dimensional[202] studies on the WDSE surface, respectively. This decrease in reactivity has been discussed in literature in terms of a shielding effect[196, 205]. The center of mass is located close to the O-atom in OH and this results in the H-atom covering a larger volume compared to the O atom. This leads to the shielding of the O by H from the approaching H_2 diatom leading to a decrease in reactivity which is evident for the YZCL2 and WSLFH surfaces. Rashed et al.[196] had studied the effect of rotation of reagents on their surface (named RB) and concluded that the WDSE surface shows less suppression of reac-

TH-1851_Sayak

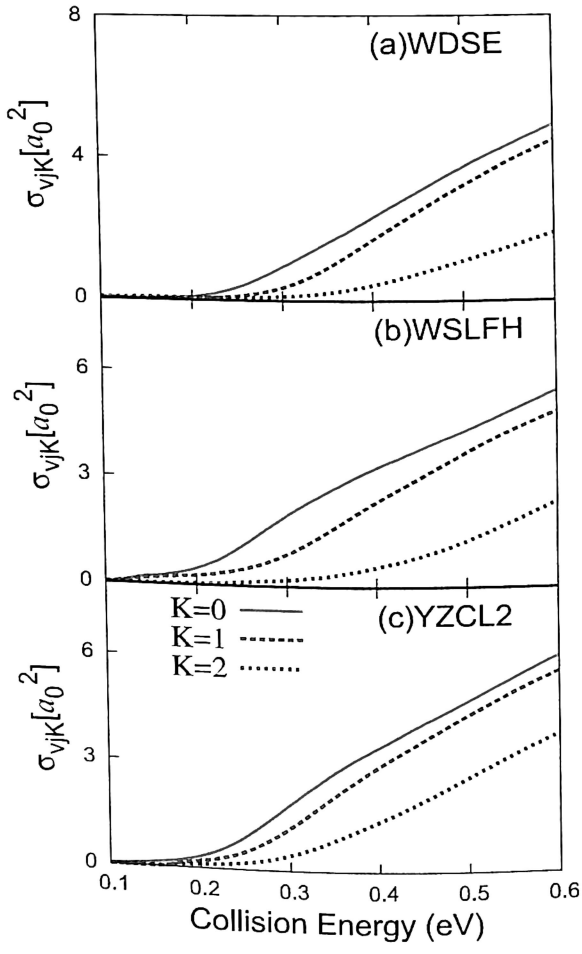


Figure 5.14: *K-dependent cross sections for $H_2(j_1 = 2)$ + $OH(j_2 = 0)$ on (a) WDSE, (b) WSLFH and (c) YZCL2 surfaces. The reagents are in their vibrational ground states.*

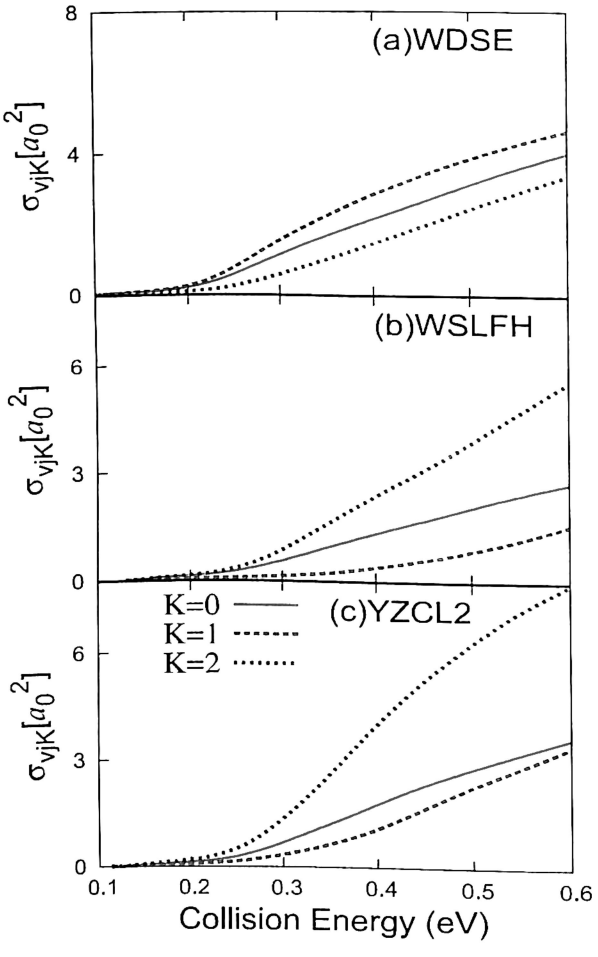


Figure 5.15: *K-dependent cross sections for $H_2(j_1 = 0)$ + $OH(j_2 = 2)$ on (a) WDSE, (b) WSLFH and (c) YZCL2 surfaces. The reagents are in their vibrational ground states.*

tivity by rotational excitation of OH and more suppression on H_2 excitation when compared with RB surface results. The long range attractive forces present on the WDSE surface were responsible for the above result. The RB surface obtained by removing the long range part from WDSE, hence, showed more decrease. The difference in the decrease of reactivity on going from WDSE to the WSLFH and YZCL2 surfaces can be traced to the absence of long range attractive forces in the later surfaces.

TH-1851_Sayak

$T(K)$	MCTDH		Literature
	WDSE	WSLFH	WDSE[a]
300	1.02E-14	1.62E-14	0.97E-14
400	3.53E-14	6.09E-14	3.72E-14
500	9.23E-14	1.53E-13	1.03E-13
600	1.99E-13	3.07E-13	2.26E-13
700	3.70E-13	5.36E-13	4.17E-13
800	6.17E-13	8.45E-13	6.81E-13

Table 5.7: *Comparison of MCTDH rate constants on the WDSE and WSLFH surfaces for* $H_2(v_1 = 0,j_1 = 2) + OH(v_2 = 0,j_2 = 0) \rightarrow H_2O+H$ *with results of* [a] *Zhang et al.[202](5D-CC).*

$T(K)$	MCTDH		Literature
	WDSE	WSLFH	WDSE[a]
300	1.57E-14	3.96E-15	1.45E-14
400	5.93E-14	2.16E-14	5.59E-14
500	1.57E-13	6.80E-14	1.55E-13
600	3.33E-13	1.59E-13	3.34E-13
700	6.00E-13	3.08E-13	6.04E-13
800	9.63E-13	5.24E-13	9.65E-13

Table 5.8: *Rate constants for* $H_2(v_1 = 0,j_1 = 0) + OH(v_2 = 0,j_2 = 2) \rightarrow H_2O+H$ *on the WDSE and WSLFH surfaces. The MCTDH results are shown in comparison to the 5D-CC results of* [a] *Zhang et al.[202].*

The dependence of cross section on K, the magnetic rotational quantum number for the diatoms, is shown in Figure 5.14 and Figure 5.15 for $H_2(j_1 = 2)$ and $OH(j_2 = 2)$, respectively. For a given j, $K = 0$ represents the planar approach of H_2 diatom towards the OH diatom, while $K = j$ represents the situation where the orbital motion of H_2 is perpendicular to the plane of motion of OH. For rotational excitation of H_2 as shown in Figure 5.14. it is observed that $K = 0$ has the maximum contribution to the cross section and $K = 2$ has the least. This is quite expected from the transition state structures of the H_3O system on the three surfaces as shown in Figure 5.9. The O-H-H angle is close to 180° on all

TH-1851_Sayak

the three surfaces considered. The planar approach for K=0 thus takes the H_2 diatom closest to that of the H_3O transition state structure leading to highest reaction probabilities its contribution is the biggest to the overall cross sections. The contributions are least for the perpendicular approach($K = 2$) as expected from the transition state structures.

For OH($j_2 = 2$) as shown in Figure 5.15, the K-dependency shows a completely different trend. For the WDSE surface K=1 accounts for the biggest contribution to the overall cross section. The H-O-H angle in the transition state is intermediate between between the perpendicular and planar configurations which explains the higher contributions from $K = 1$. For the WSLFH and YZCL2 surfaces the corresponding H-O-H angle is close to 90° which explains the dominance of the trajectory with perpendicular approach denoted by $K = j(K = 2)$.

The theoretical rate constants obtained from our MCTDH calculations for rotational excitations of both the reagents are shown in Figure 5.16 and tabulated in Tables 5.7 and 5.8 over a temperature range of 300 K to 800 K. On the WDSE surface, the rate constant shows an uniform decrease in comparison to the ground state rate constants of H_2. The MCTDH rate constants for rotational excitation of the reagents on the WDSE surface are in excellent agreement with the reference results which are 5D-CC. For $H_2(j_1 = 2)$, while the calculated rate constant at 300 K is 1.02× 10^{-14} cm^3 molecule$^{-1}s^{-1}$, the literature values are 0.99× 10^{-14} cm^3 molecule$^{-1}s^{-1}$(6D-CS) [246] and 0.97× 10^{-14} cm^3 molecule$^{-1}s^{-1}$(5D-CC)[202] for the same. The corresponding values at 800 K are 6.17× 10^{-13} cm^3 molecule$^{-1}s^{-1}$(6D-CC), 6.68× 10^{-13} cm^3 molecule$^{-1}s^{-1}$(6D-CS)[246] and 6.81× 10^{-13} cm^3 molecule$^{-1}s^{-1}$(5D-CC)[202]. It is interesting to note that the 6D-CS values are marginally closer to the 6D-CC results in comparison to the 5D-CC

TH-1851_Sayak

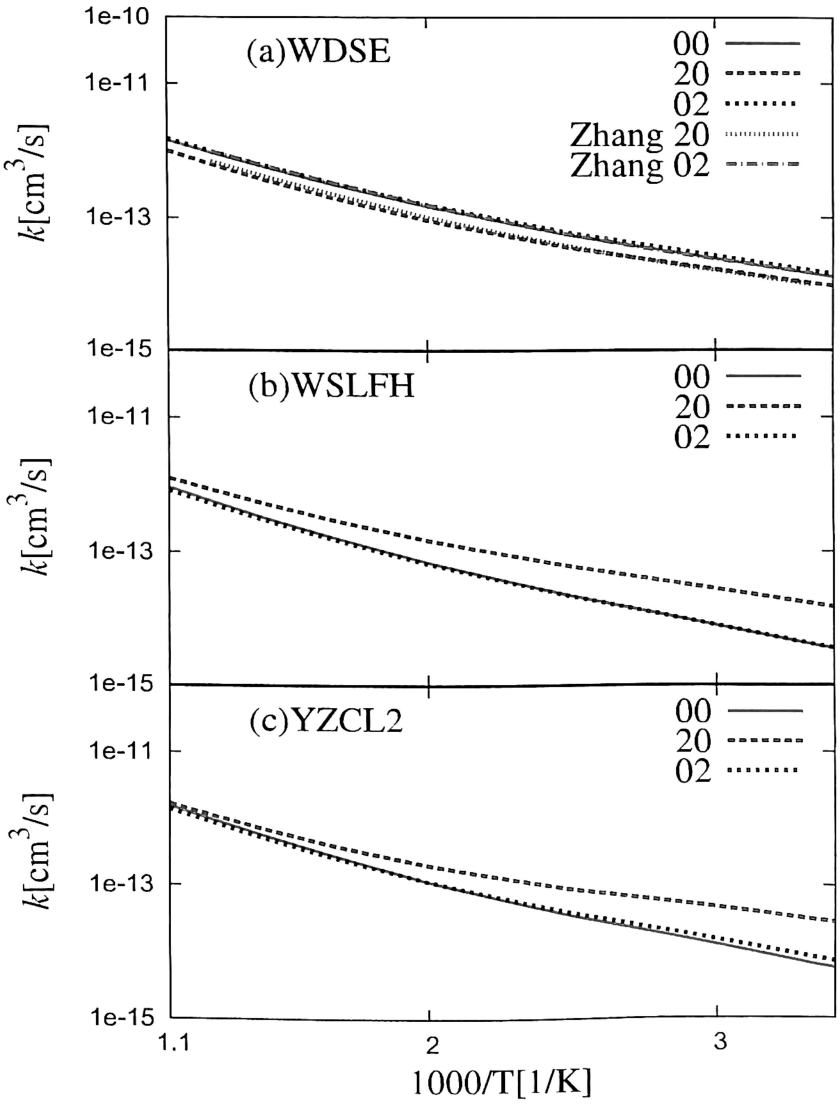


Figure 5.16: *Dependence of the rate constants on initial rotational states of the reagents. Results for* $H_2(v_1 = 0, j_1 = 2) + OH(v_2 = 0, j_2 = 0) \rightarrow H_2O+H$, *denoted as 20, and* $H_2(v_1 = 0, j_1 = 0) + OH(v_2 = 0, j_2 = 2) \rightarrow H_2O+H$, *denoted as 02, on (a) WDSE, (b) WSLFH and (c) YZCL2 surfaces are shown. The MCTDH results for ground ro-vibrational states (denoted as 00) are also shown. The mentioned reference is Zhang et al.[202](5D-CC).*

results over the entire energy range. For WSLFH, the rate constants show an increase with respect to ground state results over the entire range of temperatures, in accordance with the results of cross sections. The enhancement in rates is higher

TH-1851_Sayak

at lower temperatures compared to the enhancement at higher temperatures. The rate constant for $H_2(j_1 = 2)$ on the WSLFH surface is $1.62\times\ 10^{-14}$ cm^3 at 300 K with an enhancement factor of 4.1 while it is 1.5 at 800 K. A similar trend is observed on the YZCL2 surface with the corresponding enhancement factors being 4.7 at 300 K and 1.1 at 800 K, respectively.

The rate constants obtained for $OH(j_2 = 2)$ on the WDSE surface show an increase over the entire temperature range considered in comparison to $OH(j = 0)$. The same trend was also observed in the earlier approximate results[202]. For the WSLFH surface, the rotationally excited state values show a negligible change in comparison to those for the ground state over the entire range of temperature studied. On the YZCL2 surface, the rate constants shows a marginal increase on rotational excitation, for temperatures up to 700 K. For higher temperatures, a marginal decrease is observed in comparison to $OH(j = 0)$.

5.2.3.3 Effect of simultaneous ro-vibrational excitation

An investigation on the effect of simultaneous excitation of the reagents on the WSLFH and YZCL2 surfaces have been carried out and the results are shown in Figure 5.17 and Figure 5.18. As mentioned previously, the calculated rate constants for vibrational excitation of reagents are for the reaction at the ground rotational state of the reagents while the experimental results involve thermal averaging over the rotational state of the reagents. The effect of excitation of the reagents, in the vibrationally excited state($v_{1(2)} = 1$) and a higher rotational excited state($j_{1(2)} = 2$) have been studied. This would give a fair idea on the accuracy of the initial state selected rate constants in comparison to the experimental

TH-1851_Sayak

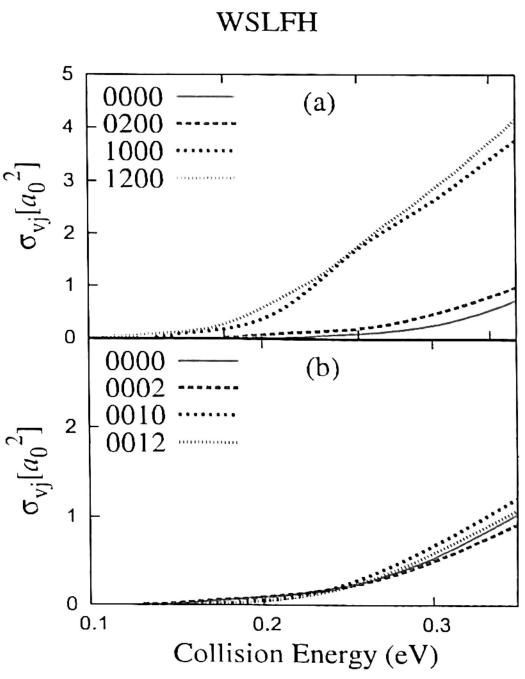


Figure 5.17: *Integral cross sections for (a)$H_2(v_1 = 1, j_1 = 2)$ + $OH(v_2 = 0, j_2 = 0)$ (denoted as 1200) and (b) $H_2(v_1 = 0, j_1 = 0)$ + $OH(v_2 = 1, j_2 = 2)$ (denoted as 0012) on the WSLFH surface. The cross sections for other ro-vibrational state combinations such as 0000, 0200 and 0002 are shown for comparison.*

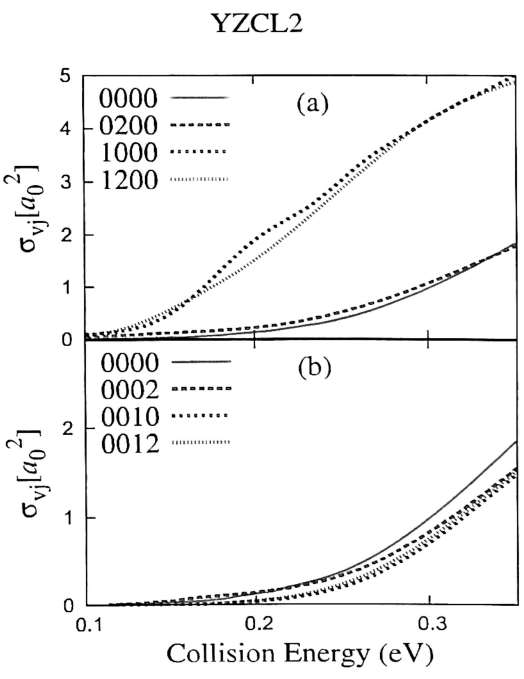


Figure 5.18: *Integral cross sections for (a)$H_2(v_1 = 1, j_1 = 2)$ + $OH(v_2 = 0, j_2 = 0)$ (denoted as 1200) and (b) $H_2(v_1 = 0, j_1 = 0)$ + $OH(v_2 = 1, j_2 = 2)$ (denoted as 0012) on the YZCL2 surface. The cross sections for other ro-vibrational state combinations such as 0000, 0200 and 0002 are shown for comparison.*

results.

For excitation of H_2 on the WSLFH surface, it is observed that the cross sections for the ($v_1 = 1$, $j_1 = 2$) state are larger than the ones for ($v_1 = 1$, $j_1 = 0$) state. The increase is significant at energies below 0.16 eV and at energies above 0.22 eV. In the intermediate energy range of 0.17-0.22 eV, the difference in cross sections for the two excited states narrows down significantly. On the YZCL2 surface, the cross sections for ($v_1 = 1$, $j_1 = 2$) state are smaller then the cross sections for ($v_1 = 1$, $j_1 = 0$) state for the intermediate energy range of 0.17-0.27 eV. Below 0.17

TH-1851_Sayak

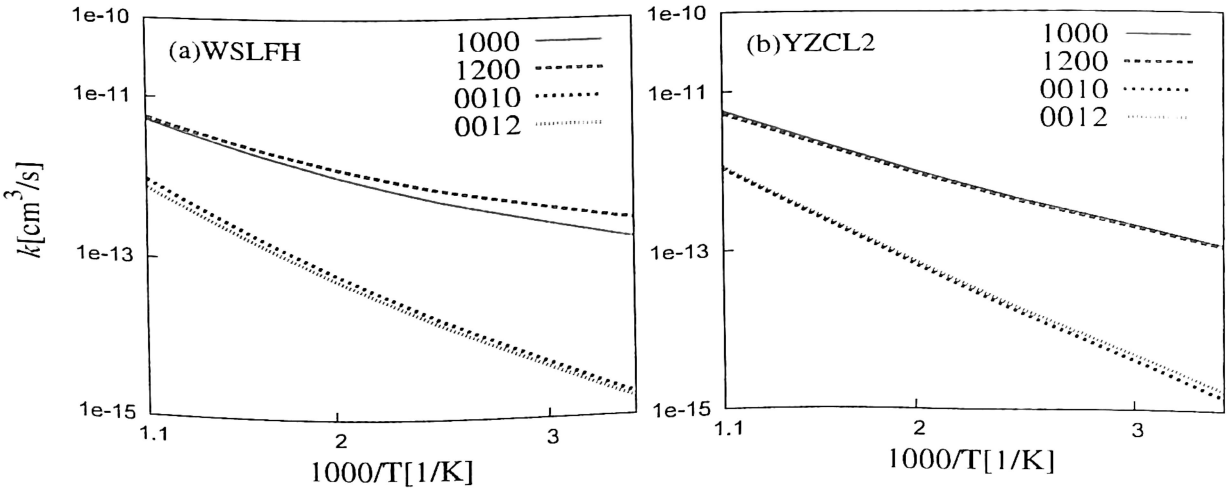


Figure 5.19: *Effect of simultaneous ro-vibrational excitation on the rate constants for $H_2(v_1,j_1)$ + $OH(v_2,j_2)$ on the (a)WSLFH and (b)YZCL2 surfaces.*

eV, the results for $v_1 = 1$, $j_1 = 2$ state are slightly larger. At higher energies, cross sections for both the excited states are almost the same.

The scenario is much simpler for the rotational excitation of OH. On the WSLFH surface, a significant decrease in cross sections is observed at energies above 0.25 eV for simultaneous ro-vibrational excitation, compared to that observed for vibrational excitation of the reagent. At lower energies, both the cross sections are similar. On the YZCL2 surface, the ($v_2 = 1$, $j_2 = 2$) cross sections are marginally larger compared to the ($v_2 = 1$, $j_2 = 0$) results over the entire energy range.

The exact effect of simultaneous ro-vibrational excitation becomes clearer with a comparative study of the reaction rate constants on both the surfaces, as shown in Figure 5.19. For simultaneous ro-vibrational excitation of H_2 on the WSLFH surface there is an increase in reaction rate at lower temperatures in comparison to the vibrationally excited state while the difference significantly narrows down at intermediate and higher temperatures. On the YZCL2 surface, the reaction rates for the ($v_1 = 1$, $j_1 = 2$) and ($v_1 = 1$, $j_1 = 0$) states show an excellent agreement

TH-1851_Sayak

over the entire energy range. The initial state selected rate constant obtained for $v_1 = 1$ on the YZCL2 surface agrees well with the experimental rate constant[95] at room temperature as has been discussed earlier. The present result shows that the initial state selected rate constants are fairly accurate on the YZCL2 surface, and inclusion of higher rotational states would show no significant change in the computed values. Simultaneous ro-vibration excitation of OH on both the surfaces show an insignificant variation in comparison to the $v_2 = 1$ rate constants on both the surfaces.

5.3 Summary and conclusions

The aim of this chapter of the thesis is two fold. Firstly, the effectiveness and applicability of the MCTDH algorithm to study reactive tetra-atomic scattering systems have been investigated. Secondly, the dependence of the reaction dynamics and kinematics of the H_2 + OH reaction on the surface characteristics and topology of the WDSE, WSLFH and YZCL2 surface have been studied.

The MCTDH methodology has been shown to be highly effective and accurate in determining reaction attributes of the H_2 + OH system. Huge amount of test calculations have been carried out to ascertain the POTFIT parameters, optimum number of single particle functions required for each mode and the size of DVR grid required for each degree of freedom to get fully converged results. The CAP parameters have been shown to strongly influence the reaction probabilities especially near the threshold. Aspects of the MCTDH methodology like "mode combination" of different degrees of freedom for a tetra-atomic system have been tested and this has been utilized to achieve an improvement in computational

TH-1851_Sayak

timing without compromising on the accuracy of the results. The importance of a perfect energy distribution of the initial wave packet has been underlined in achieving proper convergence of the reaction probabilities.

Studies performed on the WDSE and the YZCL2 surfaces for ro-vibrational ground states of the reactants showed excellent agreement with previously reported reaction probabilities, cross sections and rate constants. This motivated us to take up a study of the WSLFH surface on which the bulk of previous studies have been performed using QCT and TST methodology. The cross sections obtained on the WDSE, WSLFH and YZCL2 surfaces have been compared and the differences are explained with respect to the surface characteristics. The contrasting results have been shown to depend upon two competing factors over the entire energy range considered. At lower energies, the marginally higher cross sections on the WDSE surface have been shown to result from its incorrect "trans" structure of the transition state. The reaction on the YZCL2 surface, which has the correct "cis" structure for the transition state, encounters greater steric hindrance resulting in decreased initial reactivity at lower energies. As the translational energy increases, the reagents attain enough energy to overcome the steric hindrance and it is the energetics that become important. The lower barrier height for the YZCL2 surface favors enhanced reactivity at higher energy region in comparison to the WDSE surface. An analysis of the change in bond lengths on going from the transition state to the products lends credence to our arguments. The lower probabilities on the WSLFH surface in comparison to the WDSE and YZCL2 surface is expected to result from the absence of attractive wells in the surface unlike the spurious wells in the WDSE surface and the van der Waals minima in the YZCL2 surface.

An exhaustive study on the effects of ro-vibrational excitation of the reagents on

TH-1851_Sayak

all the three surfaces has thrown up some interesting results. These are the first quantum dynamical CC studies performed on all three surfaces for vibrational excitation of the reagents. The presence of resonating structures for $H_2(v_1{=}1)$ on the WDSE surface, similar to the previous CS studies, and their absence on YZCL2 and WSLFH shows that they arise from the inaccuracy in the WDSE surface. The excellent agreement of the ($v_1 = 1$) rate constants calculated on the YZCL2 surface with the latest experimental results shows the accuracy of the methodology and the PES. The rate constants for ($v_1 = 1$) on the WSLFH surface are close to those obtained on the YZCL2 surface, which is the most accurate surface till date. While excitation of the reactive H_2 results in enhancement in reactivity, the effect is negligible for excitation of OH.

The rotational excitation of the reagents results in contrasting results on the surfaces considered. While WDSE surface shows a significant decrease in reactivity, the YZCL2 surface shows an initial increase in reactivity at lower energies followed by a decrease at higher energies although to a much lesser extent compared to WDSE PES. For the WSLFH surface, the reactivity shows a marginal increase with increase in rotation throughout the entire energy range. The initial increment in cross sections on the YZCL2 and WSLFH surfaces results from the attainment of favorable conformation on rotation. For the WDSE surface, rotation results in moving away from the initial favored conformation resulting in a decrease in cross sections. The results obtained at higher energies are been explained on the basis of the ratio of time spent in the approach coordinate to the time required for appreciable rotation. Factors like the presence of spurious wells in the WDSE surface, a van der Waals minimum in the YZCL2 surface and the absence of wells in the WSLFH surface affect the approach time of the reagents

TH-1851_Sayak

and thus the mentioned ratio, which explains the observed results. For rotation of OH diatom, while the effect is negligible on the WDSE surface, a decrease in reactivity is observed for the WSLFH and YZCL2 surface.

A successful study of the H_2 + OH system by the MCTDH methodology motivates us to study heavier systems which would provide an even better test for the gain in computational timings envisaged in the MCTDH algorithm. Isotopic systems along with systems with higher degrees of freedom would form a logical extension of this work.

TH-1851_Sayak

Chapter 6

$H_2 + CN \rightarrow HCN + H$: Effect of Inclusion of Coriolis Coupling on Reaction Dynamics

6.1 Introduction

The H_2 + CN system is one of the few tetra-atomic systems whose dynamics has been studied thoroughly in the last three decades in both experimental and theoretical domains. Along with the H_2 + OH and CO + OH systems, the studies on the H_2 + CN system rank as one of the first attempts to give an accurate and detailed description of reactive scattering in systems involving more than three atoms. The reactive system is important in combustion[252] and atmospheric chemistry[253]. HCN, itself, is an important intermediate in the combustion reactions of hydrocarbon flames containing a nitrogen source and also play an im-

TH-1851_Sayak

portant role in the flame process of nitramine propellants. As nitrogen containing fuels are heated before entering the combustion zone it has been proposed that thermal decomposition occurs, producing low molecular weight compounds containing nitrogen. These compounds include CN and HCN as well as NH, NH_2 and NH_3. The reaction of CN and water forms a rapid equilibrium with HCN and OH. HCN is also an intermediate in many proposed mechanisms for NO_x formation in hydrocarbon/air flames.

The $H_2(v_1 = 0, j_1 = 0)$ + $CN(v_2 = 0, j_2 = 0)$ reaction is exothermic by 0.95 eV and has a barrier $\sim$ 0.14 eV along the reaction path[98]. Experimental and theoretical studies have probed the H_2 + CN reaction system from a variety of perspectives. Experimental measurement of rate constants over a wide range of temperatures and an accurate estimation of the product vibration state distributions have formed a concrete basis for understanding the reaction kinetics and the dynamics involved. Early theoretical studies performed on *ab initio* and semiemperical potential energy surfaces[254–257] served as a benchmark for development of various reduced and full dimensional methodologies to study the reactive tetraatomic system. The development of a global PES[98] paved the way for accurate theoretical studies, with the obtained results showing an appreciable concurrence with experimental results. Unlike the H_2 + OH reaction, the role of the non reactive CN bond has been ambiguous and its status as a "spectator bond" has been questioned in various experimental and theoretical studies. Accurate full dimensional theoretical studies using an exact form of the Hamiltonian is expected to confirm the exact nature of the bond.

This chapter begins with a literature survey on the exhaustive experimental studies, followed by an overview of the available potential energy surfaces and a

TH-1851_Sayak

summary of the theoretical calculations performed using various methodologies on the H_2 + CN system. This is followed by detailed discussions on the results obtained from the application of the MCTDH algorithm to study the reaction system, with reagents in the ground and vibrational excited states. A summary of the work done in this chapter along with the conclusions derived are given in the last section.

6.1.1 Experimental results

Kinetic studies [258–273] over a temperatures range 209-1500 K have been able to provide an exhaustive documentation of the kinetics of the system. Most of the studies have been on thermal rate constant measurements with the observed activation energy suggesting a barrier of about 0.13 eV. There have been several studies of product state distributions where H_2 has been replaced by a hydrocarbon or a hydrogen halide[274–276]. The rate constants measured by different groups till 1995 were reviewed by Yang and Lin[273]. Initial experimental studies using laser were performed by Li and co-workers[258] where cyanogen was photolyzed to produce known concentrations of CN radicals in the v_2 =0 and v_2 =1 levels. Contrary to expectations that vibrational energy would not play an important role in exothermic reactions with low energy barriers, rate constants increased by a factor of 2.0±0.6 for reaction of CN(v_2=1) with H_2(v_1=0) compared to the vibrational ground state rate constants[262, 264]. The study had two conclusions: firstly, vibrational enhancement does enhance rate of the chemical reaction; secondly, it was observed that vibrational energy was not as effective as translational energy thus indicating the presence of an early barrier. This agreed with the *ab*

TH-1851_Sayak

initio calculations[254] which suggested that the reaction has an early barrier and vibrational energy is not as effective as translational energy in surmounting the barrier. Studies performed by Juan et al.[259] reported a lower enhancement factor of 1.2±0.3 for CN(v_2=1), compared to the rates obtained for CN(v_2=0). Atakan et al.[263] obtained an enhancement factor of 1.4±0.2 and explained the minor enhancement in reaction rates by terming the C-N bond as a "spectator bond "which remains essentially unchanged during the course of the reaction. Sims and Smith[262] made a detailed study on rate constants for reactions of CN(v_2=0) and CN(v_2=1) with H_2(v_1=0) over a temperature range of 295-768 K. The ratio of the rate constants for CN(v_2=1) compared to CN(v_2=0) were close to one for all the temperatures studied, indicating that vibrational excitation does not usually enhance the rate of a direct atom-transfer reaction. Experimental studies performed by Sun et al.[264] over a similar temperature range found very little enhancement of the reaction by vibrational excitation of CN. There are no measurements of the rate with H_2 in its vibrationally excited state. Che and Liu[266, 267] reported the doubly differential cross section for the isotopic D_2 + CN reaction measured in their crossed-beam apparatus which was affected more by the rotation than the vibration of the CN bond. Contrary to studies portraying the CN bond as a pure spectator bond, studies on the reverse reaction by Kreher et al.[265] and Crim and co-workers[277] have provided evidence that CN vibration participated in the reaction dynamics and did not behave as a pure spectator bond. Both these groups independently reported the initial vibrational excitation on reactivity of the HCN + H reaction. Crim's group reported 23% of the product CN in v=1 while Gericke's group reported 40% for the same. Both results indicate that the *HCN + H* reaction cannot be totally described by a simple picture in which the non-reactive *CN* bond is spectator during reaction since a significant part of the

TH-1851_Sayak

available energy is distributed into CN vibrational energy. The rate constants for the reactions H_2 + CN and D_2 + CN have been reported by Macdonald and co-workers[270] over a temperature range 293-380 K. The product vibrational state distribution of HCN has also been measured by the same group[272]. The presence of significant population in the CN and CH modes provided a proof of the non-spectator nature of the CN vibration in the reaction.

6.1.2 Potential energy surface

An important aspect in accurate theoretical studies of a system is the development of a proper potential energy surface. Information about the potential energy landscape for the H_2CN system was first obtained from the *ab initio* calculations by Bair and Dunning[254] in which they characterized the geometry and vibrational frequencies of H_2CN, along with the saddle point structures. A minimum corresponding to the molecule H_2CN was found to be the most stable feature on the PES. A shallow minima was also observed for the "cis" and "trans" HCNH adducts which were connected to HCN by H-migration. A collinear saddle point was found and barrier height for the abstraction reaction was reported to be 0.26 eV(with respect to H_2 + CN). A study of rate constants for the H-atom abstraction reaction, using transition state theory by Wagner et al.[255] showed that good agreement with experiment is obtained if the theoretically predicted barrier height is reduced from 0.26 eV to 0.18 eV. This was followed by Brooks and Clary[256] developing a PES constructed from a three body LEPS surface, combined with a modified Morse potential for the CN two-body contribution. The barrier height of this PES was set at 0.24 eV. A semiemperical three dimensional potential energy

TH-1851_Sayak

surface for the title reaction was developed by Sun and Bowman[257] based in part on the *ab initio* results by Bair and Dunning[254]. A very similar potential energy surface was also reported by Clary based on *ab initio* points[278]. Both these surfaces were constructed assuming that the only four-atom stationary point is the collinear saddle point for hydrogen abstraction. This resulted in the intermediate complexes, H_2CN, "cis" and "trans" HCNH complexes, which were otherwise shown to be present in the *ab initio*[254, 255] calculations, being neglected in the resulting surface[279]. ter Horst et al.[98] developed three analytical potential energy surfaces for the H_2 + CN reaction representing different fits to highly accurate *ab initio* computational results. Almost the complete molecular configuration space was explored using high quality *ab initio* molecular orbital methods based on multireference configuration interaction (MR-CI) wave functions for various levels of complete active space (CAS) references. These PES's describe not only the hydrogen abstraction reaction channel but also the complex-formation channels those lead to the H_2CN, *cis* and *trans*-HCNH minima. The *ab initio* calculations were concentrated at geometries near the collinear abstraction path and in the region of the H_2CN complex. The global energy PESs describes all the features of the H_2 + CN and H + HCN interactions with near chemical accuracy in some regions. The three surfaces herein denoted TSH1, TSH2, and TSH3 with slightly different saddle point properties were investigated to determine the sensitivity of the dynamics on the properties of the surface. The *ab initio* barrier estimate of 0.19 eV appeared to be too high by about 0.04 eV to explain experimentally measured rate constants. The PES labeled surface TSH3, with a barrier height of 0.14 eV gave the best agreement with experiment for the temperature dependence of the calculated rates. The TSH3 PES has been used for the study of the H_2 + CN system in this work.

TH-1851_Sayak

6.1.3 Theoretical results

Initial theoretical calculations for the present system were performed by Wagner and Bair[255], using conventional transition state theory. The rate constants calculated on this surface showed a general agreement with the available experimental results[258]. Importantly, the CN vibrational frequency was found to rémain constant along the reaction path in these studies, expected as a result of early saddle point for the reaction. Approximate quantum scattering calculations, which include the exact collinear calculations by Brooks and Clary [256], the reduced dimensionality adiabatic bend approximation(RDAB) by Bowman and co-workers[257, 264, 280], the rotating bond approximation by Clary[278], concluded that the CN bond largely behaves as a spectator bond in the reaction. However, these findings can be attributed to an unrealistic character of the PES employed in these calculations[281].

With the development of the TSH3 PES by ter Horst et al., a wide range of studies using quasi-classical trajectory (QCT)[98, 282] reduced dimensional quantum[279, 281, 283] and semi-classical methods[282] have been performed on the system. Schatz et al.[283] performed quantum dynamical calculations on the TSH3 PES to study the exact nature of the CN bond. They found that the non-reactive CN stretching motion significantly affects the reaction dynamics because of substantial coupling between CN and CH stretches in HCN. The studies involving the vibrational or rotational excitation of the CN bond in quantum calculations by Takayanagi and Schatz[281] using the rotating-bond approximation on the TSH3 surface resulted in insignificant change in the cross section for the reaction. This result is consistent with the fact that the forward reaction has an

TH-1851_Sayak

early barrier. For the reverse reaction, a comparison of the effect of excitation of both the CN and CH bonds on threshold energy, puts the role of the CN bond in proper perspective. While a decrease of $\sim$ 0.272 eV was observed on excitation of the CN stretching mode, a similar excitation of the CH stretching mode resulted in a decrease of the threshold by $\sim$ 0.427 eV. Thus, while excitation of the reactive bond in the system expectedly accounts for the higher decrease in threshold energy, the effect of excitation the non-reactive bond is not insignificant. This lends credence to the theory that the CN bond is not merely a "spectator bond" and has a significant role in the reaction dynamics. The HCN vibrational state distributions for the H_2 + CN reaction were also found to show significant population in both CH and CN stretching normal modes. A similar conclusion was also derived by Bethardy et al.[282] in their QCT studies based on the observation that the CN normal mode of the HCN product does contain some local mode C-H stretching character which establishes the coupling between the CH and CN stretching modes.

Manthe and Matzkies[284] computed the rate constants and cumulative reaction probabilities by carrying out quantum dynamical calculations in five dimensions using a flux-flux correlation function approach which avoids resorting to the state-resolved scattering calculations. Six dimensional (6D) wave packet calculations under the centrifugal sudden (CS) approximation have also been performed for a few vibrational[285] and rotational[286] states of both the diatoms. These approximate calculations[285] reported a slight decrease in the reaction cross section on the vibrational excitation of CN while the vibrational excitation of H_2 considerably enhances the reaction. A comparison with experimental rate constants[257, 262] showed an appreciable agreement at higher temperatures, while the theoretical

TH-1851_Sayak

results were considerably lower at lower temperatures. In view of this, Zhu et al.[285] concluded that the effective barrier on the TSH3 surface may be too high by about 0.01 eV. The other explanation proposed for this discrepancy was the exclusion of higher rotational states in the calculations, which are included in calculation of experimental thermal rate constants. Quantum-classical calculations performed by Coletti and Billing[287] included the higher rotational states but the discrepancy still remained thus lending credence to the proposition that the surface was flawed. The only 6D study including the Coriolis coupling (CC) on this system is by Zhang and Lee[286]. They calculated the reaction cross sections for the ro-vibrational ground states of the two diatoms which show a significant difference from the CS results at high energies. It was also shown that rotational excitations of CN had essentially no effect on the cross section but H_2 rotational excitations caused a decline in calculated cross sections. Recent studies using the variational transition state theory performed by Ju et al.[288] concluded that CN can be regarded as a spectator in the title reaction. Thus it can be summarized from previous studies that the exact nature of the CN bond is still highly ambiguous and merits further investigation.

In the present work, we aim to make a comparison of the reaction cross sections calculated using an exact form of the kinetic energy operator with the previous approximate results[285] for the vibrationally excited states of the two reagents. This study is justified as it will make us conclude and then explain the overall enhancing or inhibiting effects of the vibrational excitations. Unlike the H_2+OH reaction, the CC results have been shown to significantly deviate from the CS results at higher energies[286] for the ro-vibrational ground states of the reagents. This makes the accurate CC calculations extremely important to gain knowledge

TH-1851_Sayak

on the effect of vibrational excitation, given the nature of the CN bond in the dynamics of the reaction. The quantum calculations have been performed for the ground as well as for the first vibrational states of the two diatoms using the wave packet propagation method as implemented in the multiconfiguration time-dependent Hartree (MCTDH) algorithm[51–54, 66]. This is the first full dimensional study of the vibrational excitation of the reagents without the use of the CS approximation for total angular momentum $J > 0$. The present quantum dynamical calculations have been carried out on the TSH3 surface[98].

TH-1851_Sayak

No. of grid points	$N_{R_3}/N_{R_1}/N_{R_2}/N\theta_1/N\theta_2$	80/30/6/28/31
Grid points for k_1,k_2	k_{min}/k_{max}	-8/8
Extension of R_3 grid	$R_{3_{min}}/R_{3_{max}}$	3.0/13.5
Extension of R_1 grid	$R_{1_{min}}/R_{1_{max}}$	0.5/6.5
Extension of R_2 grid	$R_{2_{min}}/R_{2_{max}}$	1.85/2.45
CAP order	β_{R_3}/β_{R_1}	3
CAP strength	$\eta_{R_{3_{(v=0)}}}/\eta_{R_{3_{(v_1=1)}}}/\eta_{R_{3_{(v_2=1)}}}$	0.001/0.12/0.09
CAP strength	$\eta_{R_1(v=0)}/\eta_{R_1(v_1=1)}/\eta_{R_1(v_2=1)}$	0.0003/0.007/0.03
Starting point of CAP	R_{3_c}/R_{1_c}	8.0(12.0)/3.50
CAP length	L_{R_3}/L_{R_1}	5.5/3.0
Center of χ_0	R_0	9.0
Width of χ_0	d_R	0.22
Initial momentum of χ_0	p_0	-6.0(6.9)
Propagation time	T	200

Table 6.1: *Numerical parameters of the MCTDH calculations for the* $H_2(v_1 = 0,j_1 = 0) + OH(v_2 = 0,j_2 = 0)$ *system(in atomic units if not otherwise stated). The parameters for calculations involving vibrationally excited reagents* $H_2(v_1 = 1)$ *and* $CN(v_2 = 1)$ *are given in brackets if those differ from ground state parameters.*

6.2 Results and discussion

6.2.1 Numerical details

Table 6.1 displays the relevant parameters used in MCTDH calculation for the $H_2(v_1 = 0,j_1 = 0) + CN(v_2 = 0,j_2 = 0)$ reaction. The parameters for vibrational excited state($v_{1(2)}= 1$) calculations have been shown in brackets in the table, if those differ from the ground state parameters and are also discussed below. We have carried out extensive test calculations to check the convergence of our results with respect to the number of SPFs considered or each mode and the size of DVR grid for each DOF. We have used the optimum number of spfs to get accurate converged results with minimum usage of computational resources. Reaction probabilities are obtained from the wave packet propagations using a

TH-1851_Sayak

flux method and subsequently, the reaction cross sections and rate constants are calculated.

A set of seven coordinates was used to parametrize the Hamiltonian as has been mentioned in Chapter 3(See Figure 3.4). The H_2 and OH bond distances are represented by R_1 and R_2, respectively while R_3 is the distance between the centers of mass of the two diatoms. θ_1, θ_2 are the polar angles. The torsion angle φ is written as φ_1 and φ_2 in the E_2 frame of reference.

The R_3 and R_1 coordinates are represented by sinc-DVR grids. The grids for R_3 and R_1 extend from 3 to 13.5 and 0.5 to 6.5 a_0, respectively. A sinc DVR of 80 and 30 points is used for R_3 and R_1 respectively. For the CN binding coordinate R_2, a harmonic oscillator DVR of 6 points is used to represent the grid. For the angles, a two-dimensional "extended Legendre DVR"[150] has been employed.

Optimum CAP parameters are used to avoid the wave packet being reflected from the grid ends. The reaction parameters for both the ground and excited state calculations have been found to be highly sensitive to the CAP parameters. The CAP used to absorb the wave function beyond the analysis point starts at $R_3 = 8.0$ a_0 and $R_3 = 12.0$ a_0 for ground state and excited state calculations, respectively. For R_1, it starts at 3.50 a_0 for both the states. The strengths and orders of the CAPs are (0.001,3) and (0.0003,3), along R_3 and R_1. CAPs of strengths and orders of (0.12,3) and (0.09,3) are used along R_3 and R_1, respectively. for the vibrational excitation of the H_2 bond. For the CN excited state calculations, the corresponding values are (0.007,3) and (0.03,3).

Calculations have been carried out to obtain reaction attributes upto a translational energy range of 0.5 eV. The initial Gaussian is centered at R_3= 9.0 a_0

TH-1851_Sayak

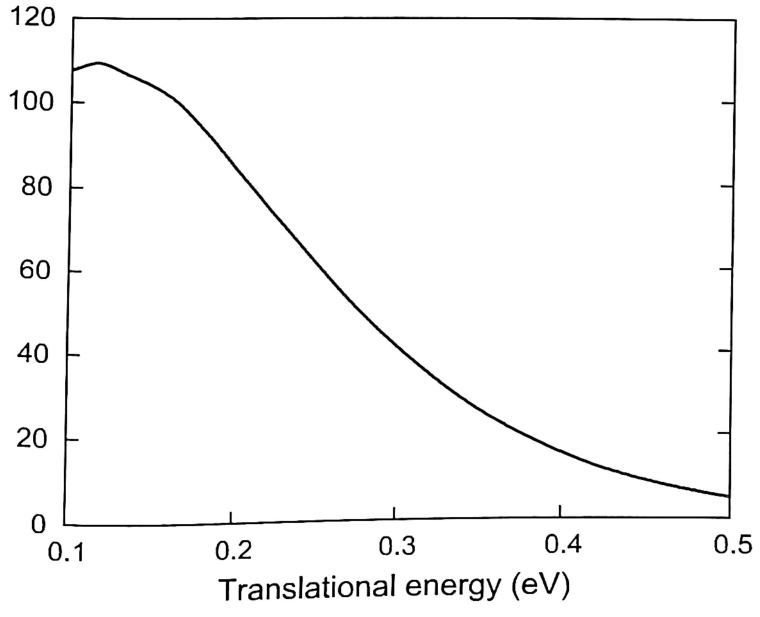


Figure 6.1: *Energy distribution of the initial wave packet on the TSH3 surface with a momentum of 6.0 a_0 and width of 0.22 a_0.*

while the width of the Gaussian wave function is $d_R = 0.22\ a_0$. Having a very large distribution in the low energy regime ensures a good convergence in that region. The momentum(p_0) of the initial wave packet is -6.0 a_0 for the ground state calculations while it is -6.9 a_0 for the excited state calculations. The initial position, width and momentum of the wave packet significantly affects the reaction probabilities and the parameters used have been considered so as to cover the entire energy range. The momentum and width of the wave packet determines the energy distribution and detailed calculations have underlined the importance of a perfect energy distributions on the convergence of reaction probabilities. It has been observed that a good energy distribution strongly influences proper convergence especially at lower energies. The energy distribution of a typical initial wave packet on the TSH3 surface is depicted in Figure 6.1 over the entire energy range considered.

TH-1851_Sayak

Mode	Primitive Basis		number of SPFs	
	Type	Size	v=0	v=1
(R_3, R_1)	(sin,sin)	(80,30)	45	45
(R_2, θ_2, k_2)	(HO,KLeg)	(6,476)	45	30
(θ_1, k_1)	KLeg	527	30	15

Table 6.2: *Parameters for the primitive basis sets employed for each degree of freedom. The brackets indicate the mode combinations, and the last column gives the number of single-particle functions used for the modes. HO is a harmonic oscillator DVR; KLeg is a two-dimensional extended Legendre DVR [150].*

Number of natural potentials	l_2/l_3	30/10
Relevant region for R_3 coordinate, au	$R_{3_{min}}/R_{3_{max}}$	2.50/7.00
Relevant region for R_1 coordinate, au	$R_{1_{min}}/R_{1_{max}}$	0.8/2.30
Relevant region for R_2 coordinate, au	$R_{2_{min}}/R_{2_{max}}$	1.90/2.30
Relevant region for θ_1 coordinate,	$\theta_{1_{min}}/\theta_{1_{max}}$	0.10/2.40
Relevant region for θ_2 coordinate,	$\theta_{2_{min}}/\theta_{2_{max}}$	0.10/3.00
Number of iterations	N_{iter}	10
Potential cutoff(V_{min}=0.0 eV)	V_{max}	1.0 eV

Table 6.3: *Numerical parameters for the potential fit for the TSH3 PES.*

Mode combinations are used for the propagation. As was the case in the H_2 + OH reaction in the previous chapter, the seven degrees of freedom are combined to produce three different sets: $(R_3,R_1),(R_2,\theta_2,k_2),(\theta_1,k_1)$. The parameters for the primitive basis sets employed for each degree of freedom are shown in Table 6.2. The number of SPFs used for the combined modes are 45, 45, 30 for the ground state calculations while the numbers are 45, 30, 15 for the excited state calculations. The quality of convergence has been checked by checking the maximum over time of populations of the least occupied natural orbitals which was close to 10^{-5} for all calculations.

In the Fourier transformation of the potential, Ω_{max} was set to 1 on the TSH3 surface. Then each transformed potential was fitted separately using 585 terms.

TH-1851_Sayak

The numerical values are tabulated in Table 6.3. Instead of using the whole region of the surface while applying POTFIT, we have restricted the algorithm to concentrate on the following space: 2.50 $a_0 < R_3 < 7.0\ a_0$, 0.80 $a_0 < R_1 < 2.30\ a_0$, 1.90 $a_0 < R_2 < 2.30\ a_0$ and $V < 1.0$ eV. A total of 10 iterations was used to get an accurate fit. The relative error was found to be less than 4 meV, in the relevant region defined above.

TH-1851_Sayak

6.2.2 Reaction probabilities

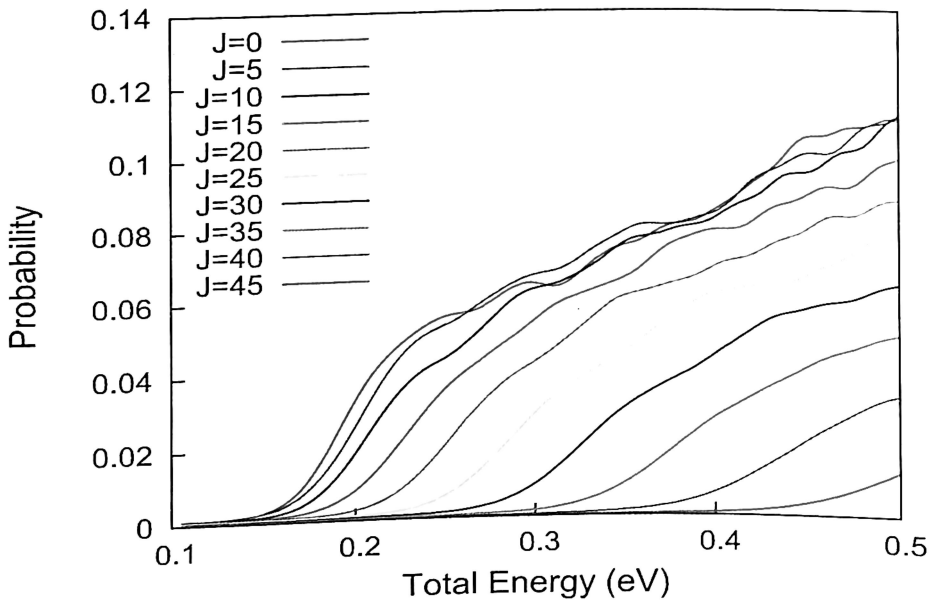


Figure 6.2: *Reaction probabilities for $H_2(v_1 = 0, j_1 = 0)$ + $CN(v_2 = 0, j_2 = 0)$ for selected J's as a function of translational energy.*

The wave packet propagation has been carried out for J = 0-50. A few selected reaction probabilities are shown in Figure 6.2 over the energy range 0.1-0.5 eV. The accuracy of the reaction probabilities has been found to be significantly dependent on the initial position and the width of the initial wave packet. As mentioned previously, proper convergence of the reaction probability is achieved by having a good energy distribution over the entire energy range considered. The reaction probability for J=0 shows an energy threshold close to 0.1 eV in accordance with the reported results[285]. The probabilities for lower J's upto J = 10 exhibit small resonance structures at higher energies. These oscillatory features highlight the fact that at certain energies the probabilities for J=5 are larger than the probabilities for J=0. These features eventually smoothen out with increase in J. The reaction probabilities for higher J values exhibit a smooth curve without any ma-

TH-1851_Sayak

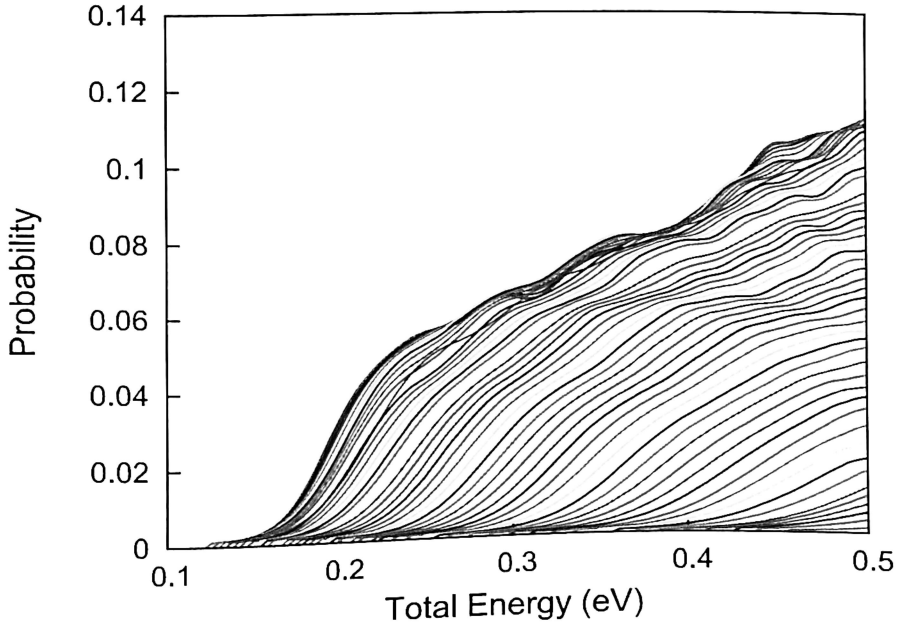


Figure 6.3: *Interpolated reaction probabilities for* $H_2(v_1 = 0, j_1 = 0) + CN(v_2 = 0, j_2 = 0)$ *for* $J = 0$-50.

jor structural distortions or oscillatory behavior. We have used the J-interpolation algorithm[61] which gives us the interpolated probabilities between two accurately calculated probabilities. Every fifth reaction probability has been accurately calculated and the intermediate reaction probabilities have been obtained using the J interpolation algorithm. The interpolated reaction probabilities for all the J values are shown in Figure 6.3. Extensive tests have been carried out to ensure that the interpolated algorithms are not in substantial variance with the exact ones for the same.

6.2.3 Integral cross sections

Figure 6.4 displays the reaction cross sections obtained using the MCTDH method along with the previous wave packet results of Zhang and Lee[286] on the TSH3

TH-1851_Sayak

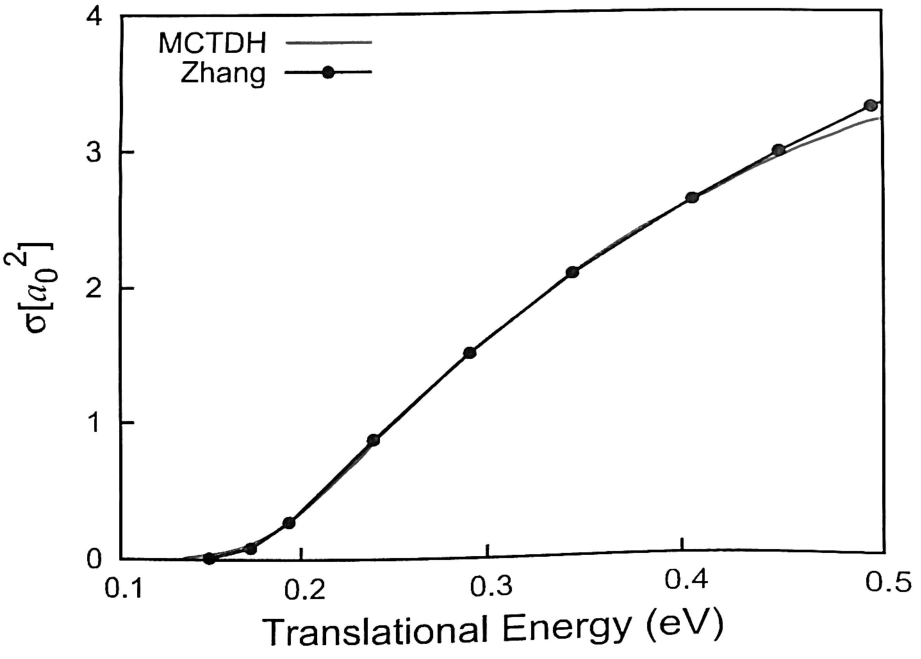


Figure 6.4: *Comparison of MCTDH integral cross sections for the $H_2(v_1 = 0)$ + $CN(v_2 = 0)$ reaction as a function of translational energy with results of Zhang et al.[286].*

potential energy surface for ground ro-vibrational states of the reactants. Our results show an excellent agreement with the full dimensional quantum results of Zhang and Lee[286], over the considered energy range. It is important to mention here that the wave packet results of Zhang et al.[286] were obtained by including the Coriolis coupling in their calculations. Although the H_2 + CN system is heavier and more complicated system than the H_2 + OH system discussed in the previous chapter, the agreement with the previous theoretical results is as good as it was for the the H_2 + OH system.

The effect of vibrational excitations of CN and H_2 on the reaction cross sections are shown in Figure 6.5 and Figure 6.6. The MCTDH results are compared with the earlier quantum results reported by Zhu et al.[285] using a J-shifting approx-

TH-1851_Sayak

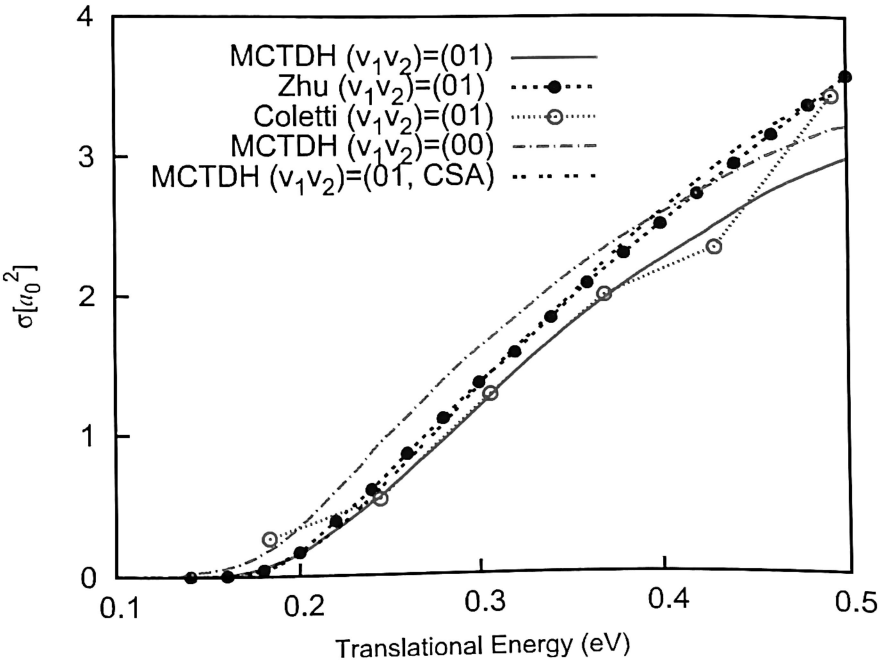


Figure 6.5: *Comparison of the CC and CSA integral cross sections with the J-shifting results from Zhu et al.[285] for the* $H_2(v_1 = 0, j_1 = 0) + CN(v_2 = 1, j_2 = 0)$ *reaction as a function of translational energy with both the diatoms at their respective rotational ground states. The mixed quantum-classical results of Coletti et al.[287] and the present CC cross sections for* $H_2(v_1 = 0, j_1 = 0) + CN(v_2 = 0, j_2 = 0)$ *are also plotted for reference. The reactants are in their respective rotational ground states.*

imation. The present results obtained using an exact kinetic energy operator and shown in the figures help us to comment on two important aspects regarding the reaction dynamics of this system: the effect of having an approximate Hamiltonian for the propagation and the role played by the CN bond in the reaction. For the H_2 + OH system(see Ref. [248] and the references therein), the results obtained within the CS approximation show a good agreement with the CC results for the ground ro-vibrational states of the reagents while for rotationally excited reagents, the CS cross sections were found to be smaller than the CC results in the whole energy range. The present CC cross sections are slightly larger than both

TH-1851_Sayak

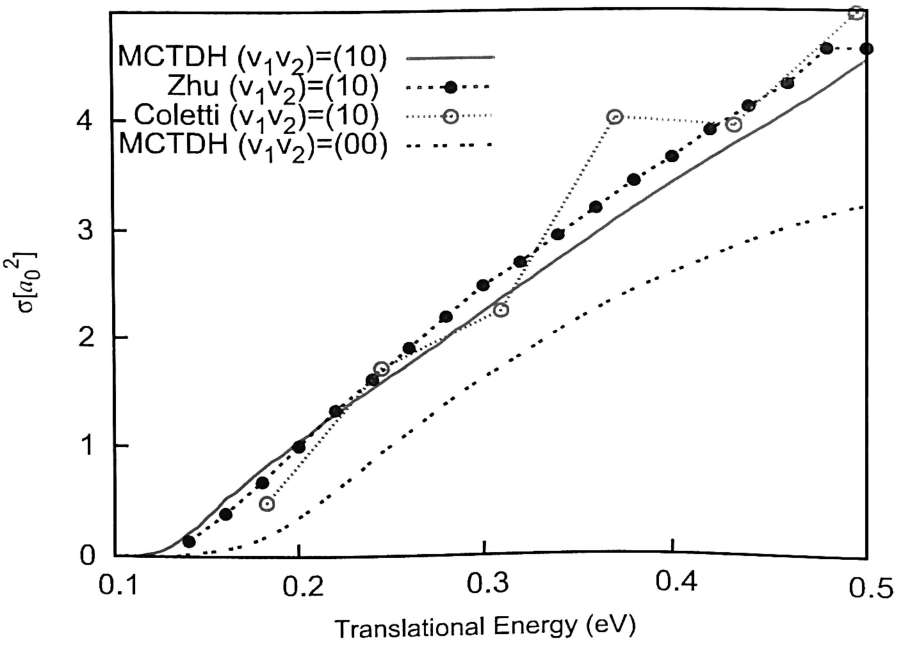


Figure 6.6: *Comparison of CC integral cross sections with the approximate cross sections of Zhu et al.[285] for the $H_2(v_1 = 1, j_1 = 0)$ + $CN(v_2 = 0, j_2 = 0)$ reaction. The mixed quantum-classical results of Coletti et al.[287] and the CC cross sections for $H_2(v_1 = 0, j_1 = 0)$ + $CN(v_2 = 0, j_2 = 0)$ are also shown for reference.*

the approximate results in the low energy range, till 0.21 eV of collision energy, as shown in Figure 6.5 for the CN diatom in its first excited vibrational state. Beyond this, the exact cross sections are consistently smaller than both the CS and J-shifting results. For H_2 vibrational excitation, the CC results are again smaller than the J-shifting results beyond 0.18 eV. A similar behavior was also observed in the ro-vibrational ground state results by Zhang and Lee[286]. The J-shifting method used by Zhu et al.[285] to compute the cross sections clearly overestimates the results in the higher energy region. This is understandable as the J-shifting approximation involved only the computation of the $J = 0$ reaction probability and then the results for higher J's are approximated by a shift in the collision energy with a rotational constant of 1.2 cm^{-1}. As mentioned already, the

TH-1851_Sayak

present cross sections are obtained by a J-interpolation algorithm. But since we computed the probabilities for every fifth J value in the range $0 \leq J \leq 50$, we consider that our interpolation is better converged for direct reactions than the different versions of the J-shifting algorithm. To check this, we also carried out exact calculations for two intermediate J values and the interpolated results were found to be super-imposable with the exact results. The CS approximation, which disregards the coupling between different K-states, systematically produces larger probabilities in the high energy region. The importance of Coriolis coupling in H_2 + CN system for the reactants in ground vibrational state has been discussed by Zhang et al.[286] and looking at the present results for excited vibrational states, the same explanations apply here too. The figures also show the mixed quantum classical cross sections by Coletti and Billing[287] without the error bars. The results for vibrationally excited CN, surprisingly, show a good agreement with the CC results between 0.25-0.38 eV. But the results are larger than the present results in the low energy and high energy regimes. For H_2, the mixed quantum classical results are higher than the CC results in the whole energy range beyond 0.23 eV.

The exact role played by the CN bond in the reaction dynamics has been debated over the last two decades in various theoretical and experimental studies. Our study being the first study on vibrational excitation of reagents which includes the Coriolis coupling, it is expected to confirm the exact nature of the CN bond. Our study shows a decrease in the value as shown in Figure 6.5 and can be attributed[281] to a higher adiabatic barrier for $v_2 = 1$ state of CN than the ground vibrational state. This is consistent with the results obtained by Zhu et al.[285] within the CS approximation and the results of the mixed quantum classical cal-

TH-1851_Sayak

culations by Coletti et al.[287]. Zhu et al.[285] performed wave packet studies and compared the results of a potential averaged five dimensional calculation, where the CN is treated as a spectator bond, with a full six dimensional study. The 6D calculation being fully exact for $J = 0$ took into consideration the effect of coupling between the CN vibration and the motions of other degrees of freedom. The absence of any significant difference in the two probabilities suggested that the CN bond can be treated as a spectator bond at least for the ground vibrational state of CN although a decrease in the values were obtained in the cross sections. Takayanagi and Schatz[283] arrived at a similar conclusion and suggested that the CN bond behaves like a spectator bond for the forward reaction than for the reverse reaction. This was explained by the fact that the H_2 + CN PES reaction has an early barrier along the reaction path. All these results are in sync with the experimental results by Sims and Smith[262] which resulted in negligible enhancement of the reaction. But the present results obtained using an exact form of kinetic energy operator shows a significant decrease from the values for vibrational ground states of the reagent CN. Hence, although there is no enhancement, the decrease still questions the role of the CN bond or rather, the correctness of the potential energy surface.

The effect of vibrational excitation of H_2 is shown in Figure 6.6 and a substantial increase in reaction cross sections over the entire energy range is clearly evident. This is again in accordance with the previous theoretical results obtained using J-shifting results[285]. The usual behavior of the H_2 vibrational excitation to increase the reaction rate by helping to overcome the activation barrier is again confirmed in the present case. But there are large discrepancies between the approximate and the current exact results, particularly at higher energies where

TH-1851_Sayak

the J-shifting results clearly overestimate the exact results for the vibrational excitation of H_2. This can again be explained in terms of the inaccuracies involved in the calculation of the shifting constant.

6.2.4 Rate constants

The initial state selected rate constants obtained from our MCTDH calculations

$T(K)$	MCTDH	Literature	
		Theory[a]	Experiment[b,c]
200	1.09E-15	7.74E-16	
209	1.62E-15		2.97E-15[c]
250	7.01E-15	5.56E-15	
251	7.23E-15		8.61E-15[c]
294.5	2.27E-14		2.40E-14[b]
296.5	2.38E-14		2.55E-14[b]
297	2.40E-14		2.51E-14[c]
300	2.57E-14	2.24E-14	
350	6.78E-14	6.17E-14	7.18E-14[c]
364	8.52E-14		8.64E-14[b]
368	9.08E-14		8.70E-14[c]
400	1.44E-13	1.35E-13	
447	2.54E-13		2.30E-13[b]
450	2.63E-13	2.52E-13	
500	4.31E-13	4.19E-13	
540	6.03E-13		5.38E-13[c]
568	7.43E-13		6.48E-13[b]
600	9.23E-13	9.20E-13	
700	1.61E-12	1.65E-12	
740	1.93E-12		2.45E-12[c]
768	2.16E-12		1.91E-12[b]
800	2.44E-12	2.58E-12	

Table 6.4: *Comparison of the present initial state selected rate constants for* $H_2(v_1 = 0, j_1 = 0) + CN(v_2 = 0, j_2 = 0)$ *with theoretical results of* [a] *Zhang et al.[286]. Experimental results of* [b] *Sims et al.[262] and* [c] *Sun et al.[264] are also shown for comparison.*

TH-1851_Sayak

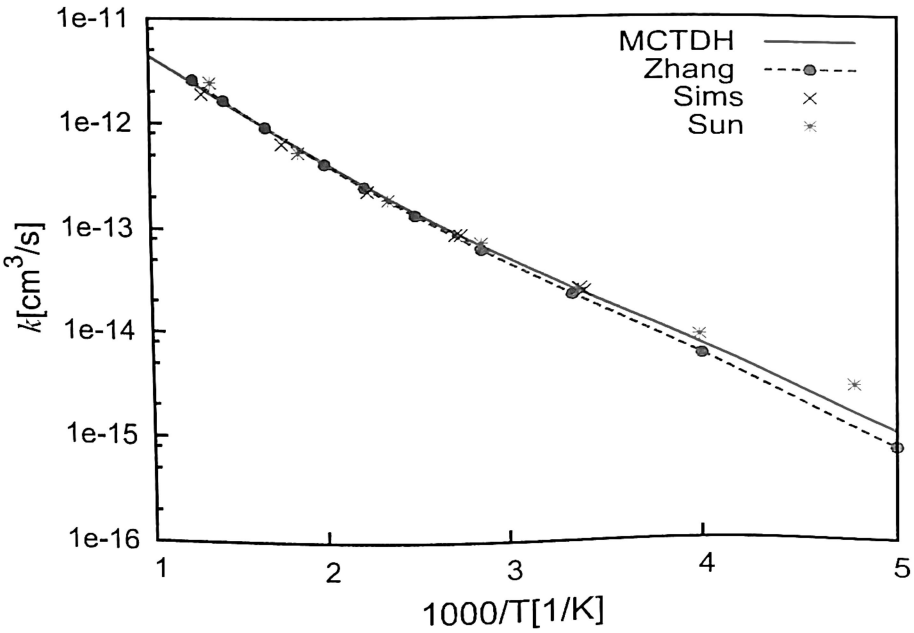


Figure 6.7: *Comparison of the present initial state selected rate constants for* $H_2(v_1 = 0, j_1 = 0)$ + $CN(v_2 = 0, j_2 = 0)$ *with CS results of Zhang et al.[286] and experimental results of Smith et al.[262] and Sun et al.[264].*

are plotted in Arrhenius form in Figure 6.7 along with initial state selected theoretical reference results of Zhang et al.[286], experimental results of Smith et al.[262] and Sun et al.[264]. The rate constants are tabulated in Table 6.4. We should keep in mind that our rate constants are obtained for the reagents in their ground rotational states while the experimental results involve thermal averaging over the rotational state of the reagents. The thermal averaging over rotational states of H_2 have been seen to decrease the reaction rate as reported and discussed in literature[286]. The MCTDH rate constants agree reasonably well with both experimental and reference theoretical results at higher temperatures. At lower temperatures, both the MCTDH and results of Zhang et al.[286] are lower than the experimental results, which has been attributed to incorrectness in the barrier height in the PES used. But certainly, the full-dimensional quantum results

TH-1851_Sayak

obtained using MCTDH are closer to the experimental results. The MCTDH algorithm is seen to give fairly accurate results for tetra-atomic reactive scattering systems as was also seen for the H_2 + OH system in the previous chapter. The CS results seem to diverge from the exact results as the temperature is lowered. At 209 K, the calculated rate constant of 1.62×10^{-15} cm^3 molecule$^{-1}s^{-1}$ is lower than the experimental rate constant of 2.97×10^{-15} cm^3 molecule$^{-1}s^{-1}$, by a factor of 1.8. At an intermediate temperature of 364 K, the calculated rate constant of 8.52×10^{-14} cm^3 molecule$^{-1}s^{-1}$ agrees well with the experimental value of 8.64×10^{-14} cm^3 molecule$^{-1}s^{-1}$. For higher temperatures, the calculated rate constants are marginally higher in comparison to the experimental results[262].

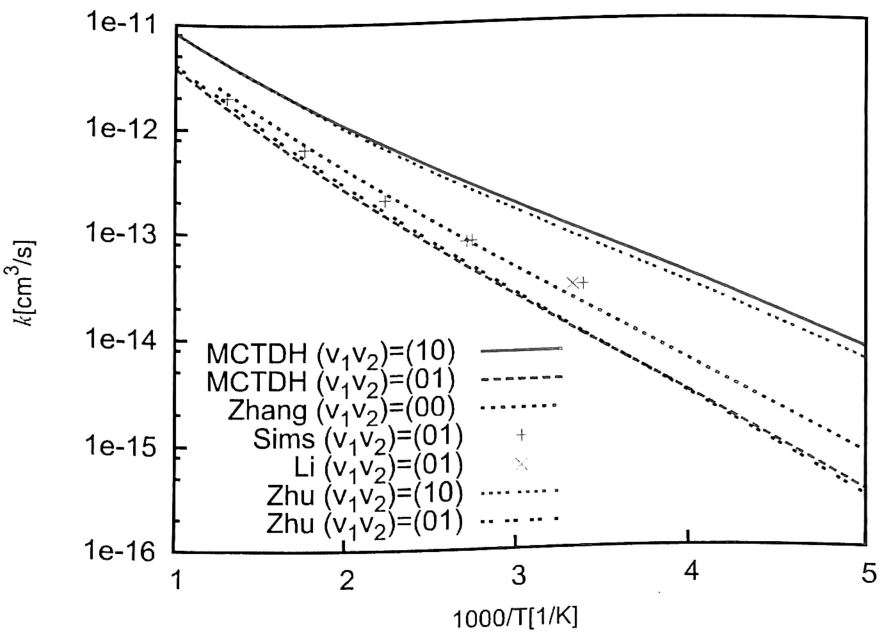


Figure 6.8: *Comparison of the present initial state selected rate constants for the reaction $H_2(v_1, j_1 = 0)$ + $CN(v_2, j_2 = 0)$ with the theoretical results of Zhang et al.[286], Zhu et al.[285] and experimental results of Sims et al.[262] and Li et al.[258].*

The rate constants obtained from our MCTDH calculations for vibrational ex-

TH-1851_Sayak

citation of reagents are shown in Figure 6.8 along with the theoretical results of Zhang et al.[286] and Zhu et al.[285]. for both the ground and vibrationally excited states of the reagents. The corresponding rate constant values are tabulated in Table 6.5. The vibrationally excited H_2 results in significant enhancement in the rate constant. As evident from the tabulated values. the enhancement factor in comparison to the ground state rate constant is 7 at 200 K while it decreases at higher temperatures to a factor of 3 and 2 at 400 K and 800 K respectively. Vibrational excitation of CN leads to a decline in cross sections. These are in accordance with the results reported by Zhu et al.[285] although there are obvious differences between the approximate and the exact quantum results. For H_2. present rate constants are also compared with the available experimental results in the same figure. Disagreements between the experimental and theoretical results for CN($v_2 = 1$) are clearly seen. At 294.5 K, the experimental rate constant is about 3 times higher than our calculated result, while at higher temperatures the difference narrows down to a factor of ≈ 1.2 at 768 K. It should be mentioned here that there are no experimental results available for the vibrational excitations of H_2.

There could be two reasons for the discrepancy observed in case of CN as proposed by Coletti and Billing[287] : the barrier height of the TSH3 potential and the rotational population of the excited vibrational state. The present rate constants have been calculated by Boltzmann averaging over translational energy only and it is assumed that thermal averaging over reagent rotations has a negligible effect. The mixed quantum classical results of Coletti and Billing[287] which included higher rotational states in their calculations showed no improvement in the theoretical rates. Also the CC results by Zhang and Lee[286] showed that the CN

TH-1851_Sayak

$T(K)$	MCTDH		Literature		
			Theoretical[a]		Experimental[b,c]
	$(v_1v_2 = 10)$	$(v_1v_2 = 01)$	$(v_1v_2 = 10)$	$(v_1v_2 = 01)$	$(v_1v_2 = 01)$
200	7.61E-15	3.47E-16	5.90E-15	3.10E-16	
294.5	9.68E-14	1.02E-14			2.96E-14[b]
298.5	1.03E-13	1.11E-14			
300	1.07E-13	1.17E-14	9.00E-14	1.2E-13	3.00E-14[c]
364	2.86E-13	4.40E-14			8.30E-14[b]
368	3.01E-13	4.71E-14			8.20E-14[b]
400	4.38E-13	7.83E-14	3.90E-13	8.50E-14	
447	6.96E-13	1.47E-13			2.08E-13[b]
500	1.07E-12	2.63E-13	1.00E-12	2.90E-13	
568	1.68E-12	4.81E-13			6.53E-13[b]
600	2.01E-12	6.13E-13	2.00E-12	6.80E-13	
700	3.24E-12	1.15E-12	3.20E-12	1.30E-12	
768	4.21E-11	1.62E-12			2.01E-12[b]
800	4.70E-12	1.87E-12	4.70E-12	2.10E-12	

Table 6.5: Comparison of initial state selected rate constants for the reaction $H_2(v_1, j_1 = 0) + CN(v_2, j_2 = 0)$ obtained using MC TDH with the theoretical results of [a]Zhu et al.[285] and experimental results of [b]Sims et al. [262] and [c]Copeland et al.[274].

rotational excitation up to $j_2 = 7$ has no effect on the cross section. But the H_2 rotational excitations were shown to decrease the overall cross section and hence, the rate constants are lowered upon rotational averaging. These wave packet results by Zhang et al.[286] were obtained by including all important Coriolis couplings. Hence, the inclusion of the excited rotational states of CN is not expected to contribute much to the overall rate constant. But the averaging with respect to H_2 rotational excitations will again result in lowering the theoretical rates, although an explicit study of rotational excitations is not a part of the present study. Thus it is evident that the TSH3 potential energy surface is probably unable in describing the reaction and a more accurate PES is required to study the dynamics. On

TH-1851_Sayak

the other hand, the theoretical rates for the isotopic D_2 + CN[289] reaction are in quite good agreement with experimental results which implies that the effective reaction barrier is almost right for the D_2 + CN reaction but a little too high for the H_2 + CN reaction.

6.3 Summary and conclusions

The study of the H_2 + CN system was taken up with the aim of looking into four important aspects involving the reaction and the methodology. Firstly, a successful application of the MCTDH algorithm to study H_2 + OH system, as shown in the previous chapter, brings forth the question of the effectiveness and applicability of the system for heavier tetra-atomic systems. With our previous study on the H_2 + OH reaction with MCTDH, it was natural to extend the study to heavier systems. With two out of the four atoms in the system being C and N, this system presented an even bigger challenge for proper convergence of the reaction parameters using the MCTDH algorithm. The most important factor for successful application of MCTDH to a system is to achieve a proper balance between numerical accuracy along with minimized usage of computational resources. We have been able to get converged results without using a significant higher number of spfs in comparison to the much simpler H_2 + OH system. The use of an optimum number of spfs is highly important for this system as the time factor shows a huge increase with a minor enhancement in the number of spfs. The energy distribution of the initial wave packet and the CAP parameters strongly influence the convergence, both near the threshold and at the higher energy range. We have successfully shown that the MCTDH algorithm can be applied to tetra-atomic systems having heavy

TH-1851_Sayak

atoms, using both CS approximation and CC methodology while achieving the same level of accuracy as obtained for simpler systems.

Secondly, our studies on the importance of using the exact Hamiltonian for the present reaction system yielded some interesting results. For the H_2 + CN system, it is observed that the present CC results show strong deviations from the previous approximate results, signifying the importance of inclusion of Coriolis coupling in the reaction dynamics. It is observed that the CS approximate results for CN($v_2 = 1$) strongly overestimate the accurate results which include Coriolis coupling. It can thus be emphasized that the general notion on the inclusion of Coriolis coupling for direct reactions is too simplistic and accurate calculations on similar systems should take the importance of an exact Hamiltonian into account. Although the inclusion of the Coriolis Coupling makes the calculations prohibitive for numerically exact wave packet propagations of heavier systems, the MCTDH algorithm presents a good alternative.

Thirdly, the exact role played by the CN bond in the reaction dynamics has been investigated by performing CC calculations. It is observed that vibrational excitation of CN leads to a significant decrease in reaction cross sections. This is contrary to the negligible effect of CN excitation envisaged by previous approximate calculations. The present observations clearly establish a non-negligible role for the CN bond on the TSH3 surface.

The accuracy of the barrier height of the TSH3 PES has been debated in various studies over the last two decades. A comparison of rate constants obtained for both ro-vibrational ground state and CN($v_2 = 1$) with available experimental results show that the values obtained at lower temperatures are significantly lower

TH-1851_Sayak

than experimental results. There can be two reasons for the present observation: an inaccurate barrier height of the TSH3 potential and the rotational population of the excited vibrational state. The present rate constants have been calculated by Boltzmann averaging over translational energy only and it is assumed that thermal averaging over reagent rotations has a negligible effect. Previous theoretical studies have shown that the inclusion of the excited rotational states of CN is not expected to contribute much to the overall rate constant. On the other hand, the theoretical rates for the isotopic D_2 + CN reaction are in quite good agreement with experimental results which implies that the effective reaction barrier is almost right for the D_2 + CN reaction but a little too high for the H_2 + CN reaction. Thus we can sum it up conclusively that the TSH3 is not accurate for the study of the H_2 + CN system and an improvement in the barrier height is required for attaining convergence of theoretical results with the experimental values.

TH-1851_Sayak

Chapter 7

Summary and Conclusions

The dynamics of three different systems, a tri-atomic and two tetra-atomic, have been studied using the MCTDH algorithm. Extensive calculations have been performed for both ground and ro-vibrational excited states of the reagents. All the calculations have been performed with an exact form of the Hamiltonian and the results have been compared with literature results obtained using CS approximation. In cases where CS results are not available, calculations for the same have also been performed using the MCTDH methodology. The dependence of the reaction dynamics on the surface topology and transition state structures have been explored. The significance of initial orientation of the reagents and the importance of a preferred pathway of approach in the reaction dynamics has been investigated. Reaction probabilities, integral cross sections and rate constants have been reported and adequate comparison with available experimental data has been made wherever possible.

For the He + H^+He reaction, the reaction probability curves are characterized

TH-1851_Sayak

by sharp resonance structures, especially at the threshold, while the intensity of the peaks decrease followed by subsequent broadening at higher energies. Both CS and CC studies have been performed using the MCTDH methodology, while the studies performed using the split operator method have been carried out under CS approximation. The CS results obtained from both the MCTDH and the split-operator methodologies, show an excellent agreement with each other for all J values considered. The CC results are distinctly different regarding the structure of the peaks and threshold characteristics when compared with the CS results. A significantly smaller number of resonance peaks are observed in the CC studies over the entire energy range, compared to the CS results. This has been explained by the fact that the Coriolis coupling provides an important decay mechanism for the complex resulting in a sharp decrease in the resonance structures. The CC cross sections are significantly higher at the threshold and at lower energies, while the difference narrows down at higher energies. The breaking of the collision complex to products is much less favorable within the CS approximation. The presence of a short lived reaction intermediate and the phenomenon of sudden collisions occurring at higher energies explain the agreement between the CS and CC cross sections in this regime. Comparison of CC and CS results for $v = 1$ shows larger cross sections for CS at lower energies, while the trend reverses at higher energies. Excitation to higher rotational states($j = 1$ and 2) does not affect the CC cross sections in a significant manner. But there is a significant decrease in cross sections for j =1, in comparison to $j = 0$, for the CS results. This underlines the inadequacy of the CS methodology in predicting the orientational dynamics for initial rotational excitations. The variations in reaction probabilities and cross sections with m(the initial magnetic rotational quantum number of the diatom) have shown the importance of the initial orientation of the reagents in the reaction

TH-1851_Sayak

dynamics of this system.

The excellent agreement of the MCTDH reaction probabilities and cross sections obtained for the H_2 + OH reaction on the WDSE and YZCL2 surfaces with the literature values underlines the accuracy of the MCTDH algorithm in studying the tetra-atomic reactive systems. The significant difference observed for the ground state reaction probabilities and cross sections on the three surfaces, have been explained on the basis of differences in transition state structures and initial orientation of the reagents. The $v_{1(2)} = 1$ CC results on the WDSE surface have been compared with previously reported CS results and no significance difference is observed. The reaction rate constants for $H_2(v_1 = 1)$ obtained on the most accurate YZCL2 surface show an excellent agreement with recent experimental results. Rotational excitation of H_2 on the three surfaces, presents an interesting case. While it leads to a uniform decrease in cross sections in comparison to $j = 0$ on the WDSE surface, an uniform increase is observed on the WSLFH surface. On the YZCL2 surface, a marginal increase in cross sections at lower energies is followed by a decrease at higher energies. The increase in cross sections at lower energies on the YZCL2 surface is explained by the attainment of a favorable geometry on rotation, unlike that obtained for the WDSE surface. The observations at higher energies are explained on the basis of the ratio of time spent in the approach coordinate to the time required for appreciable rotation of the diatoms. This is determined by the presence or absence of wells and van der Waals minima in the surfaces. The study of the reaction cross sections and rate constants for the ro-vibrational excited states of the diatoms reveals a significant dependence of the reaction attributes on the properties of the surfaces considered along with the pathways of approach and the initial orientation of the reactants.

TH-1851_Sayak

The application of the MCTDH algorithm to study the H_2 + CN reaction, explains some ambiguous phenomenon related to the reaction dynamics of the system. The studies establish conclusively that the TSH3 potential is not accurate for the study of the H_2 + CN system and an improvement in the barrier height is required for attaining convergence of theoretical results with the experimental values. The exact role of the CN bond in the reaction dynamics on the TSH3 surface is investigated in this study. Although the vibrational excitation of the CN bond does not lead to an enhancement in reaction cross sections, a significant decrease is observed for the same. It is concluded that the CN bond plays a significant part in the overall reaction dynamics and assigning it the nomenclature of a spectator bond is erroneous. Both CS and CC studies have been performed for a better understanding of the factors affecting the reaction dynamics in the vibrationally excited state. It is observed that the present CC results show strong deviations from the previous approximate results signifying the importance of inclusion of Coriolis coupling in the reaction dynamics. The CS approximate results for CN($v_2 = 1$) strongly overestimate the accurate results which include Coriolis coupling. It can thus be emphasized that the general notion on the inclusion of Coriolis coupling for direct reactions is too simplistic and accurate calculations on similar systems should take the importance of an exact Hamiltonian into account. Although the inclusion of the Coriolis Coupling makes the calculations prohibitive for numerically exact standard wave packet propagations of systems with higher degrees of freedom, the MCTDH algorithm presents an efficient and accurate alternative.

TH-1851_Sayak

Bibliography

[1] M. Born and R. Oppenheimer. Zur Quantentheorie der Molekeln. *Ann. Phys.*, 84:457, 1927.

[2] M. Born and K. Huang. *Dynamical Theory of Crystal Lattices.* Oxford University Press, New York, 1954.

[3] C. D. Sherill. Frontiers in electronic structure theory. *J. Chem. Phys.*, 132:110902, 2010.

[4] J. Hirschfelder, H. Eyring, and B. Topley. Reactions involving hydrogen molecules and atoms. *J. Chem. Phys.*, 4:170, 1936.

[5] H. M. Hulburt and J. O. Hirschfelder. The transmission coefficient in the theory of absolute reaction rates. *J. Chem. Phys.*, 4:170, 1936.

[6] T. P. Schafer, P. E. Siska, J. M. Parson, F. P. Tully, Y. C. Wong, and Y. T. Lee. Crossed molecular beam study of F + D_2. *J. Chem. Phys.*, 53:3385, 1970.

[7] Aron Kuppermann, George C. Schatz, and M. Baer. Quantum mechanical reactive scattering for planar atom+diatom systems. I. Theory. *J. Chem. Phys.*, 65:4596, 1976.

[8] G. C. Schatz and A. Kuppermann. Quantum mechanical reactive scattering for three-dimensional atom plus diatom systems. II. Accurate cross sections for H+H_2. *J. Chem. Phys.*, 65:4668–4692, 1976.

[9] G. C. Schatz and A. Kuppermann. Quantum mechanical reactive scattering for three-dimensional atom plus diatom systems. I. Theory. *J. Chem. Phys.*, 65:4642, 1976.

[10] J. M. Bowman and G. C. Schatz. Reactive molecular collision calculations. *Computer Phys. Comm.*, 17:117, 1979.

[11] V. Mohan and N. Sathyamurthy. Quantal wave packet calculations of reactive scattering. *Computer Phys. Rep.*, 7:213, 1988.

TH-1851_Sayak

[12] W. H. Miller. Recent advances in quantum mechanical reactive scattering theory (Including comparison of recent experiments with rigorous calculations of state-to-state cross sections for the H/D+H_2 → H_2/HD+H reactions). *Ann. Rev. Phys. Chem.*, 41:245, 1990.

[13] J. M. Bowman and G. C. Schatz. Theoretical studies of polyatomic bimolecular reaction dynamics. *Ann. Rev. Phys. Chem.*, 46:169, 1995.

[14] N. Balakrishnan, C. Kalyanaraman, and N. Sathyamurthy. Time-dependent quantum mechanical approach to reactive scattering and related processes. *Phys. Rep.*, 280:79, 1997.

[15] S. C. Althorpe and D. C. Clary. Quantum scattering calculations on chemical reactions. *Ann. Rev. Phys. Chem.*, 54:493, 2003.

[16] W. Hu and G. C. Schatz. Theories of reactive scattering. *J. Chem. Phys.*, 125:132301, 2006.

[17] D. C. Clary. Quantum dynamics of chemical reactions. *Science*, 321:789, 2008.

[18] D. C. Clary. Theoretical studies on bimolecular reaction dynamics.. *Proc. Nat. Acad. Sci.*, 105:12649, 2008.

[19] J. Mazur and R. J. Rubin. Quantum-mechanical calculation of the probability of an exchange reaction for constrained linear encounters. *J. Chem. Phys.*, 31:1395, 1959.

[20] E. A. McCullough and R. E. Wyatt. Quantum dynamics of the collinear (H,H_2) reaction. *J. Chem. Phys.*, 51:1253, 1969.

[21] E. A. McCullough and R. E. Wyatt. Dynamics of the collinear (H.H_2) reaction. I. Probability density and flux. *J. Chem. Phys.*, 54:3578, 1971.

[22] M. D. Feit, J. A. Fleck Jr., and A. Steiger. Solution of the Schrödinger equation by a spectral method. *J. Comp. Phys.*, 47:412–433, 1982.

[23] M. D. Feit and J. A. Fleck Jr. Solution of the Schrödinger equation by a spectral method II: Vibrational energy levels of triatomic molecules. *J. Chem. Phys.*, 78:301, 1983.

[24] D. Kosloff and R. Kosloff. A Fourier-method solution for the time-dependent Schrödinger equation as a tool in molecular dynamics. *J. Comp. Phys.*, 52:35, 1983.

[25] J. C. Light, I. P. Hamilton, and J. V. Lill. Generalized discrete variable approximation in quantum mechanics. *J. Chem. Phys.*, 82:1400, 1985.

TH-1851_Sayak

[26] J. V. Lill, G. A. Parker, and J. C. Light. Discrete variable representations and sudden models in quantum scattering theory. *Chem. Phys. Lett.*, 89:483–489, 1982.

[27] R. Kosloff. Time-dependent quantum-mechanical methods for molecular dynamics. *J. Phys. Chem.*, 92:2087, 1988.

[28] H. Tal-Ezer and R. Kosloff. An accurate and efficient scheme for propagating the time dependent Schrödinger equation. *J. Chem. Phys.*, 81:3967, 1984.

[29] R. Kosloff and D. Kosloff. Absorbing boundaries for wave propagation problems. *J. Comp. Phys.*, 63:363, 1986.

[30] D. Neuhauser and M. Baer. Wave-packet approach to treat low-energy reactive systems: Accurate probabilities for $H+H_2$. *J. Phys. Chem.*, 93:2872, 1989.

[31] D. Neuhauser and M. Baer. The time-dependent Schrödinger equation: Application of absorbing boundary conditions. *J. Chem. Phys.*, 90:4351, 1989.

[32] D. Neuhauser and M. Baer. The application of wave packets to reactive atom-diatom systems: A new approach. *J. Chem. Phys.*, 91:4651, 1989.

[33] D. Neuhauser, M. Baer, R. S. Judson, and D. J. Kouri. The application of time-dependent wavepacket methods to reactive scattering. *Computer Phys. Comm.*, 63:460, 1991.

[34] D. Neuhauser, R. S. Judson, R. L. Jaffe, M. Baer, and D. J. Kouri. Total integral reactive cross sections for $F+H_2 \rightarrow HF+H$: Comparison of converged quantum, quasiclassical trajectory and experimental results. *Chem. Phys. Lett.*, 176:546, 1991.

[35] J. G. Muga, J. P. Palao, B. Navarro, and I. L. Egusquiza. Complex absorbing potentials. *Phys. Rep.*, 395:357, 2004.

[36] G. G. Balint-Kurti, R. N. Dixon, and C. C. Marston. Time-dependent and time-independent wavepacket approaches to reactive scattering and photodissociation dynamics. *Int. Rev. Phy. Chem.*, 11:317, 1992.

[37] B. Jackson. Time-dependent wave packet approach to quantum reactive scattering. *Ann. Rev. Phys. Chem.*, 46:251, 95.

[38] G. G. Balint-Kurti. Wavepacket theory of photodissociation and reactive scattering. *Adv. Chem. Phys.*, 128:249, 2003.

[39] S. C. Althorpe. The plane wave packet approach to quantum scattering theory. *Int. Rev. Phy. Chem.*, 23:219, 2004.

TH-1851_Sayak

[40] T.-S. Chu, Y. Zhang, and K.-L. Han. The time-dependent quantum wave packet approach to the electronically nonadiabatic processes in chemical reactions. *Int. Rev. Phy. Chem.*, 25:201, 2006.

[41] G. G. Balint-Kurti. Time-dependent and time-independent wavepacket approaches to reactive scattering and photodissociation dynamics. *Int. Rev. Phy. Chem.*, 27:507, 2008.

[42] G. G. Balint-Kurti. Wavepacket quantum dynamics. *Theo. Chem. Acc.*, 127:1, 2010.

[43] A. Askar and A. S. Cakmak. Explicit integration method for the time-dependent Schrödinger equation for collision problems. *J. Chem. Phys.*, 68:2794, 1978.

[44] R. B. Gerber, M. A. Ratner, and V. Buch. Simplified time-dependent self-consistent field approximation for intramolecular dynamics. *Chem. Phys. Lett.*, 91:173, 1982.

[45] R. B. Gerber, V. Buch, and M. A. Ratner. Time-dependent self-consistent field approximation for intramolecular energy transfer. I. Formulation and application to dissociation of van der Waals molecules. *J. Chem. Phys.*, 77:3022, 1982.

[46] R. H. Bisseling, R. Kosloff, R. B. Gerber, M. A. Ratner, L. Gibson, and C. Cerjan. Exact time-dependent quantum mechanical dissociation dynamics of I_2He: Comparison of exact time-dependent quantum calculation with the quantum time-dependent self-consistent field (TDSCF) approximation. *J. Chem. Phys.*, 87:2760, 1987.

[47] J. Kucar, H.-D. Meyer, and L.S. Cederbaum. Time-dependent rotated Hartree approach. *Chem. Phys. Lett.*, 140:525, 1987.

[48] N. Makri and W. H. Miller. Time-dependent self-consistent (TDSCF) approximation for a reaction coordinate coupled to a harmonic bath: Single and multiconfiguration treatments. *J. Chem. Phys.*, 87:5781, 1987.

[49] Z. Kotler, A. Nitzan, and R. Kosloff. Multiconfiguration time-dependent self-consistent field approximation for curve crossing in presence of a bath. A fast Fourier transform study. *Chem. Phys. Lett.*, 153:483, 1988.

[50] A. D. Hammerich, R. Kosloff, and M. A. Ratner. Quantum mechanical reactive scattering by a multiconfigurational time-dependent self-consistent field (MCTDSCF) approach. *Chem. Phys. Lett.*, 171:97, 1990.

TH-1851_Sayak

[51] H.-D. Meyer, U. Manthe, and L. S. Cederbaum. The multi-configurational time-dependent Hartree approach. *Chem. Phys. Lett.*, 165:73–78, 1990.

[52] U. Manthe, H.-D. Meyer, and L. S. Cederbaum. Wave-packet dynamics within the multiconfiguration Hartree framework: General aspects and application to NOCl. *J. Chem. Phys.*, 97:3199, 1992.

[53] M. H. Beck, A. Jäckle, G. A. Worth, and H.-D. Meyer. The multiconfiguration time-dependent Hartree method: A highly efficient algorithm for propagating wavepackets. *Phys. Rep.*, 324:1, 2000.

[54] H.-D. Meyer and G. A. Worth. Quantum molecular dynamics: Propagating wavepackets and density operators using the multiconfiguration time-dependent Hartree (MCTDH) method. *Theo. Chem. Acc.*, 109:251–267, 2003.

[55] H.-D. Meyer, F. Gatti, and G. A. Worth. *Multidimensional Quantum Dynamics: MCTDH Theory and Applications.* Wiley-VCH, Weinheim, 2009.

[56] H.-D. Meyer. Studying molecular quantum dynamics with the multiconfiguration time-dependent hartree method. *Wiley Interdisciplinary Reviews : Comput. Mol. Sci.*, 2011.

[57] A. Jäckle and H.-D. Meyer. Reactive scattering using the multiconfiguration time-dependent Hartree approximation: General aspects and application to the collinear $H+H_2 \rightarrow H_2+H$ reaction. *J. Chem. Phys.*, 102:5605, 1995.

[58] A. P. J. Jansen and H. Burghgraef. MCTDH study of CH_4 dissociation on Ni(III). *Surf. Sci.*, 344:149, 1995.

[59] A. Jäckle and H.-D. Meyer. Calculation of $H+H_2$ and $H+D_2$ reaction probabilities within the multiconfiguration time-dependent Hartree approach employing an adiabatic correction scheme. *J. Chem. Phys.*, 109:2614, 1998.

[60] R. Milot and A. P. J. Jansen. Ten dimensional wavepacket simulations of methane scattering. *J. Chem. Phys.*, 109:1966, 1998.

[61] S. Sukiasyan and H.-D. Meyer. Reaction cross sections for the $H+D_2(v_0=1) \rightarrow HD+D$ and $D+H_2(v_0=1) \rightarrow DH+H$ systems. a multiconfiguration time-dependent Hartree (MCTDH) wave packet propagation study. *J. Chem. Phys.*, 116:10641, 2002.

[62] C. Crespos, H.-D. Meyer, R. C. Mowrey, and G. J. Kroes. Multiconfiguration time-dependent Hartree method applied to molecular dissociation on surfaces: $H_2+Pt(III)$. *J. Chem. Phys.*, 124:074706, 2006.

TH-1851_Sayak

[63] F. Huarte-Larrañaga and U. Manthe. Vibrational excitation in the transition state: The CH_4+H $\rightarrow$ CH_3+H_2 reaction rate constant in an extended temperature interval. *J. Chem. Phys.*, 116:2863, 2002.

[64] M. Nest and H.-D. Meyer. Benchmark calculations on high-dimensional Henon-Heiles potentials with the Multi-Configuration Time-Dependent Hartree (MCTDH) Method. *J. Chem. Phys.*, 117:10499–10505, 2002.

[65] D. J. Haxton, Z. Zhang, H.-D. Meyer, T. N. Rescigno, and C. W. McCurdy. Dynamics of dissociative attachment of electrons to water through the $^2B_1$ metastable state of the anion. *Phys. Rev. A*, 69:062714, 2004.

[66] U. Manthe, H.-D. Meyer, and L. S. Cederbaum. Multiconfigurational time-dependent Hartree study of complex dynamics: Photodissociation of NO_2. *J. Chem. Phys.*, 97:9062, 1992.

[67] U. Manthe and A. D. Hammerich. Wavepacket dynamics in five dimensions. Photodissociation of methyl iodide. *Chem. Phys. Lett.*, 211:7, 1993.

[68] S. Woittequand, C. Toubin, B. Pouilly, M. Monnerville, S. Briquez, and H.-D. Meyer. Photodissociation of a HCl molecule adsorbed on ice. *Chem. Phys. Lett.*, 406:202–209, 2005.

[69] H. Nauendorf, G.A. Worth, H.-D. Meyer, and O. Kühn. Multi-configuration time-dependent Hartree dynamics on an ab initio reaction surface: Ultrafast laser -driven proton motion in Phthalic Acid Monomethylester. *J. Phys. Chem.*, 106:719–724, 2002.

[70] I. Craig, M. Thoss, and H. Wang. Proton transfer reactions in model condensed-phase environments: Accurate quantum dynamics using the multilayer multiconfiguration time-dependent hartree approach. *J. Chem. Phys.*, 127:144503, 2007.

[71] T. Hammer and U. Manthe. Intramolecular proton transfer in malonaldehyde: Accurate multilayer multi-configurational time-dependent hartree calculations. *J. Chem. Phys.*, 134:224305, 2011.

[72] O. Vendrell, M. Brill, F. Gatti, D. Lauvergnat, and H.-D Meyer. Full dimensional (15-dimensional) quantum-dynamical simulation of the protonated water-dimer III: Mixed jacobi-valence parametrization and benchmark results for the zero point energy, vibrationally excited states, and infrared spectrum. *J. Chem. Phys.*, 130:234305, 2009.

[73] O. Vendrell, F. Gatti, and H.-D Meyer. Full dimensional (15-dimensional) quantum-dynamical simulation of the protonated water-dimer IV: Isotope

TH-1851_Sayak

effects in the infrared spectra of $D(D_2O)_2^+$, $H(D_2O)_2^+$, and $D(H_2O)_2^+$ isotopologues. *J. Chem. Phys.*, 131:034308, 2009.

[74] A. Raab, G. Worth, H.-D. Meyer, and L. S. Cederbaum. Molecular dynamics of pyrazine after excitation to the S_2 electronic state using a realistic 24-mode model Hamiltonian. *J. Chem. Phys.*, 110:936–946, 1999.

[75] A. Markmann, G.A. Worth, S. Mahapatra, H.-D. Meyer, H. Köppel, and L.S. Cederbaum. Simulation of a complex spectrum: Interplay of five electronic states and 21 vibrational degrees of freedom in $C_5H_4^+$. *J. Chem. Phys.*, 123:204310, 2005.

[76] G. A. Worth, H.-D Meyer, H. Köppel, and L. S. Cederbaum. Using the MCTDH wavepacket propagation method to describe multimode non-adiabatic dynamics. *Int. Rev. Phy. Chem.*, 27:569, 2008.

[77] F. Gatti and H.-D. Meyer. Intramolecular vibrational energy redistribution in Toluene: A nine dimensional quantum mechanical study using the MCTDH algorithm. *Chem. Phys.*, 304:3–15, 2004.

[78] G. Pasin, C. Iung, F. Gatti, and H.-D. Meyer. Theoretical investigation of highly excited vibrational states in DFCO: Calculation of the out-of-plane bending states and simulation of the intramolecular vibrational energy redistribution. *J. Chem. Phys.*, 126:024302, 2007.

[79] G. Pasin, C. Iung, F. Gatti, F. Richter, C. Léonard, and H.-D. Meyer. Theoretical investigation of intramolecular vibrational energy redistribution in HFCO and DFCO induced by an external field. *J. Chem. Phys.*, 129:144304, 2008.

[80] G. A. Worth. Accurate wave packet propagation for large molecular systems: The multi-configuration time-dependent Hartree (MCTDH) method with selected configurations. *J. Chem. Phys.*, 112:8322–8329, 2000.

[81] H. Wang and M. Thoss. Multilayer formulation of the multiconfiguration time-dependent Hartree theory. *J. Chem. Phys.*, 119:1289, 2003.

[82] U. Manthe. A multilayer multiconfigurational time-dependent Hartree approach for quantum dynamics on general potential energy surfaces. *J. Chem. Phys.*, 128:164116, 2008.

[83] O. Vendrell and H.-D. Meyer. Multilayer multiconfiguration time-dependent hartree method: Implementation and applications to a henon-heiles hamiltonian and to pyrazine. *J. Chem. Phys.*, 134:044135, 2011.

TH-1851_Sayak

[84] O. E. Alon, A. I. Streltsov, and L. S. Cederbaum. Multiconfigurational time-dependent hartree method for bosons: Many-body dynamics of bosonic systems. *Phys. Rev. A*, 77:033613, 2008.

[85] J. Zanghellini, M. Kitzler, C. Fabian, T. Brabec, and A. Scrinzi. An MCTDHF approach to multi-electron dynamics in laser fields. *Laser Phys.*, 13:1064, 2003.

[86] H. M. Kunttu, J. Seetula, M. Räsänen, and V. A. Apkarian. Photogeneration of ions via delocalized charge transfer states. I. Xe_2H^+ and Xe_2D^+ in solid Xe. *J. Chem. Phys.*, 96:5630, 1992.

[87] H. M. Kunttu and J. A. Seetula. Photogeneration of ionic species in Ar, Kr and Xe matrices doped with HCl, HBr and HI. *Chem. Phys.*, 189:273, 1994.

[88] T. D. Fridgen and J. M. Parnis. Electron bombardment matrix isolation of Rg/Rg/methanol mixtures (Rg= Ar, Kr, Xe): Fourier-transform infrared characterization of the proton-bound dimers Kr_2H^+, Xe_2H^+, $(ArHKr)^+$ and $(ArHXe)^+$ in Ar matrices and $(KrHXe)^+$ and Xe_2H^+ in Kr matrices. *J. Chem. Phys.*, 109:2155, 1998.

[89] T. D. Fridgen and J. M. Parnis. Density functional theory study of the proton-bound rare-gas dimers Rg_2H^+ and $(RgHRg')^+$ (Rg=Ar, Kr, Xe): Interpretation of experimental matrix isolation infrared data. *J. Chem. Phys.*, 109:2162, 1998.

[90] L. Khriachtchev, A. Lignell, and M. Räsänen. Neutralization of solvated protons and formation of noble-gas hydride molecules: Matrix-isolation indications of tunneling mechanisms? *J. Chem. Phys.*, 123:064507, 2005.

[91] S. P. Walsh and J. T. H. Dunning. A theoretical study of the potential energy surface for $OH+H_2$. *J. Chem. Phys.*, 72:1303, 1980.

[92] G. C. Schatz and H. Elgersma. A quasi-classical trajectory study of product vibrational distributions in the $OH + H_2 \rightarrow H_2O + H$ reaction. *Chem. Phys. Lett.*, 73:21, 1980.

[93] G. Wu, G. C. Schatz, G. Lendvay, D.-C. Fang, and L. B. Harding. A new potential surface and quasiclassical trajectory study of $H+H_2O \rightarrow OH+H_2$. *J. Chem. Phys.*, 113:3150, 2000.

[94] M. Yang, D. H. Zhang, M. A. Collins, and S.-Y. Lee. *Ab initio* potential-energy surfaces for the reactions $OH+H_2 \leftrightarrow H_2O+H$. *J. Chem. Phys.*, 115:174–178, 2001.

TH-1851_Sayak

[95] A. Hanf, H. R. Volpp, and J. Wolfrum. *Determination of kinetic parameters in laminar flow reactors. II. Experimental aspects* . Springer Publications, Berlin- Heidelberg, 2005.

[96] R. Zellner and W. Steinert. Vibrational rate enhancement in the reaction OH + H_2(v = 1) → H_2O + H. *Chem. Phys. Lett.*, 81:568, 1981.

[97] G. P. Glass and B. K. Chaturvedi. The effect of vibrational excitation of H_2 and of OH on the rate of the reaction H_2 + OH → H_2O +H. *J. Chem. Phys.*, 75:2749, 1981.

[98] M. A. ter Horst, G. C. Schatz, and L. B. Harding. Potential energy surface and quasiclassical trajectory studies of the CN+H_2reaction. *J. Chem. Phys.*, 105:558, 1996.

[99] P. A. M. Dirac. Note on Exchange Phenomena in the Thomas Atom. *Proc. Cambridge Philos. Soc.*, 26:376–385, 1930.

[100] J. Frenkel. *Wave Mechanics*. Clarendon Press, Oxford, 1934.

[101] U. Manthe. On the integration of the multi-configurational time-dependent hartree (MCTDH) equations of motion. *Chem. Phys.*, 329:168, 2006.

[102] A. Jäckle and H.-D. Meyer. Product representation of potential energy surfaces. *J. Chem. Phys.*, 104:7974, 1996.

[103] A. Jäckle and H.-D. Meyer. Product representation of potential energy surfaces II. *J. Chem. Phys.*, 109:3772, 1998.

[104] C. Leforestier and R. E. Wyatt. Optical potential for laser induced dissociation. *J. Chem. Phys.*, 78:2334, 1983.

[105] D. Neuhauser and M. Baer. A new time-independent approach to the study of atom-diatom reactive collisions: Theory and application. *J. Phys. Chem.*, 94:185, 1990.

[106] A. Vibok and G. G. Balint-Kurti. Reflection and transmission of waves by a complex potential — a semiclassical Jeffreys-Wentzel-Kramers-Brillouin treatment. *J. Chem. Phys.*, 96:7615, 1992.

[107] U. V. Riss and H.-D. Meyer. Calculation of resonance energies and widths using the complex absorbing potential method. *J. Phys. B*, 26:4503, 1993.

[108] U. V. Riss and H.-D. Meyer. Reflection-free complex absorbing potentials. *J. Phys. B*, 28:1475, 1995.

TH-1851_Sayak

[109] U. V. Riss and H.-D. Meyer. Investigation on the reflection and transmission properties of complex absorbing potentials. *J. Chem. Phys.*, 105:1409, 1996.

[110] D. J. Tannor and D. E. Weeks. Wave packet correlation function formulation of scattering theory: The quantum analog of classical S-matrix theory. *J. Chem. Phys.*, 98:3884, 1993.

[111] A. Jäckle and H.-D. Meyer. Time-dependent calculation of reactive flux employing complex absorbing potentials: General aspects and application within MCTDH. *J. Chem. Phys.*, 105:6778, 1996.

[112] J. Z. H. Zhang. *Theory and Application of quantum molecular dynamics.* World Scientific, Singapore, 1999.

[113] A. R. Offer and G. Balint-Kurti. Time-dependent quantum mechanical study of the photodissociation of HOCl and DOCl. *J. Chem. Phys.*, 101:10416, 1994.

[114] A. N. Panda and N. Satyamurthy. Bound and quasibound states of He_2H^+ and He_2D^+. *J. Phys. Chem. A*, 107:7125, 2003.

[115] F. Gatti, C. Iung, M. Menou, Y. Justum, A. Nauts, and X. Chapuisat. Vector parametrization of the n-atom problem in quantum mechanics. I. Jacobi vectors. *J. Chem. Phys.*, 108:8804, 1998.

[116] F. Gatti, C. Iung, M. Menou, and X. Chapuisat. Vector parametrization of the n-atom problem in quantum mechanics. II. Coupled-angular-momentun spectral representations for four atom systems. *J. Chem. Phys.*, 108:8821, 1998.

[117] F. Gatti. Vector parametrization of the n-atom problem in quantum mechanics. iii separation into two sub-systems. *J. Chem. Phys.*, 111:7225, 1999.

[118] F. Gatti, F. Otto, S. Sukiasyan, and H.-D. Meyer. Rotational excitation cross sections of para-H_2+para-H_2 collisions. a full-dimensional wave-packet propagation study using an exact form of the kinetic energy. *J. Chem. Phys.*. 123:174311, 2005.

[119] A. N. Panda, F. Otto, F. Gatti, and H.-D. Meyer. Rovibrational energy transfer in ortho-H_2+ para-H_2 collisions. *J. Chem. Phys.*, 127:114310, 2007.

[120] F. Gatti and C. Iung. Exact and constrained kinetic energy operators for polyatomic molecules: The polyspherical approach. *Phys. Rep.*, 484:1, 2009.

[121] W. P. Kraemer. V. Špirko, and O. Bludský. Bound and low-lying quasibound rotation-vibration energy levels of the ground and first excited electronic states of HeH_2^+. *Chem. Phys.*, 276:225, 2002.

TH-1851_Sayak

[122] R. E. Grisenti, W. Schöllkopf, J. P. Toennies, G. C. Hegerfeldt, T. Köhler, and M. Stoll. Determination of the bond length and binding energy of the helium dimer by diffraction from a transmission grating. *Phys. Rev. Lett.*, 85:2284, 2000.

[123] K. T. Tang, J. P. Toennies, and C. L. Yiu. Accurate analytical He-He van der Waals potential based on perturbation theory. *Phys. Rev. Lett.*, 74:1546, 1995.

[124] S. M. Cybulski and R. R. Toczylowski. Ground state potential energy curves for He_2, Ne_2, Ar_2, He-Ne, He-Ar, and Ne-Ar: A coupled-cluster study. *J. Chem. Phys.*, 111:10520, 1999.

[125] F-M. Tao. *Ab initio* calculation of the interaction potential for the krypton dimer: The use of bond function basis sets. *J. Chem. Phys.*, 111:2407, 1999.

[126] N. G. Adams, D. K. Bohme, and E. E. Ferguson. Reactions of He_2^+, Ne_2^+, Ar_2^+, and Rare-Gas Hydride Ions with Hydrogen at 200 K. *J. Chem. Phys.*, 52:5101, 1970.

[127] V. E. Bondybey and G. C. Pimentel. Infrared Absorptions of Interstitial Hydrogen Atoms in Solid Argon and Krypton. *J. Chem. Phys.*, 56:3832, 1972.

[128] J. Lundell and H. Kunttu. Structure, spectra, and stability of argon hydride ion (Ar_2H^+), krypton hydride ion (Kr_2H^+), xenon hydride ion (Xe_2H^+): An effective core potential approach. *J. Phys. Chem.*, 96:9774, 1992.

[129] J. Lundell. Density functional approach on ground state RgH^+ and $RgHRg^+$ (Rg = Ar, Kr, Xe) ions. *J. Mol. Struct.*, 355:291, 1995.

[130] F. A. Gianturco and F. Filippone. Structure and dynamics of small protonated rare-gas clusters using quantum and classical methods. *Computer Phys. Comm.*, 145:78, 2002.

[131] J. Y. Qu, W. Li, R. Guo, and X. S. Zhao. A global potential energy surface of Ar_2H^+ based on *ab initio* calculations. *J. Chem. Phys.*, 117:2592, 2002.

[132] S. T. Kim and J. S. Lee. *Ab initio* study of He_2H^+ and Ne_2H^+ : Accurate structure and energetics. *J. Chem. Phys.*, 110:4413, 1999.

[133] K. T. Giju, S. Roszak, and J. Leszczynski. A theoretical study of protonated argon clusters: Ar_nH^+ (n=1-7). *J. Chem. Phys.*, 117:4803, 2002.

[134] T. Ritschel. Cationic Van der Waals complexes: Theoretical study of Ar_2H^+ structure and stability. *Zeits. für Phys. Chem.*, 218:377, 2004.

TH-1851_Sayak

[135] T. Ritschel, Ch. Zuhrt L. Zülicke, and P. J. Kuntz. Structure and dynamics of cationic Van der Waals clusters II. dynamics of protonated argon clusters. *Eur. Phys. J. D*, 41:127, 2007.

[136] R. D. Poshusta, J. A. Haugen, and D. F. Zetik. *Ab Initio* predictions for very small ions. *J. Chem. Phys.*, 51:3343, 1969.

[137] R. D. Poshusta and W. F. Siems. *Ab Initio* calculations on He_2H^+. *J. Chem. Phys.*, 55:1995, 1971.

[138] M. B. Milleur, R. L. Matcha, and E. F. Hayes. Theoretical studies of hydrogen-rare gas complexes: He_nH and He_nH^+ clusters. *J. Chem. Phys.*, 60:674, 1974.

[139] C. E. Dykstra. The strong hydrogen bond in $HeHHe^+$ and its weak counterpart in HeH_3^+. *J. Mol. Struct. (Theochem)*, 103:131, 1983.

[140] J. S. Lee and D. Secrest. A calculation of the rotation-vibration states of He_2H^+. *J. Chem. Phys.*, 85:6565, 1986.

[141] I. Baccarelli and F. A. Gianturco. Stability and fragmentation of protonated helium dimers from ab initio calculations of their potential energy surfaces. *J. Phys. Chem. A*, 101:6054, 1997.

[142] F.A. Gianturco and F. Filippone. Competitive shell-filling in protonated helium clusters. *Chem. Phys.*, 241:203, 1999.

[143] B. Balta and F.A. Gianturco. Structural properties and quantum effects in protonated helium clusters. I.The *ab initio* interaction potential. *Chem. Phys.*, 254:203, 2000.

[144] S. Bhattacharya and A. N. Panda. Time-dependent quantum dynamics of the He + H^+He reaction. *J. Phys. B*, 42:85201, 2009.

[145] T.-S. Chu and K.-L. Han. Effect of coriolis coupling in chemical reaction dynamics. *Phys. Chem. Chem. Phys.*, 10:2431, 2008.

[146] J. Mayneris, J. D. Sierra, and M. González. Time dependent quantum dynamics study of the Ne+H_2^+(v = 0-4)→NeH^++H proton transfer reaction. *J. Chem. Phys.*, 128:194307, 2008.

[147] X. Tang, C. Houchins, K. Lau, C. Y. Ng, R. A. Dressler, Y. Chiu, T. Chu, and K.-L. Han. A time-dependent wave packet quantum scattering study of the reaction HD^+(v = 0-3;j_0 = 1)+He→HeH^+(HeD^+)+D(H). *J. Chem. Phys.*, 127:164318, 2007.

TH-1851_Sayak

[148] E. Carmona-Novillo, T. Gonzãlez-Lezana, O. Roncero, P. Honvault, J.-M. Launay, N. Bulut, F. J. Aoiz, L. Bañares, A. Trottier, and E. Wrede. On the dynamics of the H^++D_2(v = 0,j = 0)HD+D^+ reaction: A comparison between theory and experiment. *J. Chem. Phys.*, 128:14304, 2006.

[149] T. Gonzãlez-Lezana, O. Roncero, P. Honvault, J.-M. Launay, N. Bulut, F. J. Aoiz, and L. Bañares. A detailed quantum mechanical and quasiclassical trajectory study on the dynamics of the H^++H_2→H_2+H^+ exchange reaction. *J. Chem. Phys.*, 125:94314, 2006.

[150] S. Sukiasyan and H.-D. Meyer. On the effect of initial rotation on reactivity. A multi-configuration time-dependent hartree (MCTDH) wave packet propagation study on the H + D_2 and D + H_2 reactive scattering systems. *J. Phys. Chem. A*, 105:2604, 2001.

[151] P. Palmieri, C. Puzzarini, V. Aquilanti, G. Capecchi, S. Cavalli, D. De Fazio, A. Aguilar, X. Gimenéz, and J. M. Lucas. *Ab initio* dynamics of the He + H_2^+ → HeH^+ +H reaction: a new potential energy surface and quantum mechanical cross-sections. *Mol. Phys.*, 98:1835, 2000.

[152] T. E. Carroll and E. M. Goldfield. Coriolis-coupled quantum dynamics for O(^{1}D) + H_2 → OH + H. *J. Phys. Chem. A*, 105:2251, 2001.

[153] D. De Fazio and J. F. Castillo. State-to-state three-atom reactive scattering using adiabatic rotation approximations. *Phys. Chem. Chem. Phys.*, 1:1165, 1999.

[154] A. Jäckle, M.-C. Heitz, and H.-D. Meyer. Reaction cross sections for the H+D_2($\nu = 0, 1$) system for collision up to 2.5 eV: A multiconfiguration time-dependent Hartree wave-packet propagation study. *J. Chem. Phys.*, 110:241–248. 1999.

[155] K-L Yeh, D. Xie, D. H. Zhang, S-Y. Lee, and R. Schinke. Time-dependent wave packet study of the O + O_2 (v = 0, j = 0) exchange reaction. *J. Phys. Chem. A*, 107:7215, 2003.

[156] B-Y. Tang, Q-K. Tang, M-D Chen, and K.-L. Han J. Z. H. Zhang. Quantum scattering calculation of the O(^{1}D)+HBr reaction. *J. Chem. Phys.*, 120:8537, 2004.

[157] E. L. Wu. Review: Coriolis Coupling and Nonadiabaticity in Chemical Reaction Dynamics. *J. Comput. Chem.*, 31:2827, 1994.

[158] K. McLenithan and Don Sest. A recoupled states approximation for molecular scattering theory. *J. Chem. Phys.*, 80:2480, 1984.

TH-1851_Sayak

[159] D. C. Clary. Quantum reactive scattering of four-atom reactions with non-linear geometry: OH+H_2→H_2O+H. *J. Chem. Phys.*, 95:7298, 1991.

[160] M. Yang, D. H. Zhang, M. A. Collins, and S.-Y. Lee. Quantum dynamics on new potential energy surfaces for the H_2 + OH → H_2O + H reaction. *J. Chem. Phys.*, 114:4759, 2001.

[161] M. Alagia, N. Balucani, P. Casavecchia, D. Stranges, G. G. Volpi, D. C. Clary, A. Kliesh, and H. J. Werner. The dynamics of the reaction OH + D_2→ HOD + D: Crossed beam experiments and quantum mechanical scattering calculations on *ab initio* potential energy surfaces. *Chem. Phys.*, 207:389, 1996.

[162] A. D. Issacson. Harmonic and anharmonic rate constants and transmission coefficients obtained from *ab initio* data. *J. Chem. Phys.*, 107:3832, 1997.

[163] G. O. Aspuru and D. C. Clary. New potential energy function for four-atom reactions. Application to OH + H_2. *J. Phys. Chem. A*, 102:9631, 1998.

[164] R. P. Bettens, M. A Collins, M. J. T. Jordan, and D. H. Zhang. *Ab initio* potential energy surface for the reactions between H_2O and H. *J. Chem. Phys.*, 112:10162, 2000.

[165] F. Otto, F. Gatti, and H-D. Meyer. Rotational excitations in para-H_2+para-H_2 collisions: Full and reduced-dimensional quantum wave packet studies comparing different potential energy surfaces. *J. Chem. Phys.*, 128:064305, 2008.

[166] G. D-Lewis, W. E. Wilson, and A. A Westemberg. Studies of hydroxyl radical kinetics by quantitative ESR. *J. Chem. Phys.*, 44:2877, 1966.

[167] N. R. Greiner. Hydroxyl radical kinetics by kinetic spectroscopy. V. reactions with H_2 and CO in the range 300-500 K. *J. Chem. Phys.*, 51:5049, 1969.

[168] F. Stuhl and H. Niki. Pulsed vacuum-uv photochemical study of reactions of OH with H_2, D_2, and CO using a resonance-fluorescent detection method. *J. Chem. Phys.*, 57:3671, 1972.

[169] A. A. Westenberg and N. de Hass. Rates of CO + OH and H_2 + OH over an extended temperature range. *J. Chem. Phys.*, 58:4061, 1972.

[170] R. Atkinson, D. A. Hansen, and J. N. Pitts Jr. Rate constants for the reaction of OH radicals with CHF_2Cl, CF_2Cl_2, $CFCl_3$, and H_2 over the temperature range 297-434 K. *J. Chem. Phys.*, 63:1703, 1975.

TH-1851_Sayak

[171] I. W. M. Smith and R. Zellner. Rate measurements of reactions of OH by resonance absorption. *J. Chem. Soc. Faraday. Trans.*, 70:1045, 1974.

[172] R. P . Overend, G. Paraskevopaoulos, and R. J. Svetanovic. Rates of OH radical reactions. I. Reactions with H_2, CH_4, C_2H_6, and C_3H_8 at 295K. *Can. J. Chem.*, 53:3374, 1975.

[173] G. C. Light and J. H. Matsumoto. The effect of vibrational excitation in the reactions of OH with H_2. *Chem. Phys. Lett.*, 58:578, 1978.

[174] R. Zellner. Non-arrhenius behavior in bimolecular reactions of the hydroxyl radical. *J. Phys. Chem.*, 83:18, 1979.

[175] F. P. Tully and A. R. Ravishankara. Flash photolysis-resonance fluorescence kinetic study of the reactions hydroxyl + molecular hydrogen $\rightarrow$ water + atomic hydrogen and hydroxyl + methane $\rightarrow$ water + methyl from 298 to 1020 K. *J. Phys. Chem.*, 84:3126, 1980.

[176] A. R. Ravishankara, J. M. Nicovich, R. L. Thomson, and F. P. Tully. Kinetic study of the reaction of hydroxyl with hydrogen and deuterium from 250 to 1050 K. *J. Phys. Chem.*, 85:2498, 1981.

[177] G. P. Glass, H. Endo, and B. K. Chaturvedi. Vibrational energy transfer from oh to other gaseous hydrides. *J. Chem. Phys.*, 77:5450, 1982.

[178] J. V. Michael and J. W. Sutherland. Rate constants for the reactions of hydrogen atom with water and hydroxyl with hydrogen by the flash photolysis-shock tube technique over the temperature range 1246-2297 K. *J. Phys. Chem.*, 92:3853, 1988.

[179] A. Jacobs. H.-R. Volpp, and J. Wolfrum. Absolute reactive cross section for the reaction $H+D_2O \rightarrow OD+HD$: A comparison to the protonated case. *Chem. Phys. Lett.*, 196:249, 1992.

[180] A. Jacobs, H.-R. Volpp, and J. Wolfrum. Reaction dynamics, OH energy partitioning, and OH product angular momentum alignment studies: $H+H_2O \rightarrow OH+H_2$ versus $H+CO_2 \rightarrow OH+CO$. *Chem. Phys. Lett.*, 218:51, 1994.

[181] A. Jacobs. H.-R. Volpp, and J. Wolfrum. The effect of reagent translation on the reaction dynamics and the absolute reaction cross section of $H+H_2O \rightarrow OH+H_2$. *J. Chem. Phys.*, 100:1936, 1994.

[182] E. de Beer, E. H. Kim, D. M. Neumark, R. F. Gunion, and W. C. Lineberger. Transition state spectroscopy of the $OH+H_2 \rightarrow H_2O$ +H reaction via photodetachment of H_3O^- and D_3O^-. *J. Phys. Chem.*, 99:13627, 1995.

TH-1851_Sayak

[183] R. K. Talukdar, T. Gierczak, L. Goldfarb, Y. Rudich, B. S. Madhava Rao, and A. R. Ravishankara. Kinetics of hydroxyl radical reactions with isotopically labeled hydrogen. *J. Phys. Chem.*, 100:3037, 1996.

[184] P. J. Krause, D. C. Clary, D. T. Anderson, M. T. Todd, R. L. Schwartz, and M. I. Lester. Time-resolved dissociation of the H_2-OH entrance channel complex. *Chem. Phys. Lett.*, 294:518, 1998.

[185] V. L. Orkin, S. N. Kozlov, G. A. Poskrebyshev, and M. J. Kurylo. Rate constant for the reaction of OH with H_2 between 200 and 480 K. *J. Phys. Chem. A*, 110:6978, 2006.

[186] I. W. M. Smith and F. F. Crim. The chemical kinetics and dynamics of the prototypical reaction: OH + H_2 $\rightarrow$ H_2O + H. *Phys. Chem. Chem. Phys.*, 4:3543, 2002.

[187] D. L. Baulch, C. T. Bowman, C. J. Cobos, R. A. Cox, Th. Just, J. A. Kerr, M. J. Pilling, D. Stocker, J. Troe, W. Tsang, R. W. Walker, , and J. Warnatz. Evaluated kinetic data for combustion modelling. *J. Phys. Chem. Ref. Data*, 34:757, 2005.

[188] P. Frank and Th. Just. High temperature reaction rate for atomic hydrogen + molecular oxygen = hydroxyl + atomic oxygen and hydroxyl + molecular hydrogen = water + atomic hydrogen. *Ber. Buns. Phys. Chem*, 89:181, 1985.

[189] R. C. Oldenborg, G. W. Loge, D. M. Harradine, and K. R. Winn. Kinetic study of the hydrogel + hydrogen reaction from 800 to 1550 K. *J. Phys. Chem.*, 96:8426, 1992.

[190] M. Alagia, N. Balucani, P. Casavecchia, D. Stranges, and G. C. Volpi. Crossed beam studies of fouratom reactions: The dynamics of OH+D_2. *J. Chem. Phys.*, 98:2459, 1993.

[191] S. Koppe, T. Laurent, P. D. Naik, H.-R. Volpp, and J. Wolfrum. Reaction dynamics studies of a simple tetraatomic system: AA+BA $\leftrightarrow$ A + ABA. *Can. J. Chem.*, 72:615, 1994.

[192] R. A. Brownsword, M. Hillenkamp, P. Schmiechen, H.-R. Volpp, and J. Wolfrum. The dynamics of the OH + HD gas-phase reaction: absolute reaction cross section and H/D atom product branching ratio. *Chem. Phys. Lett.*, 275:325, 1997.

[193] R. A. Loomis and M. I. Lester. Stabilization of reactants in a weakly bound complex: OH-H_2 and OH-D_2. *J. Chem. Phys.*, 103:4371, 1995.

TH-1851_Sayak

[194] K. Kudla and G. C. Schatz. Theoretical studies of energy transfer and reaction in $H+H_2O$ and $H+D_2O$ collisions. *J. Chem. Phys.*, 98:4644, 1993.

[195] D. C. Clary. Quantum scattering calculations on the $OH+H_2(v=0,1)$, $OH+D_2$, and $OD+H_2$ reactions. *J. Chem. Phys.*, 96:3656, 1992.

[196] O. Rashed and N. J. Brown. A molecular dynamics study of the reaction $H_2+OH \rightarrow H_2O+H$. *J. Chem. Phys.*, 82:5506, 1985.

[197] J. A. Harrison and H. R. Mayne. The effect of reagent rotation in the reaction $OH(j)+H_2(j') \rightarrow H_2O+H$. *J. Chem. Phys.*, 88:7424, 1988.

[198] A. D. Issacson. Global potential energy surfaces from limited ab initio data. *J. Phys. Chem.*, 96:531, 1992.

[199] T. H. Dunning, L. B. Harding, and E. Kraka. *Super computer algorithms for reactivity, dynamics and kinetics of small molecules.* Springer, 1989.

[200] T. N. Truong. Direct *ab initio* dynamics studies of vibrational-state selected reaction rate of the $OH+H_2 \rightarrow H+H_2O$ reaction. *J. Chem. Phys.*, 102:5335, 1995.

[201] U. Manthe, T. Seideman, and W. H. Miller. Full-dimensional quantum mechanical calculation of the rate constant for the $H_2+OH \rightarrow H_2O+H$ reaction. *J. Chem. Phys.*, 99:10078, 1993.

[202] D. H. Zhang and S.-Y. Lee. Fully converged integral cross sections of diatom-diatom reactions and the accuracy of the centrifugal sudden approximation in the H_2+OH reaction. *J. Chem. Phys.*, 110:4435, 1999.

[203] E. M. Goldfield and S. K. Gray. A quantum dynamics study of $H_2+OH \rightarrow H_2O+H$ employing the Wu-Schatz-Lendvay-Fang-Harding potential function and a four-atom implementation of the real wave packet method. *J. Chem. Phys.*, 117:1604, 2002.

[204] A. Rodíguez, E. García, J. M. Alvariño, and A. Laganà. Progress in validating the potential energy surface of the OH + H_2 reaction: product vibrational distributions. *Chem. Phys. Lett.*, 345:219, 2001.

[205] D. Troya, M. J. Lakin, G. C. Schatz, and M. González. Variational transition state theory and quasiclassical trajectory studies of the $H_2+OH \rightarrow H_2O+H$ reaction and some isotopic variants. *J. Chem. Phys.*, 115:1828, 2001.

[206] S. K. Pogrebnya, J. Palma, D. C. Clary, and J. Echave. Quantum scattering and quasi-classical trajectory calculations for the $H_2+OH \rightleftharpoons H_2O+H$ reaction on a new potential surface. *Phys. Chem. Chem. Phys.*, 2:693, 2000.

TH-1851_Sayak

[207] G. C. Schatz, G. Wu, G. Lenday, D.-C. Fang, and L. B. Harding. Reaction of H with highly vibrationally excited water: activated or not? *Faraday Discuss. Chem. Soc.*, 113:151, 1999.

[208] D. Troya, G. C. Schatz, and M. González. A quasiclassical trajectory study of reactivity and product energy disposal in H+H_2O, H+D_2O, and H+HOD. *J. Chem. Phys.*, 114:8397, 2001.

[209] J. F. Castillo, F. J. Aoiz, and L. Bañares. A quasiclassical trajectory study of the H + H_2O → OH + H_2 reaction dynamics at 1.4 ev collision energy on a new *ab initio* potential energy surface. *Chem. Phys. Lett.*, 356:120. 2002.

[210] D. H. Zhang, M. A. Collins, and S.-Y. Lee. First-principles theory for the H+H_2O, D_2O reactions. *Science*, 290:961, 2000.

[211] C. Xiao, X. Xu, S. Liu, T. Wang, W. Dong, T. Yang, Z. Sun, D. Dai, X. Xu, D. H. Zhang, and X. Yang. Experimental and theoretical differential cross sections for a four-atom reaction: HD + OH → H_2O + D. *Science*, 333:440, 2011.

[212] G. C. Schatz and S. P. Walsh. An *ab initio* calculation of the rate constant for the OH+H_2→H_2O+H reaction. *J. Chem. Phys.*, 72:776, 1980.

[213] G. C. Schatz. A quasiclassical trajectory study of reagent vibrational excitation effects in the OH+H_2→H_2O+H reaction. *J. Chem. Phys.*, 74:1133, 1981.

[214] K. S. Bradley and G. C. Schatz. A quasiclassical trajectory study of product energy and angular distributions in OH + H_2 (D_2). *J. Phys. Chem.*, 98:3788, 1994.

[215] A. D. Issacson and D. G. Truhlar. Polyatomic canonical variational theory for chemical reaction rates. separable-mode formalism with application to OH+H_2→H_2O+H. *J. Chem. Phys.*, 76:1380, 1982.

[216] D. G. Truhlar and A. D. Isaacson. Statistical-diabatic model for state-selected reaction rates. theory and application of vibrational-mode correlation analysis to OH(n_{OH})+H_2(n_{HH})→H_2O+H. *J. Chem. Phys.*, 77:3516, 1982.

[217] D. Lu and D. G. Truhlar. Bond-distance and bond-angle constraints in reaction-path dynamics calculations. *J. Chem. Phys.*, 99:2723, 1993.

[218] M. J. Cohen and A. Willets N. C. Handy. Cumulative reaction probabilities for OH+H_2 → H_2O +H and ClH+Cl → Cl+HCl from a knowledge of the anharmonic force field. *J. Chem. Phys.*, 99:5885, 1993.

TH-1851_Sayak

[219] G. D. Billing. Quantum-classical reaction path/surface model for chemical reactions. III. the reaction H_2+OH→H_2O+H. *Chem. Phys.*, 146:63, 1990.

[220] G. D. Billing. Quantum-classical reaction-path model for chemical reactions. V. relation to transition state theory. *Chem. Phys.*, 161:245, 1992.

[221] J. Palma and D. C. Clary. Quasi classical trajectory study of the reaction H_2+OH→H_2O+H: Comparison with quantum results. *J. Chem. Soc., Faraday Trans.*, 93:841, 1997.

[222] E. Garcia, A. Saracibar, C. Sanchez, and A. Laganà. A multiproperty analysis of the OH + H_2(D_2,HD) potential energy surface. *cp*, 308:201, 2005.

[223] G. Ochoa de Aspuru and D. C. Clary. New Potential Energy Function for Four-Atom Reactions. Application to OH+H_2. *J. Phys. Chem.*, 102:9631, 1998.

[224] G. Nyman and D. C. Clary. Quantum scattering calculations on H_2O+H→H_2+OH and isotopes: Rotational distributions and cross sections. *J. Chem. Phys.*, 99:7774, 1993.

[225] D. Wang and J. M. Bowman. Reduced dimensionality quantum calculations of mode specificity in OH+H_2↔H_2O+H. *J. Chem. Phys.*, 96:8906, 1992.

[226] J. Echave and D. C. Clary. Quantum theory of planar fouratom reactions. *J. Chem. Phys.*, 100:402, 1994.

[227] H. Szichman and M. Baer. A three dimensional quantum mechanical theory to treat tetra-atom reactions: State-to-state cross sections for the H_2 + OH → H_2O + H process. *J. Chem. Phys.*, 101:2081, 1994.

[228] H. Szichman and M. Baer. Quantum mechanical treatment of the H_2 + OH ⇔ H + H_2O reactions. calculations of cross sections and rate constants. *Chem. Phys. Lett.*, 242:285, 1995.

[229] N. Balakrishnan and G. D. Billing. Integral cross sections and rate constants for the reaction OH+H_2→H_2O+H: A semiclassical wave packet approach. *J. Chem. Phys.*, 101:2785, 1994.

[230] N. Balakrishnan and G. D. Billing. A mixed quantal/classical study of the reaction OH + H_2 → H_2O + H. *Chem. Phys. Lett.*, 233:145, 1995.

[231] D. H. Zhang and J. Z. H. Zhang. Full-dimensional time-dependent treatment for diatom-diatom reactions: The H_2+OH reaction. *J. Chem. Phys.*, 101:1146, 1994.

TH-1851_Sayak

[232] U. Manthe, T. Seideman, and W. H. Miller. Quantum mechanical calculations of the rate constant for the H_2+OH→H+H_2O reaction: Full-dimensional results and comparison to reduced dimensionality models. *J. Chem. Phys.*, 101:4759, 1994.

[233] W. H. Thompson and W. H. Miller. Initial state-selected reaction probabilities for OH+H_2 → H+H_2O and photodetachment intensities for HOH_2^-. *J. Chem. Phys.*, 101:8620, 1994.

[234] D. H. Zhang and J. Z. H. Zhang. Accurate quantum calculations for H_2+OH→H_2O+H: Reaction probabilities, cross sections, and rate constants. *J. Chem. Phys.*, 100:2697, 1994.

[235] D. H. Zhang and J. Z. H. Zhang. Accurate quantum calculation for the benchmark reaction H_2+OH→H_2O +H in five-dimensional space: Reaction probabilities for J=0. *J. Chem. Phys.*, 99:5615, 1993.

[236] D. H. Zhang and J. C. Light. The cumulative reaction probability for the H_2 + OH reaction. *J. Chem. Phys.*, 106:551, 1997.

[237] J. Dai, W. Zhu, X. C. Huang, and J. Z. H. Zhang. Energy dependence of state-to-state reaction probabilities for H_2 + OH → H + H_2O in six dimensions. *J. Phys. Chem.*, 100:13901, 1996.

[238] W. Zhu, J. Dai, J. Z. H. Zhang, and D. H. Zhang. State-to-state time-dependent quantum calculation for reaction H_2+OH→H+H_2O in six dimensions. *J. Chem. Phys.*, 105:4881, 1996.

[239] D. H. Zhang, J. C. Light, and S. Lee. Quantum rate constants for the H_2+OH reaction with the centrifugal sudden approximation. *J. Chem. Phys.*, 109:79, 1998.

[240] D. Neuhauser. Fully quantal initial-state-selected reaction probabilities (j=0) for a four-atom system: H_2(v=0, 1, j=0)+OH(v=0,1, j=0)→H+H_2O. *J. Chem. Phys.*, 100:9272, 1994.

[241] M. T. Cvitaš and S. C. Althorpe. Quantum wave packet method for state-to-state reactive scattering calculations on AB + CD → ABC + D reactions. *J. Phys. Chem. A*, 113:4557, 2009.

[242] M. T. Cvitaš and S. C. Althorpe. State-to-state reactive scattering in six dimensions using reactant-product decoupling: OH + H_2 → H_2O + H (J = 0). *J. Chem. Phys.*, 134:024309, 2011.

TH-1851_Sayak

[243] P. Defazio and S. K. Gray. A quantum dynamics study of D_2 + OH → DOH + D on the WSLFH potential energy function. *J. Phys. Chem. A*, 107:7132, 2003.

[244] D. H. Zhang, M. Yang, and S.-Y. Lee. Branching ratio in the HD+OH reaction: A full-dimensional quantum dynamics study on a new *ab initio* potential energy surface. *J. Chem. Phys.*, 114:8733, 2001.

[245] D. H. Zhang. M. Yang, and S.-Y. Lee. Quantum dynamics of the D_2 + OH reaction. *J. Chem. Phys.*, 116:2388, 2002.

[246] D. H. Zhang and S. Lee. Effects of reagent rotation on the dynamics of the H_2+OH reaction: A full dimension quantum study. *J. Chem. Phys.*, 109:2708, 1998.

[247] J. D. Sierra, P. A. Enŕiquez, D. Troya, and M. Gonźalez. A QCT study of the cross-section, energy and angular distributions of the OH + D_2 → HOD + D reaction at E_T = 0.28 eV on the YZCL2 surface. *Chem. Phys. Lett.*, 399:527, 2004.

[248] S. Bhattacharya, A. N. Panda, and H.-D. Meyer. Multiconfiguration time-dependent Hartree approach to study the OH+H_2 reaction. *J. Chem. Phys.*, 132:214304, 2010.

[249] U. Manthe and F. Matzkies. Rotational effects in the H_2+OH→H+H_2O reaction rate:full-dimensional close-coupling results. *J. Chem. Phys.*, 113:5725, 2000.

[250] A. Chakraborty and G. D Truhlar. Chemical theory and computation special feature: Quantum mechanical reaction rate constants by vibrational configuration interaction: The OH + H_2 →H_2O + H reaction as a function of temperature. *Proc. Nat. Acad. Sci.*, 102:6744, 2005.

[251] J. C. Polanyi and J. L. Schreiber. The reaction of F + H_2 → HF + H. A case study in reaction dynamics. *Faraday Discuss. Chem. Soc.*, 62:267, 1977.

[252] J. A. Miller and C. T. Bowman. Mechanism and modeling of nitrogen chemistry in combustion. *Prog. Energy Combust. Sci.*, 15:287, 1989.

[253] D. F. Strobel. Photochemistry of the Reducing Atmospheres of Jupiter, Saturn and Titan. *Int. Rev. Phy. Chem.*, 3:145, 1983.

[254] R. A. Bair and T. H. Dunning. Theoretical studies of the reactions of HCN with atomic hydrogen. *J. Chem. Phys.*, 82:2280, 1985.

TH-1851_Sayak

[255] A. F. Wagner and R. A. Bair. An *Ab initio* determination of the rate constant for H_2 + CN → H + HCN. *Int. J. Chem. Kinet.*, 18:473, 1986.

[256] A. N. Brooks and D. C. Clary. Application of hyperspherical coordinates to four-atom reactive scattering: H_2+CN → H+HCN. *J. Chem. Phys.*. 92:4178, 1990.

[257] Q. Sun and J. M. Bowman. Reduced dimensionality quantum reactive scattering: H_2+CN→H+HCN. *J. Chem. Phys.*, 92:5201, 1990.

[258] X. Li, N. Sayah, and W. M. Jackson. Laser measurements of the effects of vibrational energy on the reactions of CN. *J. Chem. Phys.*, 81:833, 1984.

[259] J. D. Juan, I. W. M. Smith, and B. Veyret. Kinetics of CN(v=0) and CN(v=1) with H_2 HCl and HBr. *Chem. Phys. Lett.*, 132:108, 1986.

[260] K. Natarajan and P. Roth. *21st Symposium(International) on Combustion.* Elsevier, 1986.

[261] A. Jacobs, M. Wahl, R. Weller, and J. Wolfrum. *22nd Symposium(International) on Combustion.* Elsevier, 1989.

[262] I. R. Sims and I. W. M. Smith. Rate constants for the reactions CN(v=0), CN(v=1)+H_2, D_2 →HCN, DCN+H, D between 295 and 768 K, and comparisons with transition state theory calculations. *Chem. Phys. Lett.*, 149:565, 1988.

[263] R. Atakan, M. Jacobs, M. Weller, and J. Wolfrum. Kinetic studies of the gas-phase reactions of CN with O_2 and H_2 from 294 to 1000 K. *Chem. Phys. Lett.*, 154:449, 1989.

[264] Q. Sun, D. L. Yang, N. S. Wang, J. M. Bowman, and M. C. Lin. Experimental and reduced dimensionality quantum rate coefficients for$H_2(D_2)$+CN→H(D)CN+H(D). *J. Chem. Phys.*, 93:4730, 1990.

[265] C. Kreher, R. Theinl, and K-H. Gericke. State-to-state reaction dynamics of R+HCN $(v_1 v_2^{l_2} v_3)$→RH+CN(v,j) with R=Cl, H. *J. Chem. Phys.*, 104:4481, 1996.

[266] D. C. Che and K. Liu. A crossed-beam study of the reaction of CN + D_2. is CN really a spectator bond? *Chem. Phys. Lett.*, 243:290, 1995.

[267] D. C. Che and K. Liu. Reactive scattering of CN + D_2: the stereodynamics. *Chem. Phys.*, 207:367, 1996.

TH-1851_Sayak

[268] J-H. Wang, K. Liu, G. C. Schatz, and M. A. ter Horst. Experimental and theoretical angular and translational energy distributions for the reaction CN+D_2 →DCN+D. *J. Chem. Phys.*, 107:7869, 1997.

[269] S. Krebs and R. J. Buenker. Multireference configuration interaction study of the mixed valence-rydberg character of the C_2H_4 $^1(\pi, \pi^*)$ V state. *J. Chem. Phys.*, 106:7208, 1997.

[270] G. He, I. Tokue, and R. G. Macdonald. Thermal rate constant for CN + H_2/D_2 → HCN/DCN + H/D reaction from T = 293 to 380K. *J. Phys. Chem. A*, 102:4585, 1998.

[271] Y. Chen and M. C. Heaven. Spectroscopy and dynamics of the H_2-CN Van der Waals complex. *J. Chem. Phys.*, 109:5171, 1998.

[272] G. A. Bethardy, F. J. Northrup, G. He, I. Tokue, and R. G. Macdonald. Initial vibrational level distribution of HCN[$\tilde{X}^1\sum^+(v_1,0,v_3)$] from the CN($X^2\sum^+$)+$H_2$ →HCN+H reaction. *J. Chem. Phys.*, 109:4224, 1998.

[273] D. L. Yang and M. C. Lin. The reactions of the cn radical with molecules relevant to combustion and atmospheric chemistry. In *The Chemical Dynamics and Kinetics of Small Radicals*, River Edge, 1995. World Scientific.

[274] L. R. Copeland, F. Mohammed, M. Zahedi, D. H. Volman, and W. M. Jackson. Rate constants for CN reactions with hydrocarbons and the product HCN vibrational populations: Examples of heavy-light-heavy abstraction reactions. *J. Chem. Phys.*, 96:5817, 1992.

[275] E. Arunan, G. Manke, and R. W. Setser. Infrared chemiluminescence studies of H + BrCN and H abstraction by CN reactions. Importance of the HNC channel. *Chem. Phys. Lett.*, 207:81, 1993.

[276] G. A. Bethardy, F. J. Northrup, and R. G. Macdonald. The initial vibrational state distribution of HCN $\tilde{X}^1\sum^+(v_1,0,v_3)$ from the reaction CN($^2\sum^+$)+C_2H_6 →HCN+C_2H_5. *J. Chem. Phys.*, 102:7966, 1995.

[277] J. M. Pfeiffer, R. B. Metz, J. D Thoemke, E. Woods, and F. F. Crim. Reactions of O, H, and Cl atoms with highly vibrationally excited HCN: Using product states to determine mechanisms. *J. Chem. Phys.*, 104:4490, 1996.

[278] D. C. Clary. Product CN rotational distributions from the H + HCN reaction. *J. Phys. Chem.*, 99:13664, 1995.

[279] T. Takayanagi, M. A. ter Horst, and G. C. Schatz. Approximate quantum scattering studies of the CN+H_2 reaction. *J. Chem. Phys.*, 105:2309, 1996.

TH-1851_Sayak

[280] J. M. Bowman. Reduced dimensionality theory of quantum reactive scattering. *J. Phys. Chem.*, 95:4960, 1991.

[281] T. Takayanagi and G. C. Schatz. Reaction dynamics calculations for the $CN+H_2 \rightarrow HCN+H$ reaction: Applications of the rotating-bond approximation. *J. Chem. Phys.*, 106:3227, 1997.

[282] G. A. Bethardy, A. F. Wagner, G. C. Schatz. and M. A. ter Horst. A quasiclassical trajectory study of product state distributions from the $CN+H_2 \rightarrow HCN+H$ reaction. *J. Chem. Phys.*, 106:6001, 1997.

[283] T. Takayanagi and G. C. Schatz. Quantum reactive scattering studies of the $CN + H_2 \rightarrow HCN + H$ reaction: The role of the non-reactive CN bond. *Chem. Phys. Lett.*, 265:410, 1997.

[284] U. Manthe and F. Matzkies. Quantum calculations of thermal rate constants and reaction probabilities: $H_2+CN \rightarrow H+HCN$. *Chem. Phys. Lett.*, 282:442, 1998.

[285] W. Zhu, J. Z. H. Zhang, Y. C. Zhang, Y. B. Zhang, L X Zhan, S. L. Zhang, and D. H. Zhang. Quantum dynamics study of $H_2+CN \rightarrow HCN+H$ reaction in full dimensions. *J. Chem. Phys.*, 108:3509, 1998.

[286] D. H. Zhang and S.-Y. Lee. Effects of reagent rotation and the accuracy of the centrifugal sudden approximation in the H_2+CN reaction. *J. Chem. Phys.*, 112:203, 2000.

[287] C. Coletti and G. Billing. Quantum-classical calculation of cross sections and rate constants for the $H_2+CN \leftrightarrow HCN+H$ reaction. *J. Chem. Phys.*, 113:11101, 2000.

[288] L. P. Ju, K.-L. Han, and J. Z. H. Zhang. A theoretical study for $H_2 + CN \leftrightarrow HCN + H$ reaction and its kinetic isotope effects with variational transition state theory. *J. Theor. Comp. Chem.*, 5:769, 2006.

[289] W. Zhu, J. Z. H. Zhang, and D. H. Zhang. Full-dimensional quantum dynamics calculation for D_2+CN reaction. *Chem. Phys. Lett.*, 292:46, 1998.

540
BHA/S
P1

THESIS
Lakshminath Bezbaroa Central Library
Indian Institute of Technology Guwahati
ACC. No. TH. 1851
Date 28/3/19

TH-1851_Sayak

PUBLICATIONS

1. S. Bhattacharya and A. N. Panda. Time-dependent quantum dynamics of the He + H^+He reaction, *J. Phys. B*, 42:85201, 2009.

2. S. Bhattacharya, A. N. Panda and H.-D. Meyer. Multiconfiguration time-dependent Hartree approach to study the OH + H_2 reaction, *J. Chem. Phys.*, 132:214304, 2010.

3. S. Bhattacharya, A. Kirwai, A. N. Panda and H.-D. Meyer. Full dimensional quantum scattering study of the H_2 + CN reaction, *J. Chem. Sci.*, (**Accepted**)

4. S. Bhattacharya, A. N. Panda and H.-D. Meyer. Cross sections and rate constants for OH + H_2 reaction on three different potential energy surfaces for ro-vibrationally excited reagents. *J. Chem. Phys.*, (**Accepted**)

TH-1851_Sayak